The University of Nottingham

Dissecting the molecular mechanism regulating lateral root hydropatterning

Thesis submitted for a degree of Doctor of Philosophy

Nicola Leftley

2017

CONTENTS

Acknowledgments VI

List of figures and tables VII

List of abbreviations X

Abstract XII

Chapter 1: INTRODUCTION 2

1.1 ROOT GROWTH AND DEVELOPMENT 2

1.2 ROOT ADAPTIVE RESPONSES 3

1.2.1 Water and soil 3

1.2.2 Hydrotropism 4

1.2.3 Lateral root hydropatterning 4

1.2.4 SUMOylation 7

1.3 LATERAL ROOT DEVELOPMENT 9

1.3.1 Primary root cellular organisation 9

1.3.2 Lateral root initiation and formation 11

1.3.3 Lateral root emergence 13

1.4 AUXIN RESPONSE CONTROLS LATERAL ROOT DEVELOPMENT 14

1.4.1 Phytohormone Auxin 14

1.4.2 Auxin signalling pathway 15

1.5 GENES INVOLVED IN LATERAL ROOT FORMATION 17

1.5.1 *AUXIN RESPONSE FACTORS (ARFs)* 17

1.5.2 Role of *ARF7* and *ARF19* 18

1.6 PROJECT AIMS AND OBJECTIVES 19

Chapter 2: GENERAL MATERIALS AND METHODS 20

2.1 PLANT CULTIVATION 21

2.1.1 *Arabidopsis thaliana* material 21

2.1.2 Plasmid material 23
2.1.3 General growth conditions for *Arabidopsis thaliana* 23
2.1.4 *Arabidopsis* crosses 24
2.2 PLANT PHENOTYPING ANALYSES 25
2.2.1 Root clearing assay 25
2.2.2 Microscopy and image processing using ImageJ 25
2.2.3 Confocal microscopy and image processing using LAS AF Lite 25
2.3 MOLECULAR TECHNIQUES 26
2.3.1 Nucleic acid extraction 26
2.3.1.1 *Plant Genomic DNA extraction* 26
2.3.1.2 *Total RNA extraction* 27
2.3.1.3 *Quality control of RNA and DNA* 27
2.3.2 Sequence amplification and analysis 28
2.3.2.1 *Polymerase chain reaction* 28
2.3.2.2 *PCR purification* 28
2.3.2.3 *Gel electrophoresis* 29
2.3.2.4 *DNA Gel extraction* 29
2.3.2.5 *Restriction enzyme digestion* 29
2.4 CLONING 30
2.4.1 Gateway recombination 30
2.4.1.1 *Generating pENTRY constructs* 30
2.4.1.2 *Generating destination constructs* 31
2.4.2 Greengate cloning system 31
2.4.2.1 *Greengate pENTRY recombination* 31
2.4.2.2 *Greengate Destination recombination* 32
2.4.3 Transformation of *E.coli* $DH_5\alpha$ cells 33

2.4.3.1 *Chemical competent transformation* 33

2.4.3.2 *Electro competent transformation* 33

2.4.4 Bacterial colony screening 34

2.4.5 Plasmid DNA isolation 34

2.4.6 DNA Sequencing 35

2.4.7 Archiving of plasmids and DNA sequence information 35

2.4.8 *Agrobacterium*-mediated transformation 35

2.4.8.1 *Transformation of Agrobacterium tumefaciens* 35

2.4.8.2 *Floral dipping of Arabidopsis thaliana* 36

2.5 EXPRESSION ANALYSIS 36

2.5.1 First strand cDNA synthesis 36

2.5.2 RT-qPCR 37

2.6 STATISTICAL ANALYSIS 38

2.6.1 P-value/T-test/ANOVA/FDR correction 38

Chapter 3: *ARF7* IS ESSENTIAL FOR LR HYDROPATTERNING 39

3.1 INTRODUCTION 40

3.2 RESULTS 41

3.2.1 Optimising the LR hydropatterning phenotyping bioassay 41

3.2.2 Hydropatterning influences very early LR development 45

3.2.3 Which auxin response factor genes are important for LR hydropatterning? 49

3.2.4 *ARF7* is important for LR hydropatterning 56

3.2.5 *ARF7* is expression during early stages of LR development 66

3.3 DISCUSSION 68

Chapter 4: *ARF7* CONTROLS LR HYDROPATTERNING VIA A SUMOYLATION - DEPENDENT POST TRANSCRIPTIONAL MECHANISM 74

4.1 INTRODUCTION 75

4.2 RESULTS 76

4.2.1 LR hydropatterning is regulated post transcriptionally 76

4.2.2 SUMOylation influences LR hydropatterning 81

4.2.3 *ARF7* is a target for SUMOylation 85

4.2.4 ARF7 controls LR hydropatterning via SUMOylation 88

4.3 DISCUSSION 94

Chapter 5: DOWNSTREAM TARGETS OF *ARF7* EXHIBIT HYDROPATTERNING DEFECTS 100

5.1 INTRODUCTION 101

5.2 RESULTS 102

5.2.1 *LBD16* is a target for *ARF7* and required for LR hydropatterning 102

5.2.2 *SHY2* is important for LR hydropatterning 107

5.2.3 *IAA28* is not important for LR hydropatterning 113

5.3 DISCUSSION 117

Chapter 6: DISCUSSION 120

6.1 DISCUSSION 121

6.2 FUTURE DIRECTIONS 125

Chapter 7: REFERENCES 127

7.1 REFERENCES 128

Chapter A: APPENDICES 138

A.1 PRIMERS 139

A.1.1 Sequencing/genotyping primers 140

A.1.2 Greengate cloning primers 141

A.2 CLONING (GATEWAY AND GREENGATE) 142

A.2.1 List of Greengate pENTRY vectors 143

A.2.2 List of Greengate Destination vectors 144

A.2.3 List of Gateway plasmids 145

ACKNOWLEDGMENTS

I would like to start by expressing my sincere thanks to both my supervisors, Prof. Malcolm Bennett and Dr. Anthony Bishopp for their excellent guidance, continued support and invaluable advice throughout my PhD. I would like to add a special thanks to Prof. Malcolm Bennett for helping me get this thesis submitted. His continued encouragement enabled me to carry on.

I would also like to give a special thank you to Kamal Swarup, who is not just a colleague but also a friend when things got hard. Her dedication to the team is remarkable. She always has time even if she has a busy schedule to help. Thank you so much Kamal.

Many thanks also to the rest of the LR hydropatterning team, Emily Morris, Rahul Bhosale, Jason Banda and Daniel Von Wangenhiem here in Nottingham. Also a big thank you to the rest of the CPIB group. The sweets and biscuits provided when people returned from holidays were always a welcomed treat.

Personally, I want to say a special big thank you to Zoe Phillips, my best friend who has always been there and encouraged me to never give up. I also want to give a big thank you to Marlene Oldman who is always there with a smile.

There are so many people I want to thank. It has been a bit of a rollercoaster at times but I can honestly say, it was worth it ;)

LIST OF FIGURES AND TABLES

Figure 1.1 Schematic diagram depicting LR hydropatterning

Figure 1.2 Schematics depicting the SUMOylation pathway in *Arabidopsis thaliana*

Figure 1.3 Schematic overview of the various layers that make up the morphology of the PR in *Arabidopsis thaliana*

Figure 1.4 Schematic showing the morphological changes during LR development in the model organism *Arabidopsis thaliana*

Figure 1.5 Schematic diagram depicting developmental stages in LR formation

Table 2.1 Greengate pENTRY and Destination vectors

Figure 3.1 Schematic representation of the hydropatterning phenotyping criteria used to score emerged LRs

Figure 3.2 LSFM used to distinguish air and contact sides

Figure 3.3 *TWD1* influences epidermal root twisting

Figure 3.4 LR hydropatterning affects XP selection

Figure 3.5 *TWD1* impacts root architecture

Figure 3.6 An ARF family member is involved in LR hydropatterning

Figure 3.7 ARFs have diverse root architectures

Figure 3.8 *ARF6* exhibits normal LR hydropatterning

Figure 3.9 *ARF6* and WT (Col-0) have similar root architectures

Figure 3.10 *ARF7* is important for LR hydropatterning

Figure 3.11 *ARF7* displays a striking LR phenotype

Figure 3.12 *ARF7* domain structure specifying *arf7* alleles

Figure 3.13 Independent *arf7* alleles validate the importance of *ARF7* in LR hydropatterning

Figure 3.14 *arf7-3* has a distinct reduction in LRs

Figure 3.15 *ARF19* is not required for LR hydropatterning

Figure 3.16 *ARF19* domain structure specifying *arf19* alleles

Figure 3.17 *ARF19* alleles have reduced LR numbers

Figure 3.18 *ARF7* transcriptional and translational reporters specifying different promoter lengths

Figure 3.19 Expression patterns of the *pARF7:3xVenus* reporter with the 'shorter' promoter

Figure 3.20 Expression patterns of the *pARF7:3xVenus* reporter with the 'longer' promoter

Figure 3.21 Expression patterns of the *pARF7:gARF7:3xVenus* reporter

Figure 4.1 Overexpression of *ARF7* rescued the LR hydropatterning defect

Figure 4.2 *ARF7* overexpression has a diverse root architecture

Figure 4.3 LR Hydropatterning is regulated post transcriptionally

Figure 4.4 *ARF7* overexpression impacts root architecture

Figure 4.5 LR hydropatterning is dependent on OTS1 and OTS2

Figure 4.6 *OTS1 OTS2* has a marked reduction in LRs

Figure 4.7 Schematic representation of the ARF7 protein coding sequence that contains post-translational regulatory motifs

Figure 4.8 *ARF7* is a target for SUMOylation

Figure 4.9 Generating the mutated SUMO *ARF7* transgene

Figure 4.10 *arf7* LR hydropatterning defect rescued

Figure 4.11 Functioning protein in SUMOylatable ARF7

Figure 4.12 *ARF7* SUMOylation required for LR hydropatterning

Figure 4.13 Non-SUMOylatable ARF7 protein remained functional

Figure 4.14 Schematic representation of *ARF7* SUMOylation

Figure 4.15 ARF7-SLR/IAA14 interaction SUMO independent

Figure 4.16 ARF7-IAA3/SHY2 interaction SUMO dependent

Figure 4.17 ARF7-IAA3/SHY2 interaction dependent on SIM motif

Figure 5.1 *LBD16* is involved in LR hydropatterning

Figure 5.2 *LBD16* and *LBD18* have marked reductions in LRs

Figure 5.3 *LBD16* expression later in the elongation zone

Figure 5.4 IAA3/*SHY2* is required for LR hydropatterning

Figure 5.5 Expression patterns of *pSHY2::NLS:3xVenus* reporter

Figure 5.6 *pSHY2::NLS:3xVenus* expression in primordia

Figure 5.7 *IAA28* may be involved in LR hydropatterning

Figure 5.8 *iaa28-ko* displays diverse root architecture

Figure 5.9 *IAA28* gain of function exhibits normal LR hydropatterning

Figure 6.1 Schematic representation of enhanced *ARF7* SUMOylation

LIST OF ABBREVIATIONS

ARF	Auxin response factors
AUX	Auxin resistant 1
bp	Base pair
cDNA	Complementary DNA
DNA	Deoxyribonucleic acid
dNTP	Deoxy ribonucleotide triphosphate
FC	Founder cells
GFP	Green fluorescent protein
IAA	Indole-3-acetic acid
LBD	Lateral organ boundaries domain
LR	Lateral root
LRI	Lateral root initiation
LRP	Lateral root primordium
M	Molar
MS	Murashige & Skoog
OTS	Overly tolerant to salt
PCR	Polymerase chain reaction
PR	Primary root
RAM	Root apical meristem
RC	Root cap
RNA	Ribonucleic acid
RSA	Root system architecture
RT	Root tip
SAM	Shoot apical meristem
SIM	SUMO interacting motif
SUMO	Small ubiquitin-like modifier

TF	Transcription factor
TWD	Twisted dwarf
WT	Wild type
XP	Xylem pole
YFP	Yellow fluorescent protein

ABSTRACT

Lateral roots (LR) contribute considerably to the architecture of the root system. The hormone auxin tightly controls the regulation of LR formation in response to environmental signals. For example, roots have the ability to distinguish between wet and dry micro environments in the soil and adapt the positioning of lateral roots accordingly. This concept is referred to as LR hydropatterning and is a novel adaptive mechanism for controlling root branching.

When growing vertically down an agar plate, *Arabidopsis thaliana* roots are also exposed to an asymmetric distribution of water that causes a meniscus to form around the primary root (PR) circumference. LRs develop preferentially on the side of the PR in contact with water, rather than the side exposed to air. My project aims to elucidate the underlying molecular mechanisms controlling this novel adaptive response.

It has been revealed that the transcription factor AUXIN RESPONSE FACTOR 7 (*ARF7*) is essential for LR hydropatterning. In contrast to wild type, *arf7* loss of function mutants do not exhibit greater LR emergence on the side of the PR in contact with moisture. Ectopic expression of *ARF7* (in *35S:ARF7 arf7-1*) can rescue *arf7* LR hydropatterning, implying that *ARF7* regulates LR hydropatterning via a post-transcriptional mechanism.

One promising post-transcriptional mechanism that may control LR hydropatterning involves protein SUMOylation (a **S**mall **U**biquitin-like **Modifier**), since the SUMO mutant *ots1 ots2* phenocopies the *arf7* LR hydropatterning defect. *OTS1* and *OTS2* encode nuclear localised proteases that remove SUMO from target proteins. *ARF7* is a target for SUMO modification, containing several SUMOylation sites including one within its DNA binding domain. Expressing wild type *ARF7* and a non-SUMOylated version in *arf7* revealed that *ARF7* controls LR hydropatterning via SUMOylation. This

knowledge will help reveal how plants explore the soil and position LR to maximise water (and nutrient) foraging.

CHAPTER 1: INTRODUCTION

CHAPTER 1: INTRODUCTION

1.1 ROOT GROWTH AND DEVELOPMENT

Root system architecture (RSA) is fundamental for optimal plant development and growth. As sessile organisms, most plants have a remarkable ability in adapting their RSA to the local environment around them. This developmental plasticity enables plants to react to various abiotic stresses (reviewed in Morris *et al*., 2017). In most plant species, the RSA is made up of a primary root (PR), lateral root (LRs) (such as adventitious roots) and root hairs (RH) (Smith and De Smet, 2012 and reviewed in Verstraeten *et al*., 2014).

The model organism *Arabidopsis thaliana* belongs to a subclass of angiosperms, dicots. *Arabidopsis thaliana* is also from the mustard family *Brassicaceae* and exhibits a 'taproot' system (Smith and De Smet, 2012). This system is comprised of a main root (PR) with smaller LRs. The PR repeatedly branches to generate these LRs. It is the LRs though that contribute considerably to the architecture of the root system. LRs are positioned evenly along the PR and follow a right left altering pattern (*in vitro*) (reviewed in Lavenus *et al*., 2013).

Branching of LRs anchors the plant in the soil but also contributes to water uptake and extraction of nutrients (Casimiro *et al*., 2003 and reviewed in Van Norman *et al*., 2013). According to Osmont *et al* (2007), the ability to take up nutrients is dependent on the root system being able to respond to an ever changing soil environment. Particles of all different sizes make up the heterogeneous nature of soil (Bao *et al*., 2014). Pockets of air and varying distributions of water are interspersed in this ever changing environment. Plants have adapted their RSA in order to tap into these distant reserves of water (Smith and De Smet, 2012 and reviewed in Verstraeten *et al*., 2014). How

plants perceive water is limited. Hence, understanding how roots sense the available water and respond is of great importance to agriculture.

1.2 ROOT ADAPTIVE RESPONSES TO WATER

Over time, plants have evolved numerous adaptive mechanisms that respond to the environmental signals around them and as a result the orientation of growth (Miyazawa and Takahashi, 2007). This ability enables plants to access limited resources and react to localised environmental stresses such as drought. These adaptive responses are highly specialised and minimise the effect of such stresses on the plant. Roots play a crucial role in the plants adaptation to water stresses but how they do this is still being explored (Robbins and Dinneny, 2015). With the aid of X-ray microCT based imagery, the characterisation of new and existing root adaptive mechanisms to varying water availability are being revealed (Morris *et al*., 2017).

1.2.1 Water and soil

The heterogeneous nature of soil affects water holding capabilities (Morris *et al*., 2017). The ability of water to move through the soil is governed ultimately by soil and water properties. There are many types of soil (clay, peat, loam and sandy) and the structural composition varies greatly between them (Morris *et al*., 2017). Particles of all different shapes and sizes therefore dictate water flow. Water moves by gravity into the numerous open pores within the soil. These pores have varying amounts of water and air due to their capacity. Water readily moves within these pores creating changeable moisture gradients (Bao *et al*., 2014). This permeability therefore affects

the availability of water and nutrient uptake by the roots. Plant have evolved their RSA to respond to the ever changing soil environment (Morris *et al*., 2017).

1.2.2 Hydrotropism

The root adaptive response referred to as hydrotropism, is where the root cap (RC) senses available water and sends a signal to the elongation zone (Moriwaki *et al*., 2013). The RC responds to the ever changing environmental cues and as a result establishes a stable RSA by directional growth (Eapen *et al*., 2003). The root adaptive response requires a gradient of water for directional root growth. Growth towards or away from moisture is therefore vital to avoid drought or oversaturation. A root's ability to forage for water is dependent on ABA signalling (Dietrich *et al*., 2017). Recent studies have confirmed that, in fact, the RC is not needed to generate a hydrotropic response which was first thought (Dietrich *et al*., 2017). Both the ABA signalling kinase, SnRK2.2 and MIZU-KUSSEI 1 (MIZ1) were found to act in the cortical cells within the elongation zone (Dietrich *et al*., 2017). The elongation zone not only senses a water potential gradient but is able to direct growth during a gravitropic response.

1.2.3 Lateral root hydropatterning

Recently, it has been observed that it is not only the RC that is sensitive to the distribution of water but also the orientation of future LRs (Bao *et al*., 2014). It has been revealed that roots have the ability to distinguish between wet and dry environments and as a result adapt the positioning of lateral root branches (Bao *et al*., 2014). This newly discovered adaptive mechanism for controlling root branching, is referred to as LR hydropatterning (Bao *et al*., 2014). Local variations in water

availability results in LRs forming primarily on the side of the root that is in direct contact with water (Fig. 1.1). With the aid of X-ray microCT imagery, this highly patterned response towards water was visualised *in-situ* (Fig. 1.1) (Bao et *al*., 2014 and Morris et *al*., 2017).

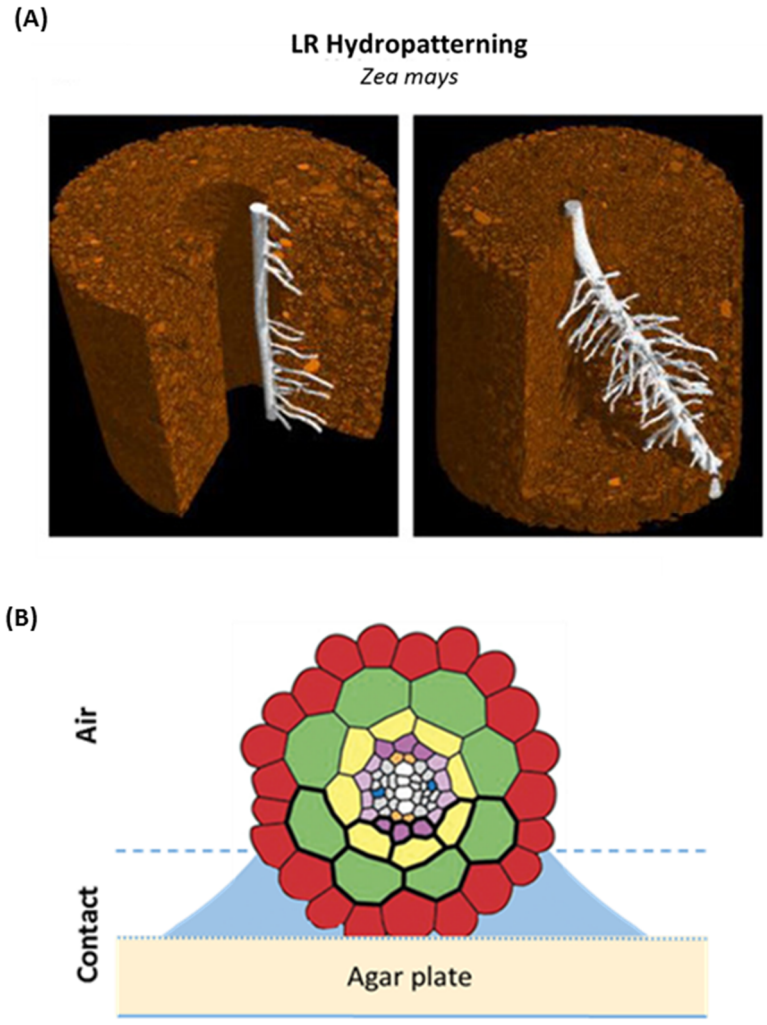


Fig. 1.1: Schematic diagram depicting LR hydropatterning. Micro-CT imaging of *Zea mays* roots growing down soil columns show clear LR hydropatterning responses (A). Roots grown down an artificial air pore position their LRs in direct contact with moisture (left). On the other hand, when roots are grown normally in soil, there is a random patterning of LRs (right) (Bao *et al*., 2014) (A). Schematic cross section of an *Arabidopsis thaliana* root showing the meniscus that forms while growing on an agar plate depicting the air/contact divide (B).

LR hydropatterning appears to be a highly conserved adaptive response in higher plants as it occurs not only in monocot but also eudicot roots (Bao *et al*., 2014). Bao *et al* (2014), hypothesised that the root systems of flowering plants have developed mechanisms to respond to differences in the environment around them. Growing roots vertically on the surface of an agar plate triggers a similar adaptive response. The formation of a meniscus results in opposite sides of the root to either be in direct contact with moisture or exposed to air (**Fig. 1.1**) (**B**). This is believed to be regulated by a differential auxin response gradient in response to an asymmetric moisture distribution (Bao *et al*., 2014). In essence, differences in water availability across the circumference of the PR causes an auxin signalling cascade.

In fact, Bao *et al* (2014) determined that auxin biosynthesis, transport and signalling were all an important part of regulating LR hydropatterning. Auxin is known to play a vital role in the earliest stages of LR development. Changes in auxin levels within the root promotes a signalling cascade (Friml *et al*., 2003). It has been well documented that this auxin activation promotes pericycle founder cell (FC) specification which overlays one of the xylem poles (De Smet *et al*., 2007; Lavenus *et al*., 2013; reviewed in Péret *et al*., 2009 and Smith and De Smet, 2012). This is the very first step in LR initiation and ultimately the development of a LR.

In *Arabidopsis thaliana* only one of the two xylem poles will be selected at any given time to develop into a LR. Bao *et al* (2014) found, with the aid of early stage markers, that LR hydropatterning acted at this point of FC specification. It is believed that moisture differences across the PR bias the xylem pole selection towards the contact side (Bao *et al*., 2014). This results in LRs emerging predominately on the contact side of the PR as opposed to that of the air side.

It is known that LR development is repressed under water limiting conditions. The ABA signalling pathway is induced if the water conditions are severe (Babe *et al*., 2012). A reduction in water potential causes ABA to translocate to the leaves and as a result alters the osmotic potential. Guard cells in the leaves then shrink thereby reducing transpiration via the xylem (Babe *et al*., 2012). Unlike, ABA signalling though, LR hydropatterning was found to be different from this classic water stress response and does not completely inhibit LR development (Bao *et al*., 2014 and De Smet *et al*., 2003). According to Bao *et al* (2014), ABA mutants such as *pyr/pyl 112458* that are highly resistant to ABA treatment, exhibited a normal LR hydropatterning response. Hence, ABA signalling pathway is not involved in LR hydropatterning. In fact, LR hydropatterning appears to be a response to drying rather than water.

1.2.4 SUMOylation

One possible drought-induced stress response is SUMOylation. Essentially, SUMOylation is a post-translational modification in response to environmental challenges such as abiotic stress (Conti *et al*., 2008 and Conti *et al*., 2014). In fact, SUMOylation is a major regulator of protein function and involved in many cellular processes such as protein localisation and stability (Park *et al*., 2011). SUMOylation is biochemically analogous to ubiquitination although functionally distinct. Rather than conjugation by ubiquitin, SUMOylation involves the covalent attachment of SUMO (**S**mall **U**biquitin-like **Mo**difier Protein) (Conti *et al*., 2014).

The dynamic nature of this post-translational modification is that it is reversible. E3 SUMO ligases make up the SUMOylation pathway along with SUMO proteases (**Fig. 1.2**). Only small fractions of protein are SUMOylated at any given time. In order for a target protein to be SUMOylated though, it must contain a SUMO site. This distinct

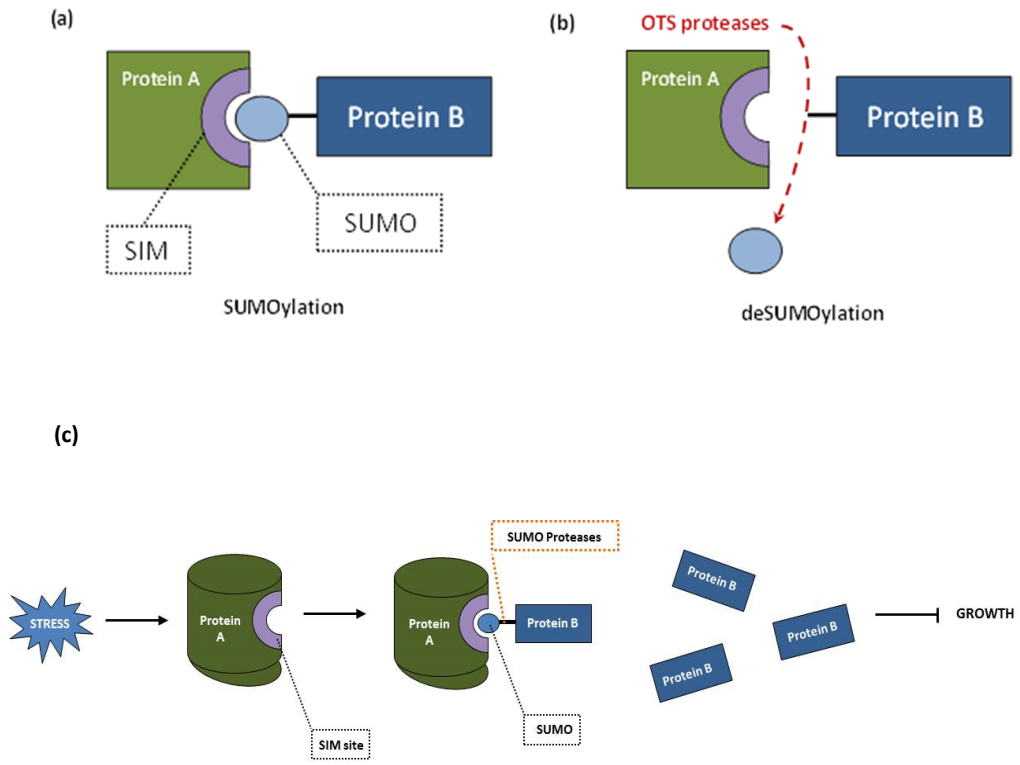


Fig. 1.2: Schematics depicting the SUMOylation pathway in *Arabidopsis thaliana*. SUMOylation is a post-translational modification response involving SUMO-SIM interactions (a). E3 SUMO ligases attach the SUMO (**S**mall **U**biquitin-like **Mo**difier Protein) covalently to the target protein (B). SUMO then forms a non-covalent interaction with a SIM (SUMO Interacting Motif) site (on protein A) during SUMOylation (a). These proteins are then targeted for ubiquitination. SUMO proteases such as OTS1 (Overly Tolerant to Salt 1), remove the SUMO from the target protein (B) during deSUMOylation (b). DeSUMOylation is an important response to environmental challenges such as drought stress. This causes an accumulation of protein (B) that inhibits growth (c).

site enables E3 SUMO ligases (such as *SIZ1*) to then attach SUMO via a covalent bond to target proteins in a similar way to the process of ubiquitination (Park *et al*., 2011). SUMO forms a non-covalent interaction with a SIM (SUMO Interacting Motif) site present on another target protein (Fig. 1.2). In essence, SUMOylation is a lock and key

mechanism causing a SUMO-substrate interaction. According to Ishida *et al* (2012), SUMO proteins are found in all eukaryotes including plants and are around 100 amino acids (12 kDa) in size. SUMO plays an important role in the mediation of interactions and recruiting components of protein complexes (Conti *et al*., 2008). It has only been in recent years though, that SUMO has emerged as a very influential key class of protein modifier (Conti *et al*., 2008).

SUMO proteases such as *OTS1* and *OTS2* (Overly Tolerant to Salt 1 and 2) remove the SUMO from the target protein during deSUMOylation (**Fig. 1.2**). *OTS1* and *OTS2* are disabled in response to environmental stresses, such as abiotic stress (Yates *et al*., 2016). Resulting in the accumulation of their SUMOylated proteins (Conti *et al*., 2008). Unlike that of ubiquitin, SUMO proteases not only affect protein abundance (by blocking degradative ubiquitination) but can modify the function of the target proteins (Johnson, 2004). The accumulation of target proteins then prevents growth. During SUMOylation, E3 SUMO ligases cause proteins to be targeted by the 26S proteasome for ubiquitination degradation (Yates *et al*., 2016). Hence, SUMOylation acts as a rapid response to modify protein behaviour under stressful environmental conditions (Yates *et al*., 2016).

1.3 LATERAL ROOT DEVELOPMENT

1.3.1 Primary root cellular organisation

Upon germination the PR emerges from the seed and grows downwards with gravity. The longitudinal organisation within the root is established by a series of development zones. This is achieved by multiple cellular divisions and subsequent cell elongation within three unique zones of growth; meristem, elongation and maturation (Scheres

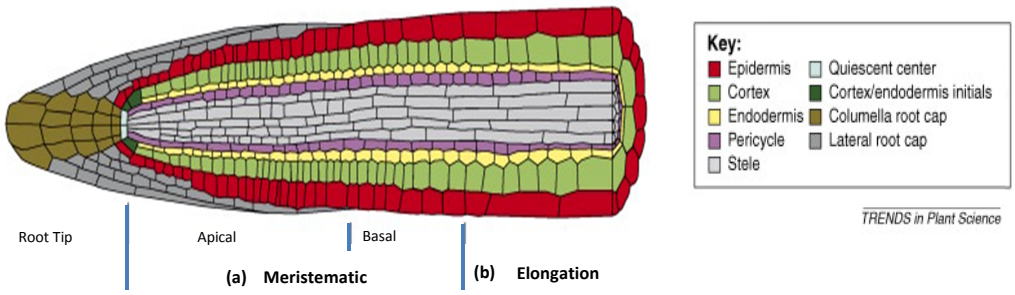


Fig. 1.3: Schematic overview of the various layers that make up the morphology of the PR in *Arabidopsis thaliana*. The PR has distinctive zones of growth – meristematic (apical and basal) (a), elongation (b) and following on from this is the differential zone. Radially, the PR is made up of different root tissues. The apical meristem comprises of the lateral and columella root caps (at the root tip), cortex/endodermal initials and the quiescent center (make up the stem cell niche). From the meristematic zone through to the hypocotyl (root-shoot junction), the PR radially consists of the epidermis, cortex, endodermis, pericycle through to the stele (the vasculature) (modified from by Péret *et al*., 2009).

et al., 2002 and reviewed in Verstraeten *et al*., 2014). These zones have been well defined and it all begins in the apical meristem at the root tip (Fig. 1.3) (reviewed in Péret *et al*., 2009; Scheres *et al*., 2002; Smith and De Smet, 2012; Verbelen *et al*., 2006 and reviewed in Verstraeten *et al*., 2014). Surrounding the tip of the root apical meristem is the RC (Fig. 1.3). This protective layer, made up of lateral and columella root caps, is forever being replaced as it relentlessly pushes downwards into the soil (Eapen *et al*., 2003 and Smith and De Smet, 2012). Just after the RC, within the centre of the root apical meristem is the stem cell niche. This is comprised of the quiescent center (QC) surrounded by initials (vascular, cortex/endodermal, epidermal/lateral root cap and columella initials) (reviewed in Clark *et al*., 2014). The QC is composed of

four mitotically inactive central cells that promotes the neighbouring cells to continuously divide (Smith and De Smet, 2012).

It is known that these initials give rise to the radial patterning of the concentric cell layers in the presence of an auxin gradient (Clark *et al*., 2014; Scheres *et al*., 2002 and reviewed in Verstraeten *et al*., 2014). The cell layers that make up the radial organisation of the PR are comprised of the epidermis, cortex, endodermis, pericycle and the stele (the vasculature) (**Fig. 1.3**) (reviewed in Péret *et al*., 2009). These cell layers still need to become specialized and mature.

The first developmental zone that is displaced from the root apical meristem (RAM) due to continuous cellular division is the basal meristem (De Smet *et al*., 2007). Cellular division slows down and cells expand within this zone. Distinct epidermal cells demarks the transition from the meristematic to elongation zones (Smith and De Smet, 2012). Transitioning from the late elongation zone, the appearance of root hairs establishes the maturation zone from where LRs originate (De Smet *et al*., 2007).

1.3.2 Lateral root initiation and formation

The initiation of the first LR occurs at a fixed distance from the RT (reviewed in Verstraeten *et al*., 2014). The initial cellular divisions that give rise to the emerged LR differ significantly from that of PR growth (Scheres *et al*., 2002 and reviewed in Péret *et al*., 2009). Over the years, the eight developmental stages that are involved in the LR formation have been well defined (Malamy and Benfey, 1997; Casimiro *et al*., 2003; reviewed in Péret *et al*., 2009 and reviewed in Lavenus *et al*., 2013) (**Fig. 1.4**).

It all begins though within the pericycle layer of the PR and is dependent on *PIN3*, *GATA23* and *ACR4* (Chen *et al*., 2015). All of which are hallmarks of LR initiation. The

stele comprises of the pericycle layer in addition to the protoxylem, phloem, xylem, their relative poles and cambium. A subset of pericycle cells adjacent to the xylem pole undergoes a cyclic pre-initiation event (reviewed in Péret *et al*., 2009 and reviewed in Lavenus *et al*., 2013). This substantiates the heterogeneous nature of the pericycle layer in LR initiation (Parizot *et al*., 2008). The xylem pole pericycle cells are then primed at pre-branch sites in the basal meristem to become founder cells (FC) (De Smet *et al*., 2007; reviewed in Lavenus *et al*., 2013 and reviewed in Péret *et al*., 2009).

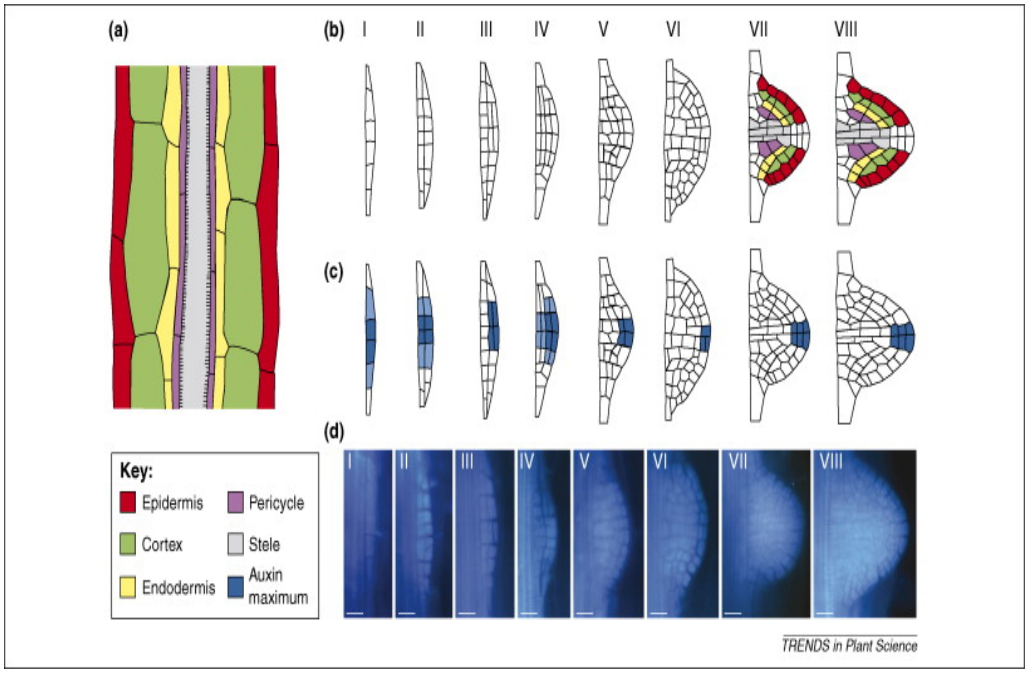


Fig. 1.4: Schematic showing the morphological changes during LR development in the model organism *Arabidopsis thaliana*. LRP originate from the pericycle founder cells within the PR. Various layers make up the morphology of the PR (a). LRP development goes through a series of eight stages (roman numerals) (b) and the auxin signalling maxima seen using the *DR5::GUS* reporter line (gradient in blue) (c). The LR animation of development was derived from aniline blue stained roots (d) (scale bars represent 20 µm) (reproduced from Péret *et al*., 2009).

The selection of pre-branch sites is aided by periods of oscillating gene expression, essentially, an internal biological clock (Moreno-Risueño *et al*., 2010). This timed oscillation event will ultimately determine the exact structure of the RSA. According to Moreno-Risueño *et al* (2010), this remarkable feature is able to compensate for variations in environmental conditions. Priming is a complex interplay between auxin transport, auxin signalling and the biological clock. However, not all primed xylem pole pericycle cells go on to trigger LR initiation (reviewed in Lavenus *et al*., 2013).

Under high auxin levels, the *PIN3*-dependent auxin reflux is mediated leading to the first anticlinal division (Chen *et al*., 2015). This gives rise to the very first anatomical phase in the formation of the lateral root primordium (LRP) (reviewed in Péret *et al*., 2009 and Smith and De Smet, 2012). FCs then go through a series of anticlinal and asymmetrical divisions that result in the LRP (reviewed in Lavenus *et al*., 2013). A single layer of cells is the very first key step in the development of the LR (Stage I) (**Fig. 1.4**). The cells then divide periclinally forming an inner and outer structure (Stage II) (**Fig. 1.4**) (reviewed in Péret *et al*., 2009). In essence, the LRP forms a dome shaped structure that occurs after many rounds of anticlinal and periclinal divisions (Stages III – VII) (**Fig. 1.4**). This dome shaped structure enables the LRP to transverse the endodermal layer (Vermeer *et al*., 2014 and Vermeer and Geldner, 2015).

1.3.3 Lateral root emergence

In order to emerge from the PR the LRP must pass through three distinct layers, the endodermis, cortex and epidermis. This process is highly regulated by a shoot to root auxin flow (reviewed in Lavenus *et al*., 2013). The developing LRP, with the aid of auxin, induces the *SHY2/IAA3* signalling cascade within the endodermis (Swarup *et al*., 2008). At the same time, the *SLR/IAA14-ARF7-ARF19* signalling cascade in the

cortex/epidermis induces *LAX3* an auxin influx carrier in addition to *PIN3* (Swarup *et al*., 2008). This thereby creates an auxin influx, positive feedback loop in the cells near the LRP. The LRP is then able to protrude with the aid of cell wall remodelling enzymes, induced by auxin (*LAX3*-dependent pathway) to promote cell separation (Lee *et al*., 2015).

As the LRP penetrates the endodermis, it acquires the same tissues that make up the parental root meristem (reviewed in Lavenus *et al*., 2013). Changes in water distribution due to turgor pressure facilitate the final emergence of the LRP (Swarup *et al*., 2008). Protrusion through the final layers (cortex and epidermis) leads to the activation of the meristem within the emerged LRP (reviewed in Péret *et al*., 2009). It is this activation of the meristem that defines the newly emerged LRP as a LR (Malamy, 2005).

1.4 AUXIN RESPONSE CONTROLS LATERAL ROOT DEVELOPMENT

1.4.1 Phytohormone Auxin

The phytohormone auxin in the endogenous form, indole-3-acetic acid (IAA) is present in all parts of the plant in varying concentrations. Auxin mediates a variety of physiological processes including the regulation of LR development (reviewed in Lavenus *et al*., 2013). Auxin is mainly synthesised at the shoot where it is then transported to other parts of the plant (Tian and Reed, 1999). Transport of auxin via the shoot occurs in the phloem and proceeds towards the RT. However, auxin synthesis also occurs at the root apex where it is necessary for the maintenance of local auxin gradients (Xuan *et al*., 2010). Both sites of auxin biosynthesis contribute to the pools of auxin available for the polar auxin transport (PAT) (Quint and Gray, 2006).

Auxin distribution via PAT is coordinated at the cellular level through influx and efflux carriers (Friml *et al*., 2003). Influx carriers *AUX1/LAX* (Auxin insensitive and like *AUX1*) diffuse auxin into cells via plasma membranes (Swarup *et al*., 2008). Once in the cell, the higher pH deprotonates IAA, that is transported out with the aid of auxin efflux carriers, *PIN3* and *PIN7* (*Pinformed1* and *7*) (reviewed in Lavenus *et al*., 2013). Auxin modulates changes in gene expression in order to elicit the many developmental processes involved in LR development.

1.4.2 Auxin signalling pathway

It has been well documented that auxin signalling plays a significant part in the very earliest stage of LR initiation by priming xylem pole pericycle cells (reviewed in Péret *et al*., 2009; reviewed in Lavenus *et al*., 2013 and Van Norman *et al*., 2013). An accumulation of auxin within these cells activates an auxin signalling cascade. It all begins with the induction of early auxin-responsive genes, Aux/IAA repressors. This triggers the $SCF^{TIR1\text{-}AFB1}$ complex (skp, cullin, F-box containing complex with the transport inhibitor response 1).

The F-box protein TIR1 (Transport Inhibitor Response1) and related proteins AFB1-6 (Auxin Signalling F-Box Protein 1 to 6) recognise auxin which essential is the 'molecular glue' holding the complex together with an Aux/IAA protein (Okushima *et al*., 2005). This complex has a high affinity for the auxin-responsive genes (Okushima *et* al., 2005 and Guilfoyle, 2007). When bound, the $SCF^{TIR1\text{-}AFB1}$ complex undergoes ubiquitination and subsequent degradation by the 26S proteasome (Guilfoyle, 2007).

It is this auxin mediated degradation of co-repressors (Aux/IAA) that enables activator auxin response factors (ARFs) to initiate gene expression (Guilfoyle, 2007). In

Arabidopsis, *Aux/IAA* genes encode 29 short lived nuclear proteins (Tiwari *et al*., 2003). These Aux/IAA proteins contain four highly conserved domains of which domain one is required to inactivate ARFs (Tiwari *et al*., 2003). ARFs activate expression by binding to the auxin response elements (AuxREs) in the promoter region of early auxin-responsive genes (Okushima *et* al., 2005). Complex interplay between the Aux/IAA with the specific ARF leads to the formation of different signalling modules (reviewed in Lavenus *et al*., 2013) (**Fig. 1.5**). Gene expression patterns result from auxin signalling modules in relation with auxin fluxes throughout the plant. Hence, along with auxin, ARFs regulate every stage of LR development.

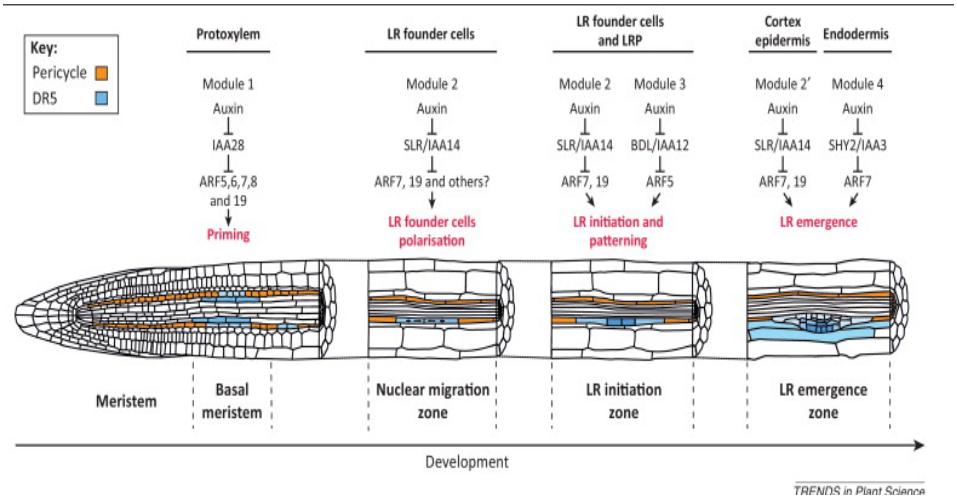


Fig. 1.5: Schematic diagram depicting developmental stages in LR formation. Modules displaying the different developmental processes (displayed in red) involved in the formation of LRs in *Arabidopsis thaliana*. Using modules, each stage focuses on the different auxin signalling pathways involved. Priming is the first key step in LR development followed by LR founder cell polarisation, LR initiation and LR emergence. The pericycle (shown in orange) clearly shows where these developmental stages are occurring. Using a *DR5* based reporter, the auxin maximum (gradient in blue) is revealed within the pericycle as the LR develops (reproduced from Lavenus *et al*., 2013).

1.5 GENES INVOLVED IN LR FORMATION

1.5.1 *AUXIN RESPONSE FACTORS (ARFs)*

In *Arabidopsis,* there are 23 ARF gene family members of which five are transcriptional activators of early auxin-responsive genes (Okushima *et al*., 2007 and Tiwari *et al*., 2003). ARFs bind to a specific conserved TGTCTC motif, or a variant of this, known as AuxRE to regulate gene expression (Tiwari *et al*., 2003). Most ARF proteins contain a DNA binding domain at the N-terminus, a middle region, a carboxy-terminal dimerization III and IV (CTD) (Tiwari *et al*., 2003). It is this middle region in the ARF domains that confers transcriptional activation or repression (Tiwari *et al*., 2003). At low auxin concentrations, Aux/IAA repressors recruit co-repressor TOPLESS (TPL) which binds to domain I (Tiwari *et al*., 2003). Hence, the inactivation of ARF protein and ability to activate auxin responsive genes.

The five activator ARFs consist of *ARF5/MONOPTEROS* (MP), *ARF6*, *ARF7*, *ARF8* and *ARF19*. One of these five activating ARFs, *ARF5/MP*, exhibits a striking phenotype in the *arf5/mp* loss of function mutant. This mutant is defective in patterning during embryogenesis (Berleth and Jurgens, 1993). This affects the developing root structure by preventing the formation of a PR and LRs. Instead, *ARF5/MP* has a basal peg in the place of a root (Berleth and Jurgens, 1993). *ARF6* and *ARF8* predominately function in the shoot apical meristem (SAM) to control stamen elongation and flower maturation (Tian *et al*., 2004). *ARF6* and *ARF8* have very similar DNA-binding and dimerization domains and normally act partially redundantly (Tian *et al*., 2004). Essentially both of these activating ARFs are essential for *Arabidopsis* reproduction. However, *ARF7* and *ARF19* are known to be involved in LR development (Goh *et al*., 2012).

1.5.2 Role of *ARF7* and *ARF19* in LR development

ARF7 and *ARF19* have been identified as key components of LR initiation (**Fig. 1.5**) (reviewed in Péret *et al*., 2009). The double knockout mutant *arf7, arf19* displays a severe reduction in the number of LRs that is not seen in the single mutants alone (Okushima *et al*., 2007). The *arf7* loss of function mutant does have a slightly reduced number of LRs when compared to both *arf19* and WT though. This data supported the fact that *ARF7* and *ARF19* are both important at the very earliest stage of LR formation (Okushima et al., 2005; Okushima et al., 2007 and reviewed in Lavenus *et al*., 2013).

In fact, *ARF7* and *ARF19* not only play a role very early on but throughout the whole process of LR development. It appears that these two ARFs have overlapping functions. During the first few steps in LR formation, *ARF7* works with *ARF19* (reviewed in Lavenus *et al*., 2013). It is known that both *ARF7* and *ARF19* are closely related and are functionally redundant without the other (Okushima *et al*., 2005). Although, *ARF7* is upstream of *ARF19* and therefore regulates more genes suggesting that it is the dominant player (Okushima *et al*., 2005). In fact, *ARF7* was identified as being positioned at the top of a gene regulatory network (GRN) (Lavenus *et al*., 2015). Hence, there are multiple genes that are regulated by *ARF7* alone.

1.6 PROJECT AIMS

The PhD project aims to discover the molecular and cellular mechanisms controlling the newly described root adaptive response termed lateral root (LR) hydropatterning.

My project objectives address the following key points:

1. Determine which components of the auxin response machinery that control LR formations, are also important for LR hydropatterning.
2. Understand how the activities of key auxin response components are regulated to control LR hydropatterning.
3. Verify in which root tissue(s) auxin response components function to control LR hydropatterning.
4. Confirm what are the downstream targets of the auxin response machinery that mediate LR hydropatterning.

CHAPTER 2: GENERAL MATERIAL AND METHODS

CHAPTER 2: GENERAL MATERIAL AND METHODS

2.1 PLANT CULTIVATION

2.1.1 *Arabidopsis thaliana* material

Arabidopsis thaliana accession, Columbia (Col) WT, was used as the control for many loss of function mutant alleles. The following mutant lines: *arf7-1*, *arf8-2*, *arf19-1*, *nph4-1, arf7-1*; *arf19-1* (double knockout), *35S::ARF7* in *arf7-1; arf19-1* and *twd1-3* were all provided from within the Prof. Malcolm Bennett group (The University of Nottingham). The *arf6-1* mutant line was supplied from the Nottingham Arabidopsis Stock Centre. The *arf19* mutant alleles: *arf19-3*, *arf19-a* and *arf19-b* were all kindly donated by Dr Rahul Bhosale (The University of Nottingham).

Collaborator, Prof. Ari Sadanandom (The University of Durham) supplied the *ots1; ots2* double knockout line. The LBD mutant lines: *lbd16-1*, *lbd18-1*, *lbd29-1*, *lbd33-1* were kindly provided from Dr Tatsuaki Goh (NAIST, Kobe University, Japan). The *lbd16-2* mutant line was donated by Dr Christa Testerink (The University of Amsterdam). Mutant lines *shy2-31*, *shy2-2* and the WT control, Landsberg *erecta* (L*er*-0) were supplied from Dr U. Voß (The University of Nottingham). *pARF7::ARF7:GFP* in *arf7-1* SUMOylated (WT) and non-SUMOylated (4xKR) lines were kindly provided by Dr Beatriz Orosa-Puente (The University of Durham).

Line pCASP1::*shy2-2* Col-0 and *shy2-101* were supplied by Dr Joop Vermeer (The University of Zurich). The mutant line *iaa28-1* (gain of function allele) was kindly supplied by Dr Bert De Rybel (Ghent University) and the *iaa28-ko* (loss of function allele) (Salk_129988C) was provided by the Nottingham Arabidopsis Stock Centre. The *Arabidopsis thaliana* accession, Wassilewskija (Ws) WT was kindly donated by Dr Kamal Swarup (The University of Nottingham).

2.1.2 Plasmid material

The pENTRY clone, used to generate a number of constructs: pDONR^{201} *ARF7*, was kindly supplied by Dr Tatsuaki Goh (NAIST, Kobe University, Japan). The *pARF7::ARF7:GFP* SUMOylated (WT) and non-SUMOylated (4xKR) constructs were kindly donated from Prof. Ari Sadanandom (The University of Durham). These were used as the DNA template to create the *pARF7::ARF7* (first intron) SUMOylated (WT) and non-SUMOylated (4KR) constructs (**Chapter 4**). The Greengate pENTRY vectors (**Table 2.1**) were supplied by Lampropoulos *et al* (2013) via Addgene. These were used to generate *ARF7* promoter specific constructs.

Table 2.1: Greengate empty vectors and modules. These vectors were supplied by Lampropoulos *et al* (2013) via Addgene. Promoter and CDS insert modules were generated using pGGA000 and pGGC000 empty vectors. These pENTRY constructs (**Appendix A.2.1**), along with the other insert modules, made up various destination constructs (**Appendix A.2.2**).

	Name	Type
pENTRY	pGGA000	Plant Promoter (Empty vector)
pENTRY	pGGC000	CDS (Empty vector)
pENTRY	pGGZ001	Destination backbone
pENTRY	pGGB003	B dummy (N-tag)
pENTRY	pGGD002	D dummy (C-tag)
pENTRY	pGGE001	RBCS terminator
pENTRY	pGGF008	Basta resistance

Destination construct, *pARF7::gARF7:Ven* was kindly provided by Jekaterina Truskina (The University of Nottingham/The University of Lyon) for transformational dipping into Col-0. Dr Joop Vermeer (The University of Zurich) supplied constructs *pCASP1::shy2-2* and *pSHY2::NLS:3xVen* for gene expression studies. The Greengate promoter module – *pXPP* (formally known as *pGRP*) was also provided by Dr Joop Vermeer. The following GATEWAY pENTRY constructs: pENTRY gene mock (Box 2) and ocsT terminator (plus stop codon) (Box 3) were kindly supplied by Jekaterina Truskina (The University of Nottingham/The University of Lyon) to generate the *pARF7::ARF7* (first intron) SUMOylated (WT) and non-SUMOylated (4xKR) constructs (**Chapter 4**).

2.1.3 General growth conditions for *Arabidopsis thaliana*

Seed lines were surface sterilized using 700 µl 50 % (v/v) bleach for 7 mins, followed by 700 µl of sterile water containing 0.1 % Triton X-100. This was followed by another 700 µl of sterile water containing 0.1 % Triton X-100 step. Five additional 1000 µl sterile water washes were used. The final wash left the seed lines immersed in 500 µl of sterile water. The seed lines were then stratified for 24 h at 4 °C in the dark. Following this, the seed lines were plated out onto the desired media containing ½ MS (2.2 g L^{-1}) (Murashige–Skoog media, Sigma), 0.5 g L^{-1} MES, 1 % sucrose and 1 % Bacto agar at pH 5.7.

All plates were sealed using thin micropore tape and returned to 4 °C (in the dark) for a further 24 h. Plates were then transferred to the required growth chamber and grown vertically for a minimum of 10 d (depending on the experimental design) under continuous temperature 22 °C and light (150 µmol m^{-2} s^{-1}) depending on the experimental design. The length of growth increased from 10 d to 13 d for the characterization of mutant alleles that displayed decreased LR numbers. Growing

these lines for longer ensured that the LR number was above a cutoff point of six LRs per seedling. Seedlings were scored based on their developmental growth prior to imaging the agar plates.

2.1.4 *Arabidopsis* crosses

In order to perform a cross between the male (♂) and female (♀) plant, the selection of flowers and buds was crucial. The flowers on the male plant needed to have visible pollen and prior to crossing, the petals were removed. It was desirable that no white petals were showing in buds on the selected female plant. Too much visible petal indicated that the carpel had already been pollenated.

The female plant was prepared using a dissecting microscope to remove extra budding flowers, leaves, petals, sepals and stamen leaving only the carpel remaining. Pollen from the male plant was carefully transferred to the prepared carpel with the aid of forceps. This process was repeated for at least four other prepared carpels upon the female plant.

Upon completion, a label was attached on the stem under the bud on the female plant. It was important to clearly write the cross indicating the female and male plants used e.g. *arf7-1* ♀ x *pLBD16::gLBD16:GFP* ♂ plus the date. The plant was then placed into a plastic sleeve to protect the cross. Crosses were then checked a few days later to ensure that they had worked (elongated carpel). Failed crosses were re-done by selecting a new bud from the flowering male plant.

2.2 PLANT PHENOTYPING ANALYSES

2.2.1 Root clearing assay

Sterilized seedlings were grown for a minimum of 5 d on media containing ½ MS, 0.5 g L^{-1} MES and 1 % agar in a vertical position. Seedlings were transferred to small pre-labeled petri dishes containing acidified methanol (0.24 M HCL in 20 % MeOH) for 15 mins. This solution was replaced with a 7 % NaOH solution containing 60 % EtOH for another 15 mins. Following on from this, the roots were rehydrated in a series of EtOH solutions (40 %, 20 % and 10 %) for 10 mins. The final step left seedlings re-suspended in a 50 % glycerol solution. Seedlings were immediately mounted onto glass microscope slides with 50 % glycerol or stored at 4 °C until needed.

2.2.2 Microscopy and image processing using ImageJ

Images of whole plates were taken using a Canon digital camera prior to root analysis under a dissecting microscope (LR emergence and number). The image data was then uploaded and converted to 8-bit TIFF using ImageJ software. With the aid of a NeuronJ plugin in ImageJ, PR length was measured and exported to an Excel spreadsheet (Microsoft Excel 2013). LR number and LR density (LR number divided by the length of the root) were also inputted into the Excel spreadsheet along with data from other root phenotypical characteristics observed.

2.2.3 Confocal microscopy and image processing using LAS AF Lite

Sterilized seedlings were grown for a minimum of 5 d on media containing ½ MS, 0.5 g L^{-1} MES, 1 % sucrose and 1 % agar in a vertical position (depending on the experimental

design). Seedlings were transferred carefully, to microscope slides. The seedlings were stained with a propidium iodide solution (15 µg ml^{-1}) to visualize the cell walls. A cover slip was placed on top of the seedlings with care to avoid introducing air bubbles. The slide was then inverted and placed onto the confocal microscope. Confocal microscopy was performed using a Leica SP5 confocal laser scanning microscope (Leica Microsystems). Scanning settings were optimized and stored for future analysis. Images were viewed, maximum projection applied (if necessary), snapshot(s) taken and final image(s) exported as a JPEG using the Leica application suite (LAS) AF Lite software.

2.3 MOLECULAR TECHNIQUES

2.3.1 Nucleic acid extraction

2.3.1.1 *Plant genomic DNA extraction*

DNA for genotyping was extracted from plant leaf material. The plant tissue was flash frozen in liquid nitrogen before being ground into fine powder. Immediately, 600 µl of DNA extraction buffer (1 M Tris-HCL, pH 7.5; 4 M NaCl; 0.5 M EDTA and 10 % SDS) was added followed by a brief vortex. The sample was centrifuged at 13,000 rpm for 5 mins. 500 µl of the supernatant was transferred to a freshly labelled Eppendorf tube.

To this, 500 µl of isopropanol was added and mixed by inverting four times. The sample was incubated on ice for 15-20 mins before being centrifuged at 13,000 rpm for 5 mins. The supernatant was then discarded and the pellet washed rapidly with 70 % ethanol and dried overnight. The pellet was re-suspended in 30 µl of RNAse free water and stored at -20 °C until needed.

2.3.1.2 *Total RNA extraction*

A fume hood was cleaned with RNAse prior to working. Seedling root tips were cut 1-2 cm from the RAM and this root tissue pooled into a sterilized pre-labelled Eppendorf tube. The root tissue was flash frozen in liquid nitrogen before being ground into a fine powder. Immediately, 500 µl of Trizol reagent was added followed by a further grinding. The sample was transferred to another pre-labelled Eppendorf tube and an additional 500 µl of Trizol reagent added and vortexed. To this, 200 µl of chloroform was added and vortexed briefly. The sample was then centrifuged at 14,000 rpm for 5 mins.

The initial 500 µl of the supernatant was transferred to a new pre-labelled Eppendorf tube. To this, 250 µl of EtOH was added and mixed by inverting four times. 750 µl of the sample was transferred to a pink RNeasy spin column (Qiagen kit). The RNA was then extracted using an RNeasy plant mini kit (for purification of total RNA, Qiagen). The purified RNA was eluted into 30 µl of RNase free water and the concentration and purity was obtained (**2.3.1.3 *Quality control of RNA and DNA***). Following on from this, the RNA was either synthesized or stored at -20 °C (for short term storage)/-80 °C (for long term storage) until needed.

2.3.1.3 *Quality control of RNA and DNA*

The DNA/RNA concentration and purity was obtained using a Nanodrop™ spectrophotometer (Nanodrop 2000, Thermo Scientific). Upon selecting the required program (for DNA, RNA or protein), the Nanodrop™ was blanked with the same buffer used to elute the DNA/RNA sample. When ready, 1.0 µl of sample material was measured. This resulted in the concentration (ng μl^{-1}) and purity (OD 260/280 nm with

the ratio of ~ 1.8 considered 'pure' for DNA and the ratio of ~ 2.0 accepted as 'pure' for RNA).

2.3.2 Sequence amplification and analysis

2.3.2.1 *Polymerase chain reaction (PCR)*

The gene of interest/sequence was amplified by PCR using a 20 µl reaction mixture, containing 2.0 µl of DNA, 4.0 µl 5 X PCR buffer (Biolabs), 0.8 µl $MgCl_2$, 0.4 µl dNTPs (10 mM), 0.2 µl Taq polymerase, 1.0 µl (stock solution 10 mM) for both the appropriated forward and reverse primers and 10.6 µl of RNase-free water. The components were mixed prior to transferring to the thermocycler. The following PCR program (for standard genotyping) was used: 94 °C for 2 mins, the next 35 cycles of 94 °C for 30 s, annealing at primer specific temperatures for 30 s, elongation at 72 °C for the required length of time (generally 1 min per 1 kb), followed by a final extension at 72 °C for 10 mins and holding at 4 °C. The PCR program was altered for specific DNA polymerases e.g. Q5® High Fidelity. The PCR product was checked by gel electrophoresis (**2.3.2.3 *Gel electrophoresis***) or stored at -20 °C until needed.

2.3.2.2 *PCR purification*

PCR products were purified using a PCR purification kit (GeneJET, Thermo Scientific). All the purifications steps were carried out at room temperature with centrifugations set to >12,000 x g. The purified DNA was eluted into 30 µl of sterile water and stored at -20 °C until needed.

2.3.2.3 *Gel electrophoresis*

The required agarose, typically 1 % (w/v) 0.05 µl was dissolved in 0.5 X TBE buffer (for a 50 ml gel) using a microwave with frequent swirling. After cooling down, 0.01 % ethidium bromide was added to the tepid liquid, mixed and poured into a gel tray with the appropriate gel comb. The gel was allowed to set for approximately 30 mins then placed into the gel tank and covered with 0.5 X TBE up to the maximum level.

The samples were mixed with loading dye (final concentration of 1 X) and 10 µl loaded into the wells. The appropriate voltage was applied (typically 80 V for 1 h). The DNA was then visualized using a UV light box (trans-illuminator) by following the required settings. The gel was either discarded appropriately or the DNA excised.

2.3.2.4 *DNA Gel extraction*

In order to extract DNA from an agarose gel, it was necessary to use a UV light box (trans-illuminator) in the dark room. The DNA was visualized very briefly (to minimise mutagenesis of the DNA) to expose the band of interest. Using a scalpel blade, the DNA was excised from the agarose gel. The excised DNA was then purified using a gel extraction kit (GeneJET, Thermo Scientific). All the purifications steps were carried out at room temperature with centrifugations set to >12,000 x g. The purified DNA was eluted into 30 µl of sterile water and stored at -20 °C until needed.

2.3.2.5 *Restriction enzyme digestion*

Enzymatic digestions were typically performed in 10 µl reactions. The mixture contained; 3.0 or 5.0 µl DNA template (for concentrations over 150 ng μl^{-1}, 3.0 µl was

used in the reaction), 2.5 or 4.5 µl sterile water (varied depending on the DNA concentration), 1.0 µl BSA (X 100), 1.0 µl restriction enzyme buffer and lastly 0.5 µl restriction enzyme (kept in an ice block). The reaction was mixed with gently pipetting and placed at 37 °C for 1 h. Following this the restriction enzyme digestion was checked by gel electrophoresis (**2.3.2.3 *Gel electrophoresis***) or stored at -20 °C until needed.

2.4 CLONING

2.4.1 Gateway recombination

Constructs were generated using the ENTRY Clone: pDONR^{201} ARF7 (donated by Dr Tatsuaki Goh) into GATEWAY binary vectors: pGWB14 (p35S 3xHA) and pGWB17 (p35S 4xMyc) (Invitrogen) (Nakagawa *et al*., 2007).

2.4.1.1 Generating *pENTRY constructs*

The first initial step in generating pENTRY constructs, involved Gateway® BP clonase™ II enzyme mix (Invitrogen). BP Clonase™ II reactions were typically performed in 10 µl reactions. The mixture contained; 1.0-7.0 µl PCR product (15-150 ng µl^{-1}), 1.0 µl donor vector (150 ng µl^{-1}), up to 8.0 µl TE buffer (pH 8.0) and lastly 2.0 µl BP clonase™ II enzyme (kept on an ice block).

The reaction was mixed with gently pipetting and briefly centrifuged before being placed at 25 °C for 1 h. The reaction was then deactivated at 37 °C for 10 mins. Following this the reaction was transformed into competent cells (**2.4.3 Transformation of *E.coli* DH$_5$α cells**) or stored at -20 °C until needed.

2.4.1.2 *Generating destination constructs*

Transferring DNA material from pENTRY to destination constructs, involved Gateway® LR clonase™ II enzyme mix (Invitrogen). LR Clonase™ II reactions were typically performed in 10 µl reactions. The mixture contained; 1.0-7.0 µl ENTRY vector (50-150 ng μl^{-1}), 1.0 µl destination vector (150 ng μl^{-1}), up to 8.0 µl TE buffer (pH 8.0) and lastly 2.0 µl LR clonase™ II enzyme (kept on an ice block). The reaction was mixed with gently pipetting and briefly centrifuged before being placed at 25 °C for 1 h. The reaction was then deactivated at 37 °C for 10 mins. Following this the reaction was transformed into competent cells (**2.4.3 Transformation of *E.coli* $DH_5\alpha$ cells**) or stored at -20 °C until needed.

2.4.2 Greengate cloning system

The Greengate cloning system was based on the Golden Gate principle. Various constructs were generated using Greengate-compatible vectors (**Appendix A.2**). This was achieved by following a protocol designed by Lampropoulos *et al.,* (2013).

2.4.2.1 *Greengate pENTRY recombination*

Promoter and CDS ENTRY vectors were constructed into reciprocated backbone modules. For promoter ENTRY vectors this was GGA0001 and GGC001 for the CDS.

In the first instance, a BsaI-HF restriction enzyme digestion was typically performed in a 50 µl reaction. The mixture contained; x µl PCR fragment (about 100 ng of gel purified), x µl sterile water (varied depending on reaction, up to 50 µl), x µl backbone module vector (ENTRY) (about 100 ng), 5.0 µl restriction enzyme CutSmart buffer and

lastly 1.0 µl BsaI-HF restriction enzyme. The reaction was mixed with gently pipetting and placed at 37 °C for 1 h. Following this the restriction enzyme digestion was deactivated at 85 °C for 10 mins.

The restriction enzyme digestion was purified using a PCR cleanup kit (**2.3.2.2 *PCR purification***) and eluted in 25 µl of RNAse free water. Following this the purified reaction was ligated with T4 DNA ligase (3 u μl^{-1}) (Promega). The mixture contained; 25 µl of the purified reaction, 3.0 µl T4 DNA ligase buffer, 1.0 µl sterile water and lastly 1.0 µl T4 DNA ligase. The reaction was mixed with gently pipetting and placed at room temperature for 1 h. This was followed by deactivated at 70 °C for 10 mins.

The final step in generating ENTRY vectors was transformation. 10 µl of ligation was transformed into $DH_5\alpha$ chemical competent cells (**2.4.4.1: *Chemical competent transformation***).

2.4.2.2 *Greengate Destination recombination*

The destination construct was generated by PCR using a 15 µl reaction mixture, containing 1.5 µl of each Greengate pENTRY module (100 ng μl^{-1}), 1.0 µl destination vector (empty vector – pGGZ001), 1.5 µl CutSmart buffer, 1.5 µl ATP (10 mM), 1.0 µl T4 DNA ligase (30 u μl^{-1}) and 1.0 µl BsaI-HF enzyme. The components were mixed prior to transferring to the thermocycler. The PCR program used was: 37 °C for 2 mins, 16 °C for 2 mins (30 cycles). This was followed by: 50 °C for 5 mins, 80 °C for 5 mins and finally, holding at 4 °C.

For more complicated constructs or those that need to be run overnight the following PCR program was used: 37 °C for 5 mins, 16 °C for 5 mins (50 cycles). This was followed by: 50 °C for 5 mins, 80 °C for 5 mins and finally, holding at 4 °C. The final step in

generating destination constructs was transformation. 6.0 µl of the PCR reaction was transformed into $DH_5\alpha$ chemical competent cells (**2.4.4.1: *Chemical competent transformation***).

2.4.3 Transformation of *E.coli* $DH_5\alpha$ cells

2.4.3.1 *Chemical competent transformation*

Competent $DH_5\alpha$ cells were allowed to thaw on ice for 10 mins. To these cells, 1.0-2.0 µl reaction mix (from LR Clonase II, DNA fragment or plasmid) was added and left on ice for a further 20 mins. The reaction was then transferred to a chilled 1.5 ml Eppendorf and immediately heat shocked at 42 °C for 45 s.

Following this, the reaction was put back onto ice for 2 mins. 450 µl of pre-warmed Luria-Bertani (LB) was then added to the reaction. The reaction was incubated in a 37 °C shaker for 1 h. 10 µl and 100 µl aliquots from the reaction were then plated out onto LB agar plates containing the required antibiotic for the plasmid construct (e.g. Ampicillin 50 µg mL^{-1}). The plates were transferred to a 37 °C incubator for 24 h.

2.4.3.2 *Electro competent transformation*

Competent $DH_5\alpha$ cells were allowed to thaw on ice for 10 mins. To these cells, 1.0-2.0 µl reaction mix (from LR Clonase II, DNA fragment or plasmid) was added and left on ice for a further 10 mins. The cell/DNA mix was carefully transferred to a chilled electroporation cuvette and gently tapped to remove air bubbles. The cuvette was then placed into the electroporator and pulsed (Bio-Rad GenePulser electroporator).

Immediately, 1000 µl of RT Luria-Bertani (LB) was added before pipetting into a 5 ml sterile universal. The reaction was then incubated in a 37 °C shaker for 1 h. 10 µl and 100 µl aliquots from the reaction were then plated out onto LB agar plates containing the required antibiotic for the plasmid construct (e.g. Spectinomycin 50 µg mL^{-1}). The plates were transferred to a 37 °C incubator for 24 h.

2.4.4 Bacterial colony screening

A select number of colonies from the plates were checked by PCR (**2.3.2.1 *Polymerase chain reaction***) to ensure they had the correct insert. In some cases, it was also necessary to perform a restriction enzyme digest (**2.3.2.5 *Restriction enzyme digestion***) for further clarification. Liquid cultures of positive colonies were incubated in a 37 °C shaker for 24 h.

2.4.5 Plasmid DNA isolation

A plasmid mini-prep kit (GeneJET, Therma Scientific) was used to isolate highly pure plasmid DNA from the overnight cultures. All the isolation steps were carried out at room temperature with centrifugations set to >12,000 x g. The plasmid DNA was eluted into 30 µl of sterile water and the concentration and purity obtained. Following on from this, the plasmid DNA was either send for sequencing (**2.4.6 DNA sequencing**) or stored at -20 °C until needed.

2.4.6 DNA sequencing

Plasmid DNA, PCR products and primers were prepared for sequencing in accordance with Source Bioscience. 5.0 µl per reaction for both the DNA and primer was needed. For plasmid DNA the concentration needed to be 100 ng μl^{-1} whereas, it was 10 ng μl^{-1} for PCR products. Primers were sent at a concentration of 3.2 pmol μl^{-1}. All tubes were clearly labelled and sent with pre-paid labels upon completion of the on-line form (www.sourcebioscience.com/services/genomics/sanger-sequencing-service/).

2.4.7 Archiving of plasmids and DNA sequence information

Benchling.com software (**https://benchling.com**) was used to assemble, design, view alignments, primer design, perform restriction enzyme digestions, store and share constructs. Constructs could be viewed as a circular or linear map with the added bonus of the sequence with added annotation. Tabs for primer design, restriction enzyme digests, CRISPR and alignments enabled everything to be done in one place.

2.4.8 *Agrobacterium* mediated transformation

2.4.8.1 *Transformation of Agrobacterium tumefaciens*

Competent *Agrobacterium tumefaciens* (GV3101 strain including pSOUP) cells were allowed to thaw on ice for 10 mins. To these cells, 1.0-2.0 µl destination construct was added and left on ice for a further 10 mins. The cell/DNA mix was carefully transferred to a chilled electroporation cuvette and gently tapped to remove air bubbles. The cuvette was then placed into the electroporator and pulsed under the Agro setting (Bio-Rad GenePulser electroporator).

Immediately, 1000 µl of RT Luria-Bertani (LB) was added before pipetting into a 5 ml sterile universal. The reaction was then incubated in a 28 °C shaker for 2-3 h. 10 µl and 100 µl aliquots from the reaction were then plated out onto LB agar plates containing the required antibiotic for the *Agrobacterium* (e.g. Rifampicin 10 µg mL^{-1}) and plasmid construct (e.g. Spectinomycin 50 µg mL^{-1}). The plates were transferred to a 28 °C incubator for 2 d. Following this the *Agrobacterium* transformants were checked via colony PCR (**2.4.4 Bacterial colony screening**).

2.4.8.2 *Floral dipping of Arabidopsis thaliana*

Arabidopsis plants (Col-0 and *arf7-1*) were transformed with *Agrobacterium* transformants (containing the gene of interest), using the floral dipping method (Clough and Bent, 1998).

Once the plants were harvested, seed was surface sterilized and plated out onto media containing ½ MS, 1 % agar and the required antibiotic or herbicide. After 14 d, the antibiotic or herbicide resistant seedlings (T1) were screened by DNA extraction (**2.3.1.1 *Plant genomic DNA extraction***) followed by PCR (**2.3.2.1 *Polymerase chain reaction (PCR)***) to ensure the seedling had the correct insert. Correct seedlings were then transferred to soil.

2.5 EXPRESSION ANALYSIS

2.5.1 First strand cDNA synthesis

The RNA (at a concentration of 100 ng $µl^{-1}$) was initially checked on an agarose gel (**2.3.2.3 *Gel electrophoresis***) to assess the integrity and visualize the 18 s and 28 s rRNA

bands. Following on from this, the SuperScript™ II Reverse transcriptase kit (Invitrogen) was used to synthesize first strand cDNA. The reverse transcription reaction was either then stored at -80 °C until needed or an RT-qPCR setup (**2.5.2 RT-qPCR**).

2.5.2 RT-qPCR

The cDNA (four replicates) was amplified using a LightCycler® 480 instrument (Roche) in a 12 µl reaction mixture, containing 5.0 µl of cDNA template, 6.0 µl 2 X SYBR Green I master mix (Roche), 0.1 µl (stock solution 100 µM) for both the appropriated forward and reverse primers and 0.8 µl of RNase-free water. Specific primer pairs were designed accordingly for real time PCR.

The components were prepared together as a master mix (apart from the cDNA that was added individually) and transferred to specific wells on a plate. The plate was covered with a membrane and centrifuged briefly prior to transfer to the cycler. The following default PCR program (40 cycles) was used: 95 °C for 10 min (first denaturation), 95 °C for 10 s, 60 °C for 30 s (amplification), 95 °C for 1 min, 60 °C for 30 s and 95 °C continuous (dissociation curve).

An internal control was used that showed no changes in *Ct* values, thereby normalizing the gene expression results obtained. Upon completion, the data was analysed with regards to expression fold changes.

2.6 STATISTICAL ANALYSIS

2.6.1 P-value/T-test/ANOVA/FDR correction

Statistical analysis of the data was performed using both a Student's t-test ($P < 0.05$) and ANOVA. The relatively straightforward Student's t-test determined if the means of two data sets (e.g. WT (Col-0) and loss of function mutant (*arf7-1*)) differed significantly from each other in relation to the null hypothesis. This took into account the differences in p-value. Having a smaller p-value ($P \leq 0.05$) indicated that there was strong evidence against that of the null hypothesis, so the null hypothesis could be rejected. Thereby, there was a significant difference between the two data sets. Asterisks were used to indicate a significant difference from that of WT (Col-0) roots based on using the Student *t* test ($P<0.05$). On the other hand, a larger p-value ($P > 0.05$) indicated that the evidence was weak so the null hypothesis could not be rejected.

ANOVA was used when there was more than two data sets to compare. The analysis of variance, one-way ANOVA took into account the total number of observations, means, standard deviations (or standard error) within each data set. Using GenStat, multiple comparisons, Tukey HSD (Honest Significant Difference) test was applied at the 0.05 significance level (95% confidence interval) to each data set. The Tukey HSD test, uses the Tukey-Kramer formula when treatments (i.e. sample groups) have unequal observations (i.e. unbalanced observations). Letters were used to indicate significance levels between all the data sets. Similar letters stated that there were no significant differences observed. Whereas, different letters indicated that there was a significant difference observed between the data sets.

Chapter 3: *ARF7* IS ESSENTIAL FOR LR HYDROPATTERNING

Author list:

Nicola Leftley – Figures 3.1, 3.3, 3.4, 3.5, 3.6, 3.7, 3.8, 3.9, 3.10, 3.11, 3.12, 3.13, 3.14, 3.15, 3.17, 3.18, 3.20 and 3.21

Daniel Von Wangenheim (Contributed data) – Figure 3.2

Rahul Bhosale (Contributed image) – Figure 3.16

Jekaterina Truskina (Contributed data) and Nicola Leftley – Figure 3.19

Chapter 3: *ARF7* IS ESSENTIAL FOR LR HYDROPATTERNING

3.1 INTRODUCTION

The heterogeneous nature of the soil has a marked impact on the RSA of the plant. The soil environment is forever changing resulting in disparities of water availability. Roots need to be able to adapt and tap into these heterogeneous reserves of water and nutrients (Morris *et al*., 2017). By being plastic, roots are able to optimise foraging and respond to the many localised environmental stresses (Osmont *et al*., 2007).

Plants employ a newly discovered adaptive mechanism termed lateral root hydropatterning to position their branches. This root adaptive response comes about from local variations in water availability. This results in LRs forming primarily on the side of the root that is in direct contact with water. With the aid of X-ray microCT imagery, this highly patterned response towards water was visualised *in-situ* (Bao et *al*., 2014 and reviewed in Morris et *al*., 2017). Essentially, the RSA is being shaped by environmental signals due to a water deficit. LR hydropatterning appears to be a highly conserved adaptive response in higher plants as it occurs in monocot and dicot roots (Bao *et al*., 2014). Growing roots vertically on the surface of an agar plate triggers this same adaptive response. The formation of a meniscus results in opposite sides of the root to either be in direct contact with moisture or exposed to air (**Fig. 3.1**) (**G**).

Up until more recently, the differences in spatial asymmetries observed by growing *Arabidopsis thaliana* roots on agar plates had not been explored (Bao *et al*., 2014). The plant hormone auxin is the main instigator in all aspects of plant growth from the shoot to the root. There is a complex interplay with auxin biosynthesis, transport and signalling in the formation of a LR (Overvoorde *et al*., 2010). Polar auxin

transport (PAT) transports IAA via a cell-to-cell manner generating localised auxin gradients in the RT. This results in an auxin signalling cascade occurring prior to the onset of LR initiation (Okushima *et al*., 2007 and Overvoorde *et al*., 2010). Pulses of auxin signalling in the basal meristem, promotes priming of neighbouring protoxylem cells (De Smet *et al*., 2007). A subset of pericycle cells then undergo a cyclic pre-initiation event at pre-branch sites to become founder cells (reviewed in Lavenus *et al*., 2013).

It was suggested by Bao *et al* (2014), that LR hydropatterning may act very early on in the development of a LR, prior to FC specification, via sensing of the local environment at the RT. It was found that higher levels of auxin were detected on the contact side as opposed to the air with the aid of a *pDR5::GUS* reporter (Bao *et al*., 2014). Thereby suggesting that auxin biosynthesis is moisture induced. The asymmetric moisture environment is known to trigger an auxin response gradient across the radius of the root that results in LRP forming predominately on the contact side (Bao *et al*., 2014). This therefore provided a link between the external environmental signals and the activation of LR development. However, the mechanistic basis behind this radial auxin response gradient remains unclear. This chapter investigates the auxin – based molecular mechanism(s) regulating LR hydropatterning and describes a new role for the transcription factor *ARF7*.

3.2 RESULTS

3.2.1 Optimising the LR hydropatterning phenotyping bioassay

An experimental system for studying how roots sense their microenvironment around them has recently been developed (Bao *et al*., 2014). When growing *Arabidopsis thaliana* roots on agar plates, one side of the PR is either in direct

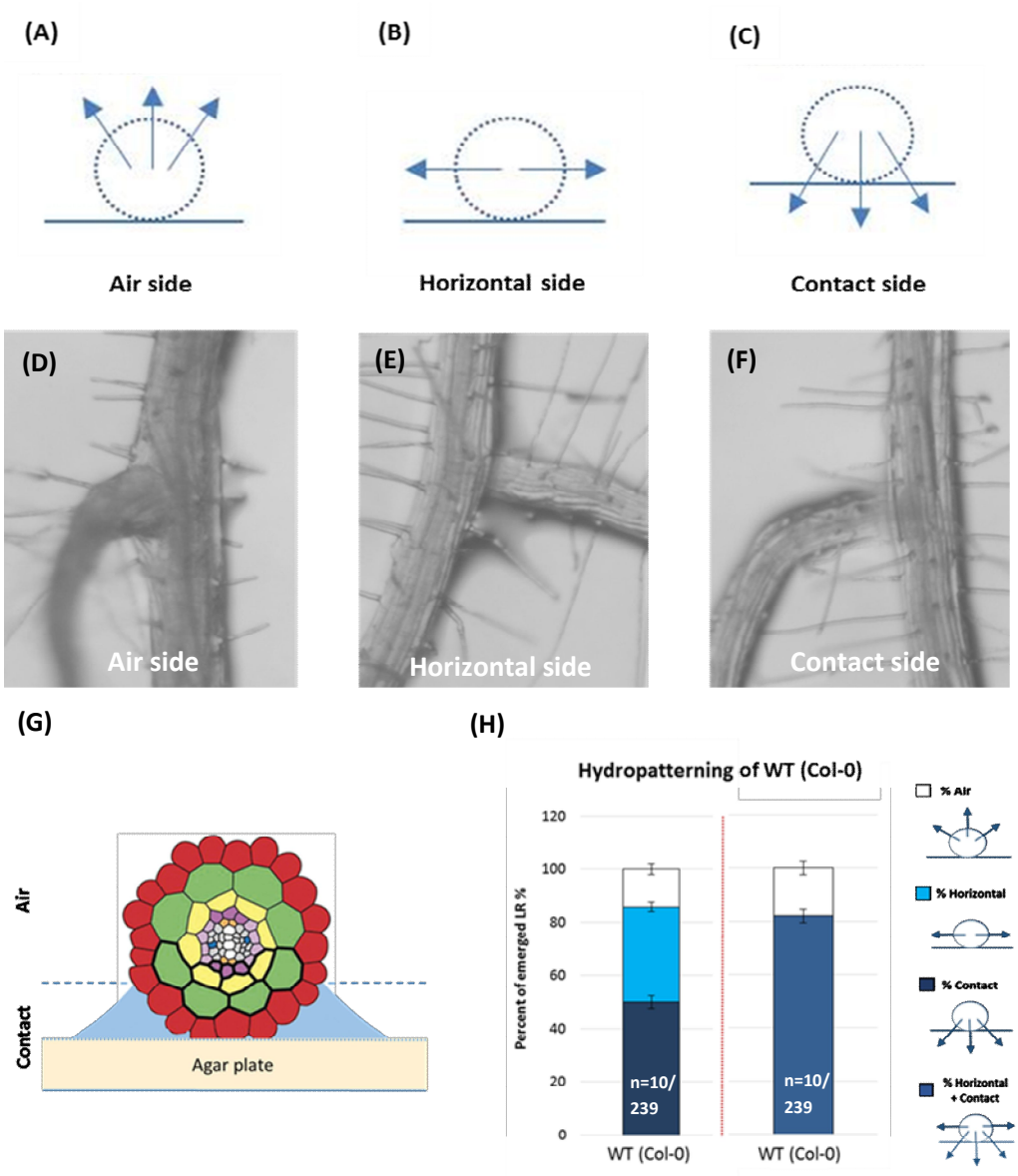


Fig. 3.1: Schematic representation of the hydropatterning phenotyping criteria used to score emerged LRs. The initial screen was adapted from Bao *et al* (2014). Using a dissecting microscope emerged LRs were placed into one of three groups based on their point of emergence, air (seen from above) (A), horizontal (B) and contact (seen from below) (C). LR primordia emerging from the air side (D), horizontal side (E) and contact side (F) of the PR. Schematic cross section of an *Arabidopsis thaliana* root showing the meniscus that forms while growing on an agar plate (G). Graph showing LR emergence patterns in WT (Col-0) roots. The percent of emerged LRs were placed initially into one of the three groups (H) that was later changed to air versus contact (including horizontal) (I). Data shown is mean values ± S. E, (n = number of seedlings/number of lateral roots analysed). Biological replicates (1=5) were performed.

contact with the surface of an agar plate or exposed to air. In relation to this, a meniscus forms alongside the PR creating a moisture environment between the contact and air sides (**Fig. 3.1**) (**G**).

Until recently, the orientation of emerged LRs growing on an agar plate had not been considered (Bao *et al*., 2014). It became apparent, upon closer examination that there was a clear bias for LRs to emerge from the contact side rather than the air side (**Fig. 3.2**). In order to quantify the emergence patterns of LRs, a hydropatterning phenotyping bioassay was devised by Bao *et al* (2014).

LRs were visualised using a dissecting microscope and characterised into one of three different phenotypic groups: contact (**Fig. 3.1**) (**C**), horizontal (**Fig. 3.1**) (**B**) and air side (**Fig. 3.1**) (**A**). The group that the LR was placed into was based on its initial direction of emergence from the PR, when observing the *Arabidopsis thaliana* seedling from above. LRs were characterized as emerging from the contact side if the point of emergence could not be seen from above and was below the root horizon (**Fig. 3.1**) (**F**). These LRs also appeared to be out of focus near the PR (**Fig. 3.1**) (**F**). If the plate was turned over, the point of emergence would then be seen from above. LRs were considered to be within the horizontal side group if the point of emergence could clearly be seen from the PR and LR growth was parallel across the agar (**Fig. 3.1**) (**E**). A meniscus would be seen around the emerged LR that spanned from the PR (**Fig. 3.1**) (**E**).

LRs within the air side group were characterized as growing upwards towards the microscope (**Fig. 3.1**) (**D**). There were also LRs that would emerge just above the horizontal axis. These LRs were considered to be within the air category if the meniscus was not present and there was a greater degree of angle upwards. In relation, there also had to be rings seen underneath the emerged LR, almost like a

tree branch, with a degree of angle upwards. This ensured that emerged LRs on the horizontal axis, that displayed no meniscus, were not characterized incorrectly.

Using this LR hydropatterning phenotyping criteria, wild type (WT) roots were initially analysed. It was observed that WT (Col-0) roots exhibited a striking LR hydropatterning response when grown vertically on an agar plate, consistent with Bao *et al* (2014). There was a clear bias in the positioning of LRs towards moisture. The majority of LRs were observed to originate from the contact (50%) and horizontal side (35%) rather than the air side (15%) (**Fig. 3.1**) (**H**). In essence, 85% of the emerged LRs were in contact with water (**Fig. 3.1**) (**I**).

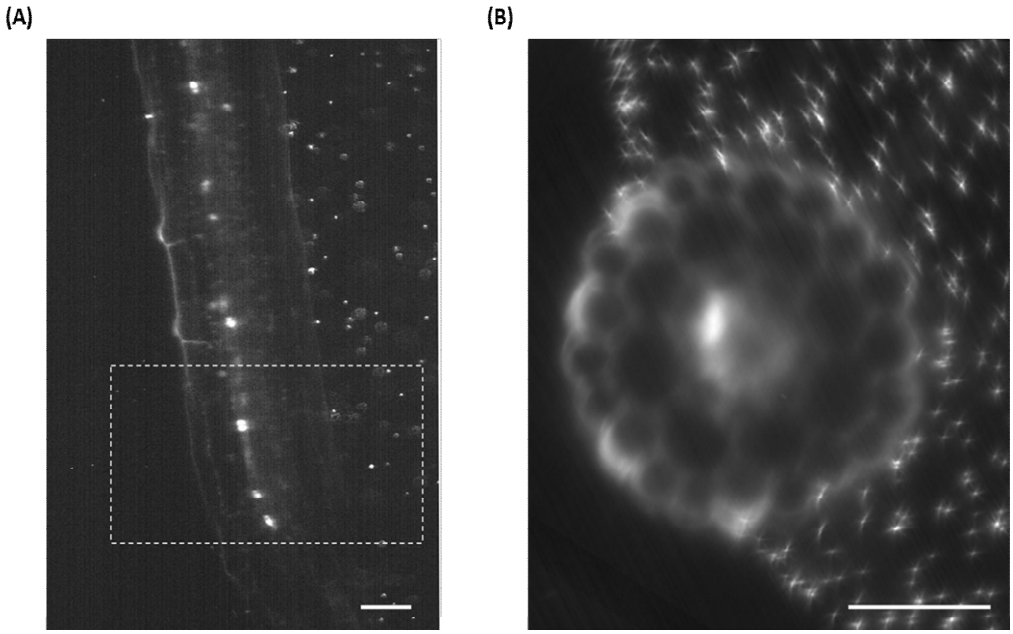


Fig. 3.2: LSFM used to distinguish air and contact sides. The Light sheet fluorescence microscope (LSFM) viewed *pLBD16::gLBD16-GFP Arabidopsis* roots from multiple angles (six views: 0°, 60°, 120°, 180°, 240° and 300° angles). Fluorescence beads (white specks) depict the air side of the root from the contact side (A). Radial cross section of the root using the sum projection along the x-z axis (boxed area in white, A) (B). Scale bar – 50 µm (A and B) (Image reproduced from data generated by Dr Daniel Von Wangenheim, The University of Nottingham).

It appeared to be water rather than direct contact with agar that was influencing the position of future LR branches. Taking this into account, the phenotyping criteria used was simplified to just score LRs as either contact or air. This data suggested that asymmetric distribution of water was an important factor in the development of a LR hydropatterning response.

In order to quantify if an asymmetric distribution of water influenced earliest stage of LR development, a Light Sheet Fluorescence microscope (LSFM) was employed to view roots from multiple angles that expressed the early LRP reporter *pLBD16::gLBD16-GFP* following as LR hydropatterning response (**Fig. 3.2**). Roots were grown normally on an agar plate then overlaid with low melting point agar containing fluorescent beads. This enabled the roots to be completely embedded in agar. Once excised, roots were then placed into a glass capillary tube before being added to the water chamber in the LSFM. Complete 360^{o} rotation enabled the roots to be visualised in all angles. The fluorescent beads depicted the air side and could be clearly seen to distinguish this side from the contact side. LSFM revealed an asymmetric pattern of *pLBD16::gLBD16-GFP* before exiting the elongation zone (**Fig. 3.2**) (**A**), while a radial cross section revealed reporter expression in nuclei of xylem pole pericycle cells oriented towards the contact side of the root (**Fig. 3.2**) (**B**).

3.2.2 Hydropatterning influences very early LR development

It is currently unclear exactly where and when a LR hydropatterning stimulus first influences LR initiation. Priming of new primordium occurs close to the root tip in the basal meristem, selecting at which xylem pole new LRs originate (De Smet *et al*., 2006). As revealed in **Fig. 3.2**, LR hydropatterning is likely to influence which XP new LRP form during this early developmental window. However, the LR hydropatterning

decision could take place much later, for example close to the end of the root elongation zone. To determine if this scenario is correct, we took advantage of the *twisted dwarf1* mutant (*TWD1*). Mutations in *TWD1* lead to a pleiotropic developmental phenotype (Geisler *et al*., 2003; Bouchard *et al*., 2006 and Wang *et al*., 2013), where organ growth throughout the plant is twisted (Fig. 3.3).

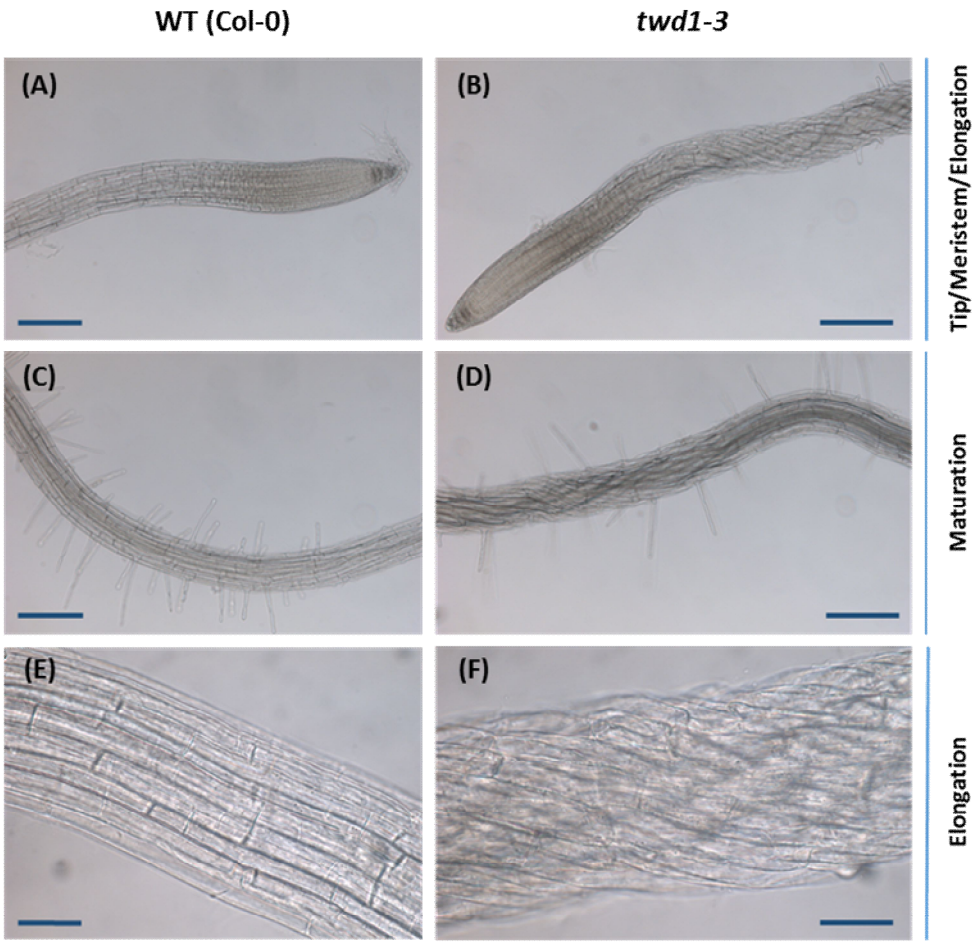


Fig. 3.3: *TWD1* influences epidermal root twisting. Compared to WT (Col-0) *Arabidopsis* roots, the loss of function allele *twd1-3* appeared to twist from the elongation zone towards the shoot apical meristem (SAM). Using a dissecting microscope, differences in the RT, meristem, elongation and maturation zones between WT (Col-0) and *twd1-3* were revealed (A to D). Zoomed in images illustrated the severe twist in the *twd1-3* loss of function allele (F) that was not present in WT (Col-0) (E) roots. Scale bars – 200 µm (A to D) and 50 µm (E and F).

The loss of function mutant *twd1-3* was observed to have a striking root twisting phenotype compared to that of WT (Col-0) roots (Fig. 3.3) (A to F). Epidermal twisting began in the *twd1-3* elongation zone and continued throughout the root (Fig. 3.3) (B, D and F) up to the shoot apical meristem (SAM). This rotation does not just affect the epidermis but all the cell files within the root itself. If LR hydropatterning influences LR positioning early in the elongation zone (i.e. prior to twisting cell files), then LRP emerging would still exhibit a bias. Alternatively, if this decision is made at a later stage, then LR patterning would be random (Fig. 3.4).

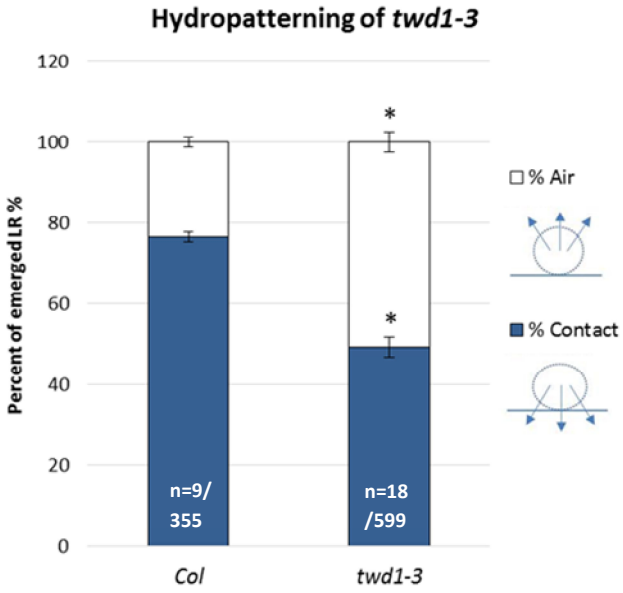


Fig. 3.4: LR Hydropatterning affects XP selection. WT (Col-0) *Arabidopsis* roots exhibit a LR hydropatterning response that was severely disrupted by the *twd1-3* loss of function mutant allele. The percent of LRs emerging towards the air side in the *twd1-3* loss of function mutant allele was over half that seen by WT (Col-0) roots. The distribution of LRs was clearly randomised with 50% emerging on either side. Data shown is mean values ± S. E, (n = number of seedlings/number of LRs analysed). Asterisks indicate a significant difference from that of WT (Col-0) roots based on using a Student *t* test ($P<0.05$). Biological replicates (1=3) were performed.

Interestingly, it was observed that there was a sporadic patterning of LRs from all sides of the PR in the loss of function *twd1-3* mutant (Fig. 3.4).

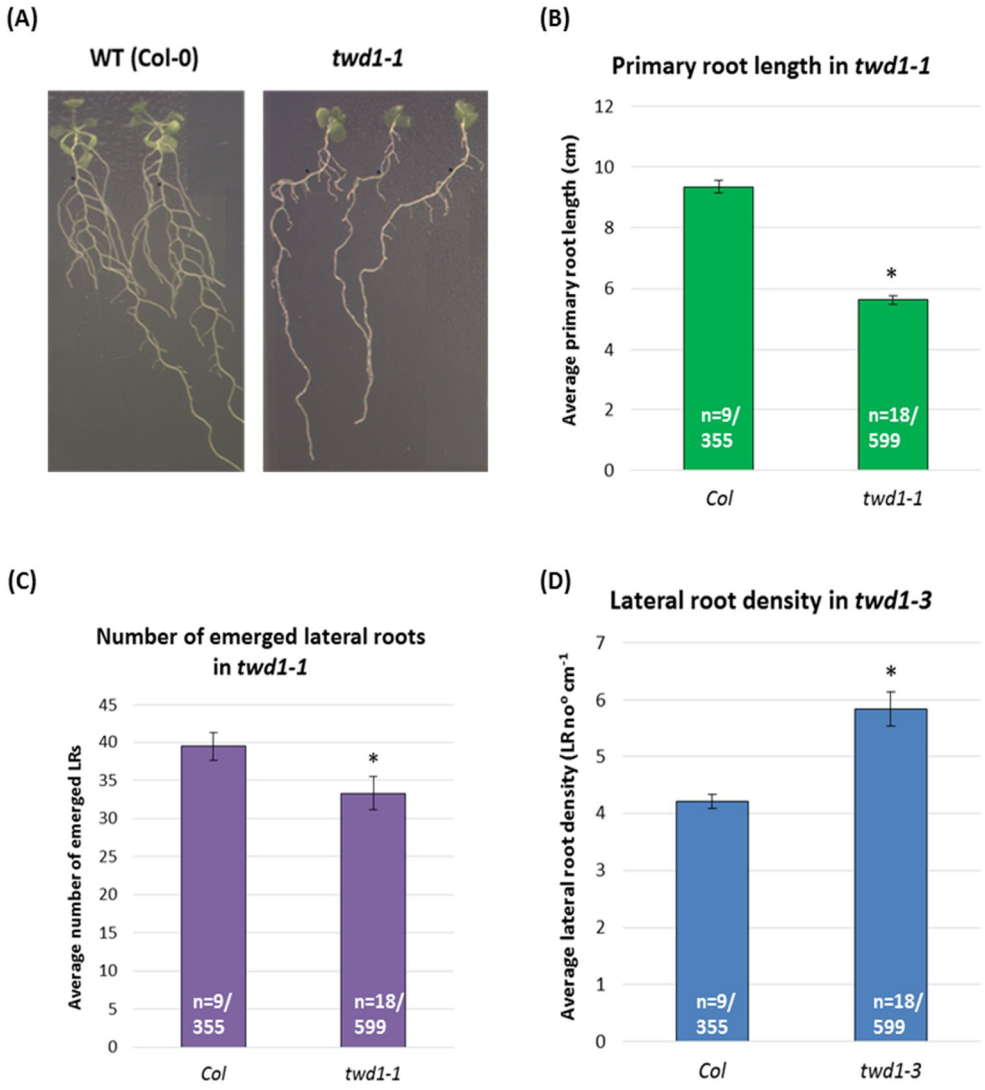


Fig. 3.5: *TWD1* impacts root architecture. Compared to WT (Col-0) *Arabidopsis* roots the *twd1-3* loss of function mutant exhibited a more striking phenotype resulting in shorter twisted LRs (A). Primary root length was severely stunned in *twd1-3* loss of function mutant roots (B). The number of emerged LRs was reduced in *twd1-3* loss of function mutant (C) but the overall density of LRs per cm^{-1} of root was significantly increased compared to WT (Col-0) roots (D). Data shown is mean values ± S. E, (n = number of seedlings/number of LRs analysed). Asterisks indicate a significant difference from that of WT (Col-0) roots based on using a Student *t* test ($P<0.05$). Biological replicates (1=3) were performed.

There was a clear 50% divide between the contact and air sides. Unlike WT (Col-0), there was no preference for LRs to emerge towards the contact side (**Fig. 3.4**). It appeared the *twd1-3* loss of function mutant exhibited a severe inability to pattern LRs resulting in a hydropatterning defect.

Compared to WT (Col-0), the *twd1-3* loss of function mutant displayed fewer, relatively shorter, twisted LRs (**Fig. 3.5**) (**A and C**). The PR length was extremely short (**Fig. 3.5**) (**B**) consistent for a dwarfed plant (Bailly *et al*., 2013). Even though the phenotypical characteristics for the *twd1-3* loss of function mutant were severe, the LR density was significantly increased (**Fig. 3.5**) (**D**).

Nevertheless, *twd1-3* LR positioning suggests that the LR hydropatterning decision is not taken when LR founder cells are in the basal root meristem but is instead delayed until these LR stem cells are transiting the root elongation zone (**Fig. 3.2**). This makes sense if LRs are being positioned relative to water availability, given that root tips take up water in the elongation (rather than meristem) zone.

3.2.3 Which auxin response factor genes are important for LR hydropatterning?

The asymmetric moisture distribution across the radius of the root triggers a differential auxin response gradient. These localised auxin response gradients are necessary for the patterning of future pre-branch sites that later result in the development of a LR (Bao *et al*., 2014) (**Fig. 3.2**).

It has been well documented that auxin responsive gene expression is regulated by a family of transcription factors termed auxin response factors (ARFs) (Okushima *et al*., 2005; Okushima *et al*., 2007 and reviewed in Lavenus *et al*., 2013). It is known that five of the ARF gene family function as transcriptional activators

(*ARF5/MONOPTEROS* (MP), *ARF6*, *ARF7*, *ARF8* and *ARF19*) of early auxin-responsive genes (reviewed in Péret *et al*., 2009). All five activating ARFs are expressed in varying degrees in the basal meristem where LR priming occurs (De Rybel *et al*., 2010). These ARFs are also involved at some point in the formation of a LR from priming in the basal meristem, to emergence in the mature root. To determine which of these ARF gene(s) controls LR hydropatterning, *loss of function* mutant alleles were characterised.

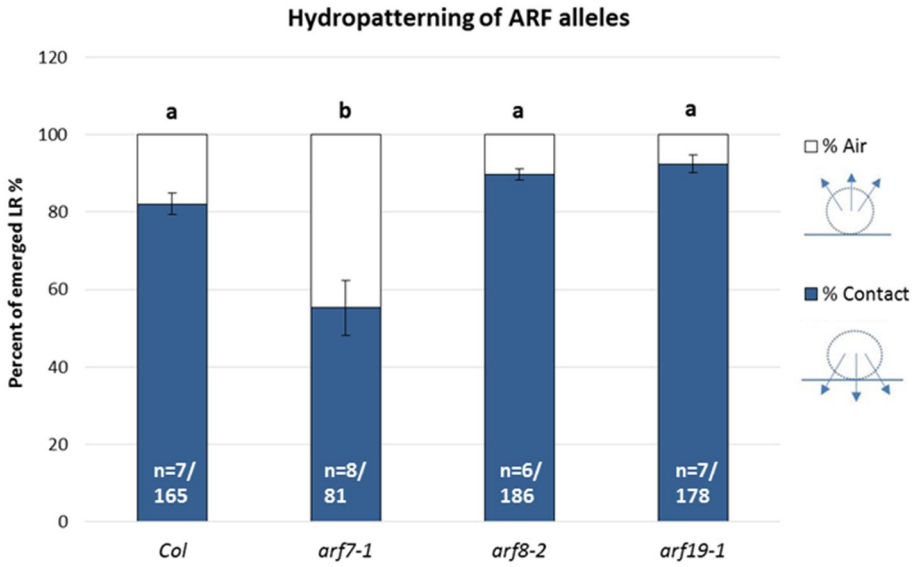


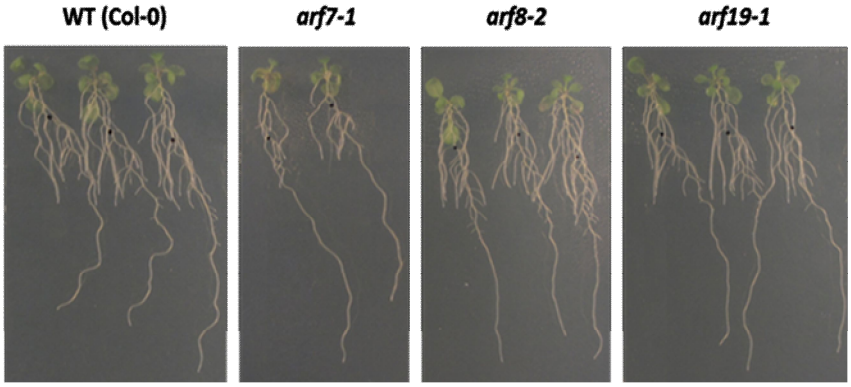
Fig. 3.6: An ARF family member is involved in LR hydropatterning. Only one of the ARFs appeared to be involved in LR hydropatterning. The *arf7-1* loss of function mutant exhibited a striking LR hydropatterning defect that was not observed in *arf8-2* and *arf19-1* loss of function mutant alleles. Instead, there was a sporadic patterning of LRs from all sides of the PR. Both *arf8-2* and *arf19-1* loss of function mutants on the other hand had a greater preference for LRs to emerge towards the contact side like WT (Col-0). Data shown is mean values ± S. E, (n = number of seedlings/number of LRs analysed). Statistical differences were analysed on the percent of emerged LRs emerging towards either contact (including horizontal) or air using a Tukey HSD test ($P<0.05$); statistically similar groups are indicated using the same letter. Biological replicates (1=5) performed.

The *arf7-1* loss of function mutant exhibited a striking LR hydropatterning response compared to that of WT (Col-0) roots (**Fig. 3.6**). Surprisingly, *arf7-1* was the only mutant disrupting an activating ARF to exhibit a LR hydropatterning defect. Instead of biasing LRs towards the contact side, the *arf7-1* loss of function mutant displayed a randomised patterning of LRs from all sides of the PR. The distribution of LRs emerging from either the air (45%) or contact (55%) side was almost equal (**Fig. 3.6**). It appeared that there was a severe inability to direct LR emergence towards the contact side as seen by WT (Col-0) roots. This suggested that LR hydropatterning may be dependent on *ARF7*.

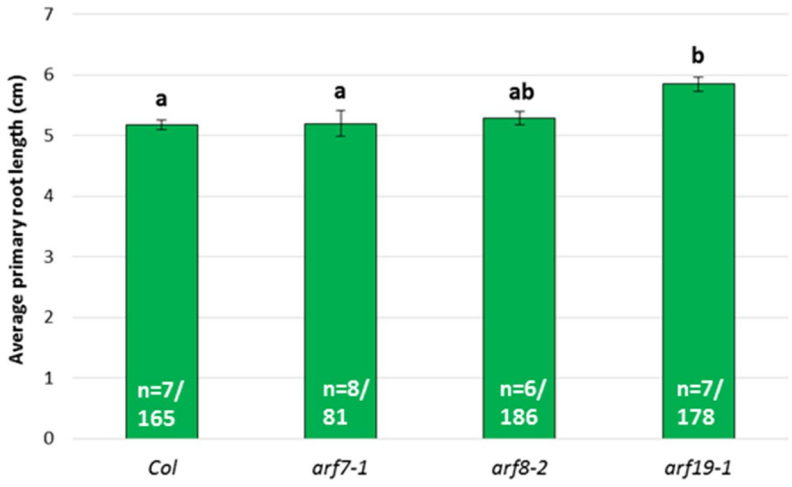
It was also apparent that the *arf7-1* loss of function mutant exhibited a prominent LR phenotype (**Fig. 3.7**) (**A to D**). Indeed, it has been well documented that the *ARF7* mutant exhibits a marked reduction in the number of LRs (Okushima et al., 2007 and reviewed in Lavenus *et al*., 2013). In fact, WT (Col-0) had double the number of emerged LRs compared to that of the *arf7-1* mutant (**Fig. 3.7**) (**C**). Even though there were fewer LRs, PR length for the *arf7-1* loss of function mutant was comparable with that of WT (Col-0) roots (**Fig. 3.7**) (**B**). This data therefore confirmed the importance of *ARF7* in LR initiation.

In contrast to *arf7-1*, the *arf6-1*, *arf8-2* and *arf19-1* loss of function mutant alleles exhibited a wildtype like LR hydropatterning response, albeit with a slightly stronger patterning of LRs towards the contact side (90%) for both the *arf8-2* and *arf19-1* mutant alleles (**Fig. 3.6**). Similarly, the same response was observed in the *arf6-1* loss of function mutant, where at least 80% of the emerged LRs were patterning towards the contact side rather than the air side (**Fig. 3.8**). Taking all this data into account it appeared that *ARF6*, *ARF8* and *ARF19* activating ARFs were not important for LR hydropatterning.

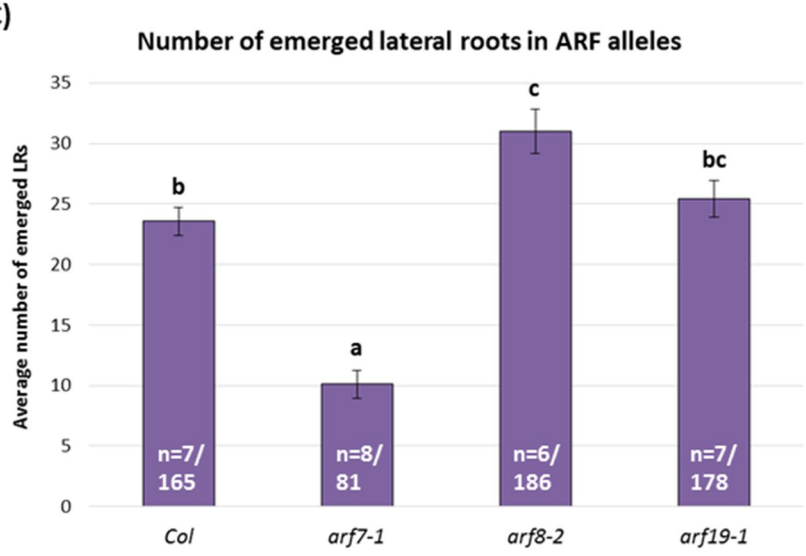
(A)


WT (Col-0)
arf7-1
arf8-2
arf19-1

(B)


Primary root length in ARF alleles
Average primary root length (cm)
0
1
2
3
4
5
6
7
a
a
ab
b
n=7/ 165
n=8/ 81
n=6/ 186
n=7/ 178
Col
arf7-1
arf8-2
arf19-1

(C)


Number of emerged lateral roots in ARF alleles
Average number of emerged LRs
0
5
10
15
20
25
30
35
b
a
c
bc
n=7/ 165
n=8/ 81
n=6/ 186
n=7/ 178
Col
arf7-1
arf8-2
arf19-1

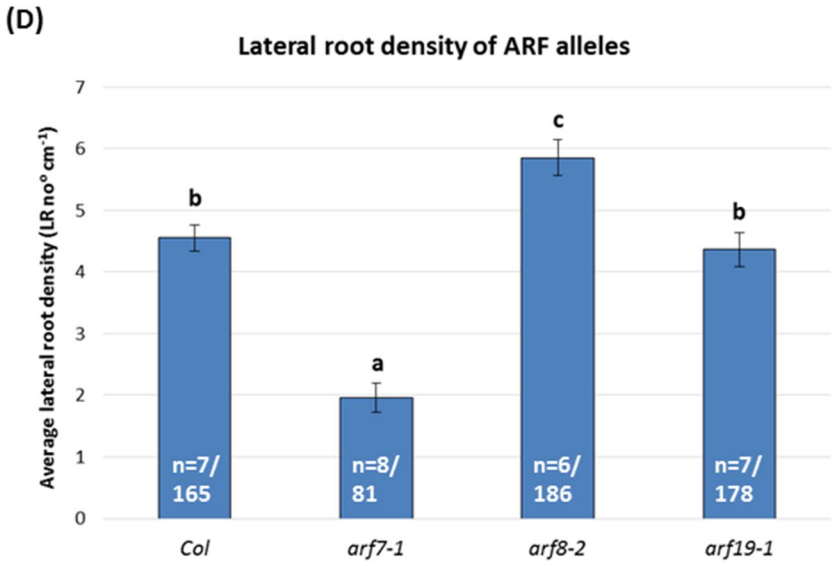


Fig. 3.7: ARFs have diverse root architectures. Compared to *arf8-2* and *arf19-1* loss of function mutants and WT (Col-0) *Arabidopsis* roots, *arf7-1* exhibited a striking phenotype that resulted in fewer LRs and a marked reduction in LR density (A) (C) (D). Primary root length was slightly enhanced in *arf19-1* loss of function roots (B). In contrast to the *arf7-1* loss of function mutant, *arf8-2* loss of function mutant had a greater number of LRs (C). This was also evident for LR density, *arf8-2* loss of function mutant had a marked difference compared to the *arf7-1* loss of function mutant. Data shown is mean values ± S. E, (n = number of seedlings/number of LRs analysed). Significant differences were analysed using the Tukey HSD test (P<0.05); statistically similar groups are indicated using the same letter. Biological replicates (1=5) were performed.

Visually, the *arf6-1*, *arf8-2* and *arf19-1* loss of function mutant alleles appeared the same as WT (Col-0) (**Fig. 3.7 and Fig. 3.9**). Although, it was apparent that the *arf8-2* loss of function mutant exhibited a slight increase in LR number (**Fig. 3.7**) (**A and C**).

Studies by Tian *et al* (2004), also observed a lateral root proliferation in *arf8* loss of function mutant alleles. Thereby supporting the lateral root density (**Fig. 3.7**) (**D**)

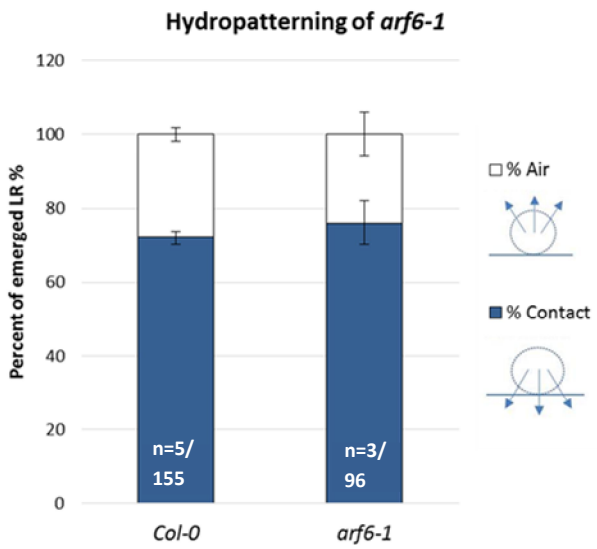


Fig. 3.8: ***ARF6*** **exhibits a normal LR hydropatterning.** WT (Col-0) *Arabidopsis* roots and the *arf6-1* loss of function mutant exhibit a LR hydropatterning response. The percent of LRs emerging towards the air and contact sides in the *arf6-1* loss of function mutant was similar to that seen by WT (Col-0) roots. Data shown is mean values ± S. E, (n = number of seedlings/number of LRs analysed). No significant difference was seen from that of WT (Col-0) roots based on using a Student *t* test ($P<0.05$). Biological replicates (1=5) were performed.

exhibited by the *arf8-2* loss of function mutant allele. It was also noted that the *arf19-1* loss of function mutant displayed a significantly longer PR length to the others (Fig. 3.7) (B). In relation to WT (Col-0) though, these difference were only marginal. Essentially, *ARF6*, *ARF8* and *ARF19* did not present any obvious phenotypical characteristics. Due to the inability of the *arf5/mp* loss of function mutant to form LRs as a result of the primary root defect, this activating ARF was unable to be analysed with regards to LR hydropatterning. It is known that *ARF5* is functionally redundant with that of *ARF7* and is involved in LR initiation (Wilmoth *et al*., 2005). However, the auxin signalling module BODENLOS (BDL)/*IAA12* - MONOPTEROS (*MP/ARF5*) only participated in LR initiation after the *SLR/IAA14* -

ARF7 - *ARF19* module has been initiated (Goh *et al.*, 2012). Therefore, it could be hypothesised that *ARF5* may also not be relevant for LR hydropatterning.

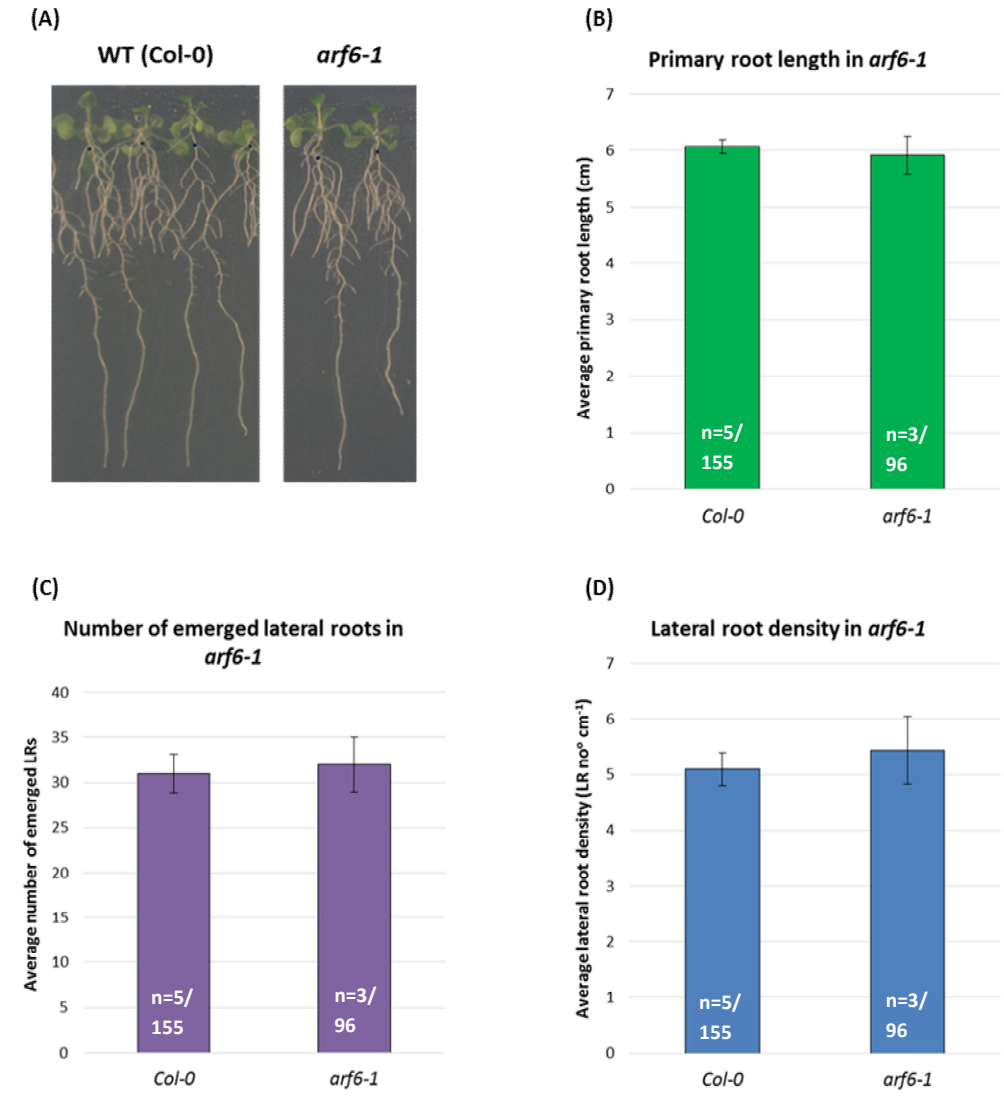


Fig. 3.9: *ARF6* and WT (Col-0) have similar root architectures. Compared to WT (Col-0) *Arabidopsis* roots the *arf6-1* loss of function mutant appeared the same (A). There was no obvious difference in primary root length (B). The *arf6-1* loss of function mutant had slightly more LRs but again nothing significant (C). This resulted in a marginal increase in LR density compared to that of WT (Col-0) roots (D). Data shown is mean values ± S. E, (n = number of seedlings/number of LRs analysed). No significant difference from that of WT (Col-0) roots was observed based on using a Student *t* test ($P<0.05$). Biological replicates (1=5) were performed.

Out of the four activating ARFs analysed, the *arf7-1* loss of function mutant was the only one to exhibit a LR hydropatterning response defect and LRP density phenotype. This suggested that, although *ARF6*, *ARF8* and *ARF19* were expressed in the basal meristem, they may not be functionally required for LR initiation. Unlike *ARF6* and *ARF8*, *ARF19* is known to be involved in LR formation with *ARF7* (reviewed in Péret *et al*., 2009). However, results obtained with *arf19-1* suggest that *ARF7* is the key ARF. Consistent with this conclusion, a recent study that built a LR gene regulatory network placed *ARF7* upstream of *ARF19* (Lavenus *et al*., 2015).

3.2.4 *ARF7* is important for LR hydropatterning

It was observed that LR hydropatterning was dependent on the transcription factor *ARF7*, since the *arf7* loss of function mutant was no longer able to exhibit a bias for LRs to emerge towards the contact side. On the other hand, *ARF19* was found not to be necessary for LR hydropatterning. Both of these genes play roles during LR development (Lavenus et al, 2013). In fact, *ARF7* is functionally redundant with that of *ARF19* (Okushima *et al*., 2007). Although, the reduced number of LRs in the *arf7-1* (but not *arf19-1*) loss of function mutant suggest that *ARF7* has a more important regulatory function in LR initiation than *ARF19* (Okushima *et al*., 2005).

To validate if *ARF7* rather than *ARF19* was truly the only activating ARF important for LR hydropatterning, several other independent *arf7* and *arf19* loss of function mutant alleles were characterised. Initially, another *arf7* loss of function mutant allele termed *nph4-1* (Non phototrophic hypocotyl 4) was analysed. Consistent with our *arf7-1* results, *nph4-1* loss of function mutant displayed a LR hydropatterning defect (**Fig. 3.10**). The distribution of LRs emerging towards the air (30%) side was far

greater than that seen by WT (Col-0) roots (15%). Like that of *arf7-1*, the *nph4-1* loss of function mutant had a marked LR phenotype (Fig. 3.11) (A to D).

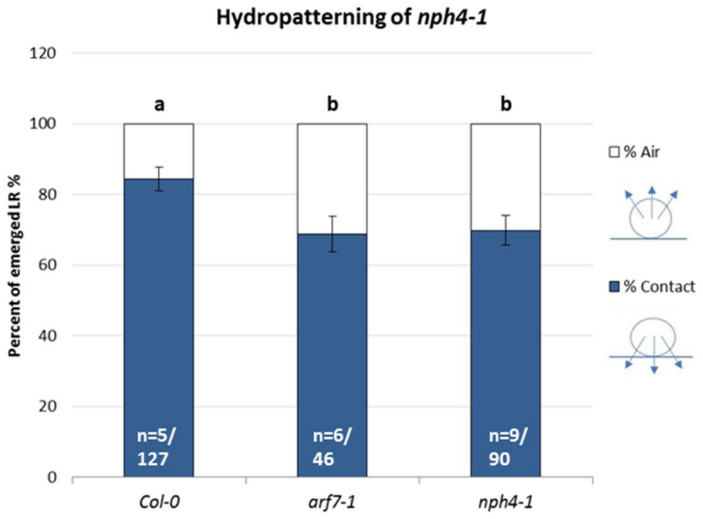


Fig. 3.10: *ARF7* is important for LR hydropatterning. WT (Col-0) *Arabidopsis* roots exhibit a LR hydropatterning response that is disrupted by *arf7* alleles. The *arf7-1* loss of function and *nph4-1* loss of function mutants displayed almost identical responses. The percent of LRs emerging towards the air side in the *arf7* alleles was greater than that seen by WT (Col-0) roots. Data shown is mean values ± S. E, (n = number of seedlings/number of LRs analysed). Statistical differences were analysed on the percent of emerged LRs emerging towards either contact (including horizontal) or air using a Tukey HSD test ($P<0.05$); statistically similar groups are indicated using the same letter. Biological replicates (1=3) were performed.

There was a significant reduction in the number of LRs compared to WT (Col-0) (Fig. 3.11) (A and C). This therefore had an impact on the LR density for both *arf7* loss of function mutant alleles (Fig. 3.11) (D). Although, compared to WT (Col-0), there was no difference in PR length (Fig. 3.11) (B).

NPH4 is known to have an inverted DNA rearrangement to that of *ARF7* with only an internal deletion (Fig. 3.12) (Harper *et al.*, 2000). The phenotypical characteristics

presented by this deletion in *nph4* are consistent with the transcriptional activators loss of function (Harper *et al.*, 2000).

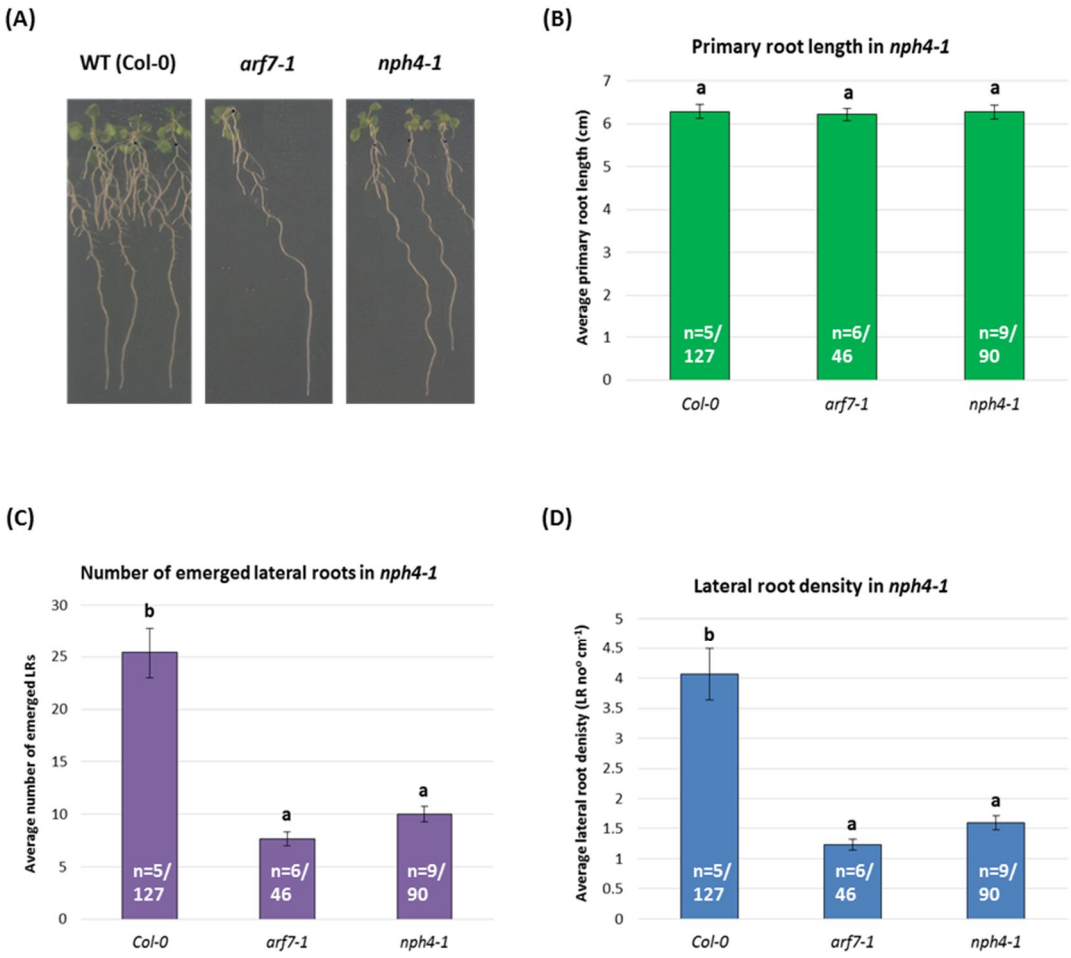


Fig. 3.11: *ARF7* displays a striking LR phenotype. Compared to WT (Col-0) *Arabidopsis* roots the *arf7-1* loss of function mutant alleles exhibit a striking LR phenotype (A). Primary root length in both the *arf7-1* loss of function and *nph4-1* loss of function mutants was comparable with WT (Col-0) (B). The number of emerged LRs on the other hand was considerably reduced in both the *arf7-1* loss of function and *nph4-1* loss of function mutant alleles (C). This reduction in LR number had a significant effect on the LR density for both *arf7* alleles (D). Data shown is mean values ± S. E, (n = number of seedlings/number of LRs analysed). Significant differences were analysed using the Tukey HSD test ($P<0.05$); statistically similar groups are indicated using the same letter. Biological replicates (1=3) were performed.

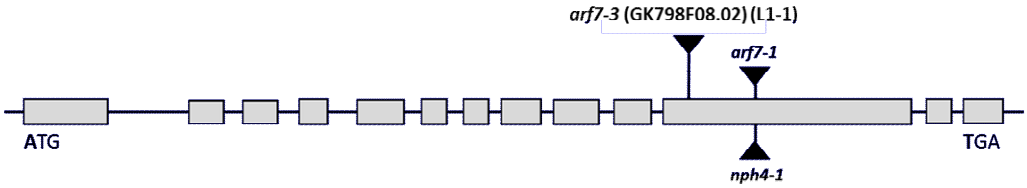


Fig. 3.12: *ARF7* domain structure specifying *arf7* alleles. Schematic representation of the *ARF7* (At5g20730) gene structure (5644 bp) and the positioning of *arf7* mutations: *arf7-1* (Salk T-DNA) (11th Exon), *nph4-1* (11th Exon) and *arf7-3* (GK798F08.02, L1-1) (11th Exon). The location of the start (**A**TG) and stop (**T**GA) codons have been indicated. Exons (boxes) and introns (lines) were determined by comparing the full length DNA sequence with that of nucleotide sequences of *arf7* mutant alleles (https://www.arabidopsis.org).

To validate these findings, another *arf7* loss of function mutant allele that we will term *arf7-3* (GK798F08.02, L1-1) was characterised. Pools of Gabi Kat (T3) seed line were selected on sulfadiazine media (75 mg/10 ml) to establishing the homozygous seed batches. The *arf7-3* loss of function mutant was also positioned in the 11th exon although much earlier compared to the other two *arf7* alleles (**Fig. 3.12**). Like *arf7-1* and *nph4-1*, the *arf7-3* loss of function mutant presented an unbiased patterning of LRs. The distribution of LRs emerging from either the air (45%) or contact (55%) side was almost equal (**Fig. 3.13**).

This identical response observed in three independent *arf7* loss of function mutant alleles, clearly showed the importance of *ARF7* in LR hydropatterning. It was also of no surprise that *arf7-3* also exhibited a matching LR phenotype to that of *arf7-1* and *nph4-1* loss of function mutant alleles (**Fig. 3.14**). Hence, the marked reduction in LR density displayed by *arf7-3* clearly showed that *ARF7* has a regulatory function in LR development (**Fig. 3.14**) (**A, C and D**). *ARF19* on the other hand has been identified as not required for LR hydropatterning.

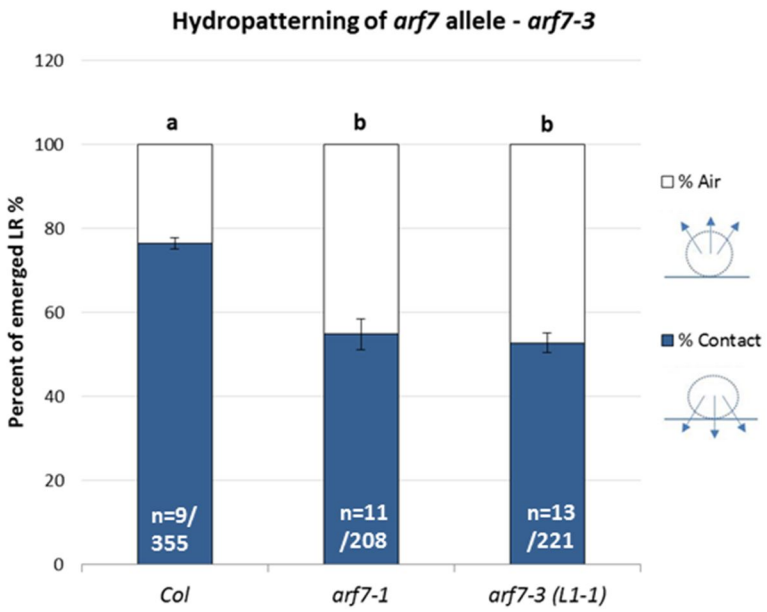


Fig. 3.13: Independent *arf7* alleles validate the importance of *ARF7* in LR hydropatterning. WT (Col-0) *Arabidopsis* roots exhibit a LR hydropatterning response that was disrupted by *arf7* alleles. Another *arf7* loss of function mutant allele, known as *arf7-3* (GK798F08.02, L1-1) displayed an identical response. The percent of LRs emerging towards the air side in the *arf7-3* (L1-1) loss of function mutant was greater than that seen by WT (Col-0) roots. There was a sporadic patterning of LRs rather than a bias towards the contact side. Data shown is mean values ± S. E, (n = number of seedlings/number of LRs analysed). Statistical differences were analysed on the percent of emerged LRs emerging towards either contact (including horizontal) or air using a Tukey HSD test ($P<0.05$); statistically similar groups are indicated using the same letter. Biological replicates (1=3) were performed.

The *arf19* loss of function mutant alleles exhibited a similar LR hydropatterning response to that of WT (Col-0) roots. The majority of the LRs emerged from the contact (80%) rather than the air side (20%) (Fig. 3.15). However, *arf19-3* and *arf19-a* loss of function mutant alleles displayed a slight increase in the number of LRs patterning towards the air side (Fig. 3.15) (at the 95% significance level there was no significant difference observed). Most of the *arf19* mutant alleles are spread

throughout the gene whereas *arf19-3* is present within the promoter region (Fig. 3.16).

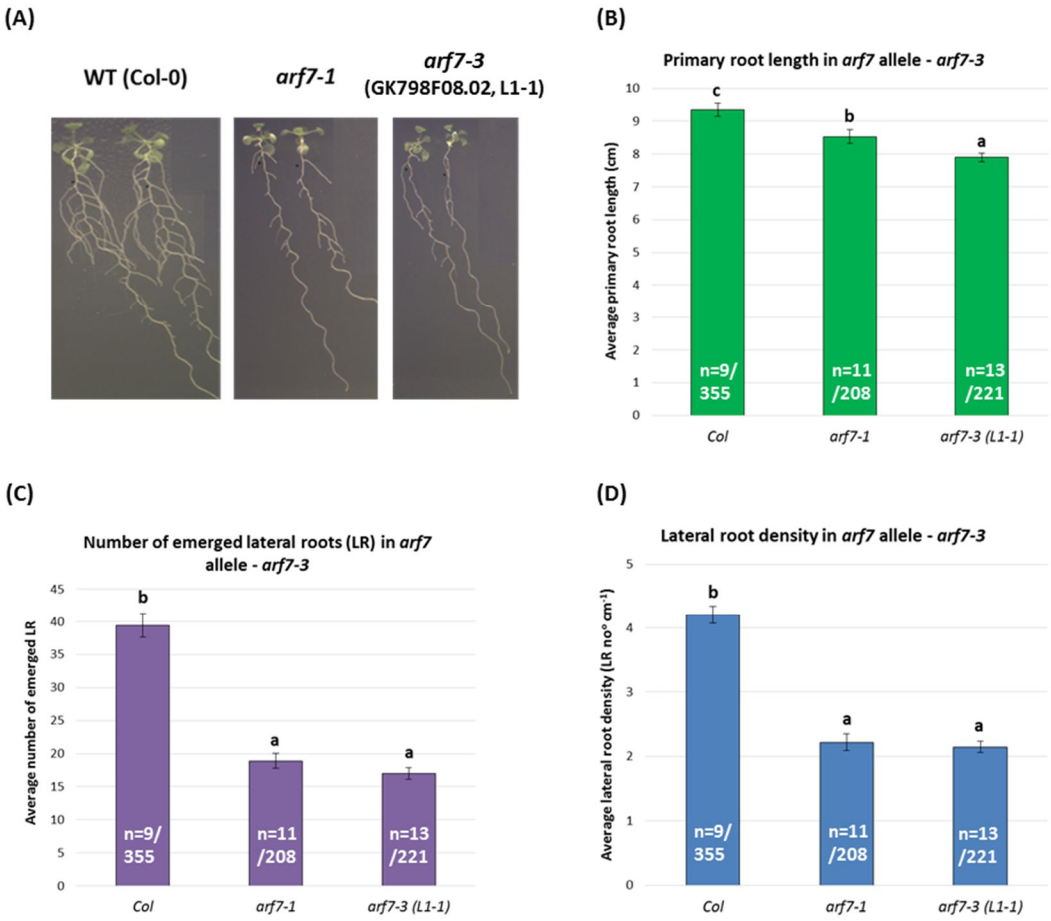


Fig. 3.14: *arf7-3* has a distinct reduction in LRs. Compared to WT (Col-0) *Arabidopsis* roots, the *arf7* loss of function mutant *arf7-3* (GK798F08.02, L1-1) exhibited a striking LR phenotype (A). Primary root length in the *arf7-3* loss of function mutant was slightly shorter than WT (Col-0) (B). Interestingly, the number of emerged LRs was considerably reduced, halved that of WT (Col-0) roots (C). This reduction in LR number therefore had a significant effect on the LR density for the *arf7-3* loss of function mutant (D). Data shown is mean values ± S. E, (n = number of seedlings/number of LRs analysed). Significant differences were analysed using the Tukey HSD test ($P<0.05$); statistically similar groups are indicated using the same letter. Biological replicates (1=3) were performed.

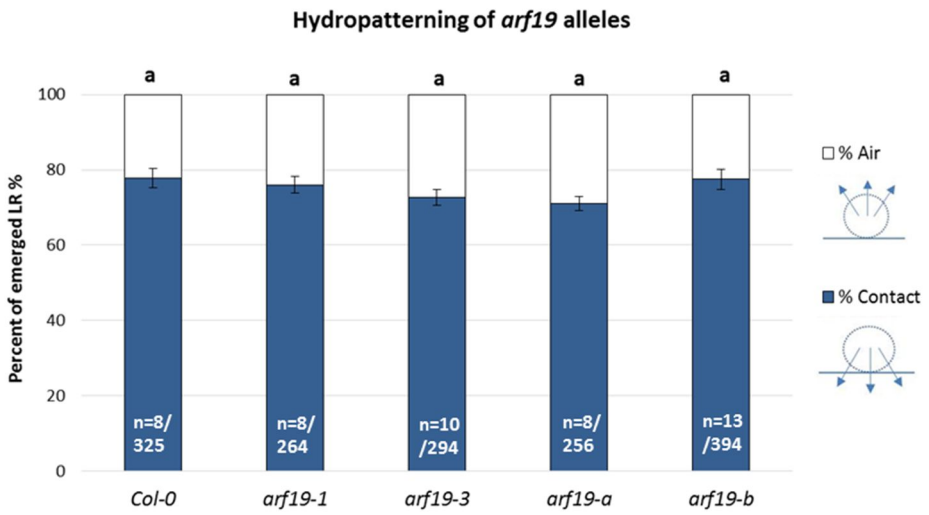


Fig. 3.15: *ARF19* is not required for LR hydropatterning. *arf19* loss of function mutant alleles exhibit a similar LR hydropatterning response to that of WT *Arabidopsis* roots. In fact, the vast majority of LRs preferred to emerge towards the contact side. Although, *arf19-3* and *arf19-a* loss of function mutant alleles showed a slight increase in the number of LRs emerging towards the air side. At 95% significance this was not significant. Data shown is mean values **±** S. E, (n = number of seedlings/number of LRs analysed). Statistical differences were analysed on the percent of emerged LRs emerging towards either contact (including horizontal) or air using a Tukey HSD test ($P<0.05$); statistically similar groups are indicated using the same letter. Biological replicates (1=3) were performed.

It was interesting to observe that *arf19-3*, *arf19-a*, *arf19-b* and *arf19-1* loss of function mutant alleles exhibited a marginal reduction in LR number compared to WT (Col-0) roots (Fig. 3.17) (C). Hence, the impact on LR density (Fig. 3.17) (D). Although visually, these differences were not obvious to see in the *arf19* loss of function mutant alleles (Fig. 3.17) (A).

It has been shown that mutations in the *ARF19* gene do not exhibit any drastic phenotypical characteristics on their own (Wilmoth et *al*., 2005). However, in

relation with *ARF7* though, this was quite the opposite. The *arf7-1*, *arf19-1* loss of function double mutant presented exacerbated developmental defects resulting in very few, if any LRs (Okushima *et al*., 2007). Mutations in both *ARF7* and *ARF19* decrease auxin induced gene activation resulting in the severe phenotype exhibited. Therefore, it was not clear if this line played a role in LR hydropatterning.

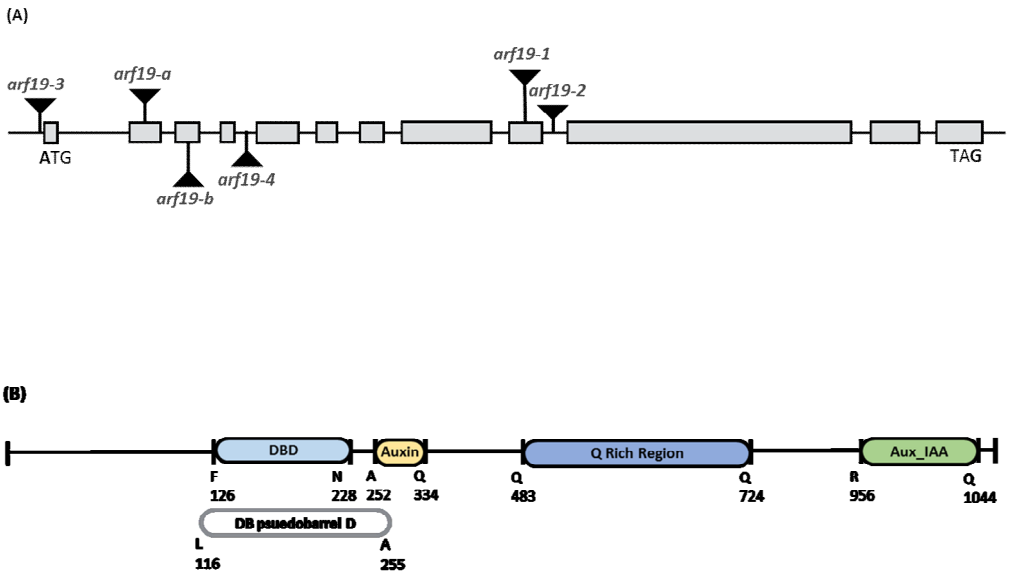
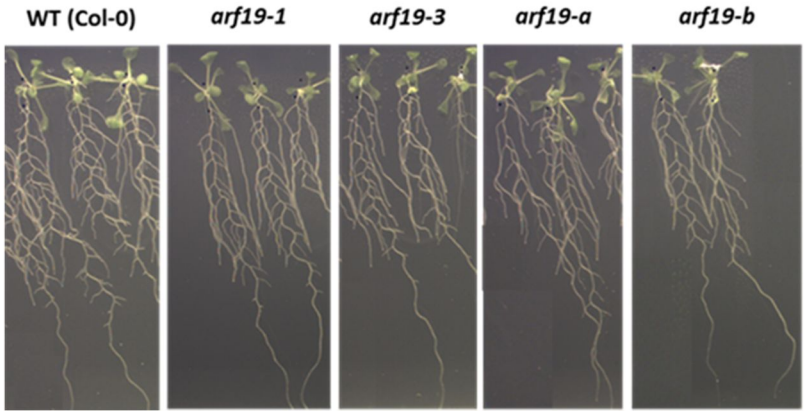
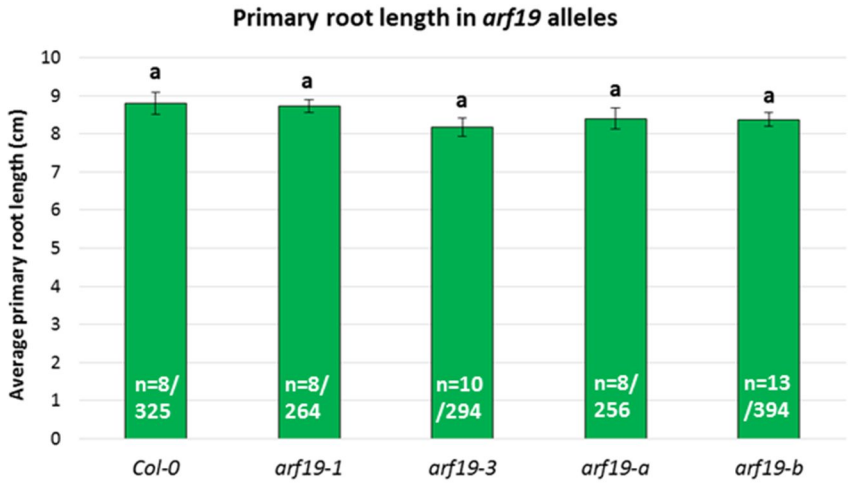


Fig. 3.16: ***ARF19* domain structure specifying *arf19* alleles.** Schematic representation of the *ARF19* (At1g19220) gene structure (4327 bp) and the positioning of *arf19* mutations (Salk T-DNA insertions): *arf19-3* (-12 bp promoter), *arf19-a* (2nd exon), *arf19-b* (3rd exon), *arf19-4* (intron between the 4th and 5th Exon), *arf19-1* (9th exon) and *arf19-2* (intron between the 9th and 10th exon). The location of the start (**A**TG) and stop (**T**AG) codons have been indicated. Exons (boxes) and introns (lines) were determined by comparing the full length DNA sequence with that of nucleotide sequences of *arf19* mutant alleles (https://www.arabidopsis.org) (A). *ARF19* domain structure depicting the DNA binding domain (DBD), Auxin, Q rich region and the Aux/IAA region (B) (Information supplied by Dr Rahul Bhosale, The University of Nottingham).

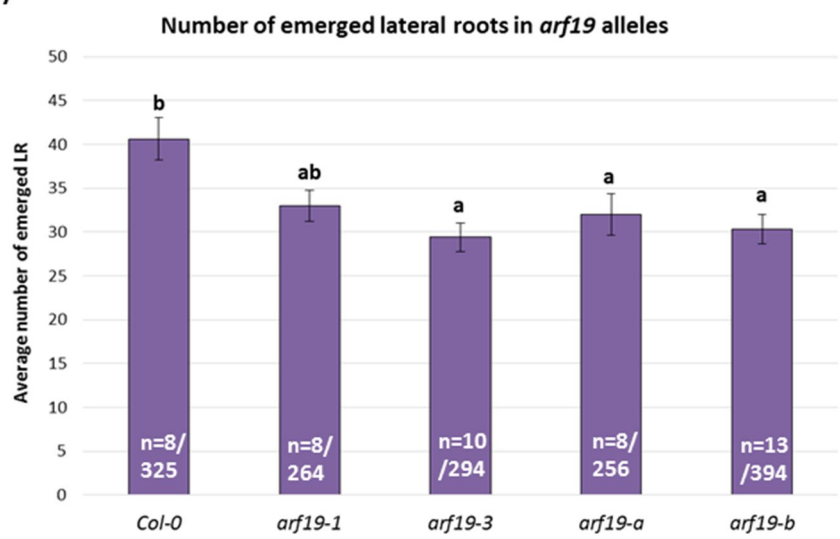
(A)


WT (Col-0)
arf19-1
arf19-3
arf19-a
arf19-b

(B)


Primary root length in arf19 alleles
Average primary root length (cm)
10
9
8
7
6
5
4
3
2
1
0
a
a
a
a
a
n=8/ 325
n=8/ 264
n=10 /294
n=8/ 256
n=13 /394
Col-0
arf19-1
arf19-3
arf19-a
arf19-b

(C)


Number of emerged lateral roots in arf19 alleles
Average number of emerged LR
50
45
40
35
30
25
20
15
10
5
0
b
ab
a
a
a
n=8/ 325
n=8/ 264
n=10 /294
n=8/ 256
n=13 /394
Col-0
arf19-1
arf19-3
arf19-a
arf19-b

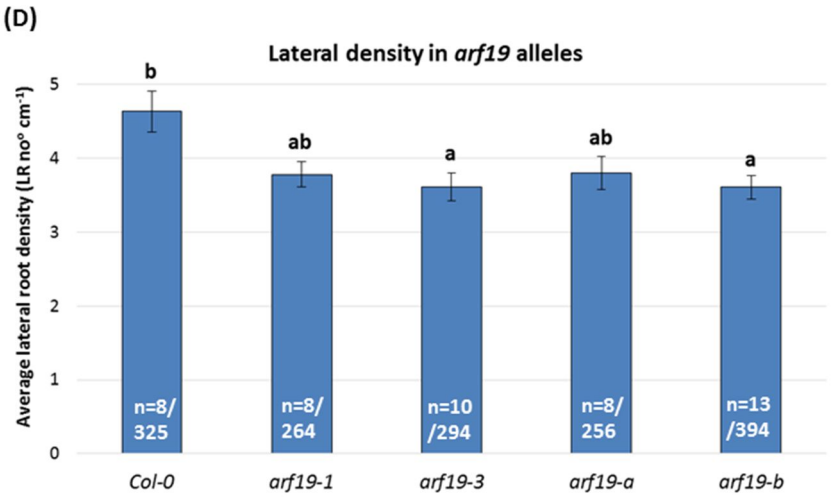


Fig. 3.17: *ARF19* alleles have reduced LR numbers. The *arf19* loss of function mutant alleles visually appeared the same as WT (Col-0) *Arabidopsis* roots, although slight differences in LR number were apparent (A). Compared to WT (Col-0) and the other *arf19* loss of function mutant alleles, *arf19-3* was marginally shorter (B). Interestingly, there was a marked reduction in the number of emerged LRs in all the *arf19* loss of function mutant alleles, especially for *arf19-3* and *arf19-b* (C). This reduction in LR number therefore had a significant effect on the LR density for the *arf19* loss of function mutant alleles (D). Data shown is mean values ± S. E, (n = number of seedlings/number of LRs analysed). Significant differences were analysed using the Tukey HSD test ($P<0.05$); statistically similar groups are indicated using the same letter. Biological replicates (1=3) were performed.

The lack of LRs in the *arf7-1*, *arf19-1* double mutant compared to WT (Col-0) though, suggested that the activation of both *ARF7* and *ARF19* are necessary components in LR development (Goh et al., 2012). In fact, it has been well documented that *ARF7* and *ARF19* work closely together to regulate LR development (Okushima *et al*., 2005; Okushima *et al*., 2007 and reviewed in Lavenus *et al*., 2013). The *arf19-1* loss of function mutant presumably does not exhibit a LR hydropatterning defect because *ARF7* plays the more dominant role in LR development. Owing to its central role in

lateral root development, it is of no surprise that *ARF7* rather than *ARF19* regulates LR hydropatterning.

3.2.5 *ARF7* is expressed during early stages of LR development

Given the importance of *ARF7* in LR hydropatterning, *Arabidopsis* roots were imaged to determine when and where this gene and protein was expressed. Two *ARF7* transcriptional reporter lines were generated: one line contained the entire promoter up to the start codon (ATG) *pARF7* (-2973 to -1 bp) fused to 3xVenus-N7 (*pARF7::3xVenus*) (**Fig. 3.18**). Subsequent transgenic lines revealed no expression close to the root tip although expression was detected in the older root (**Fig. 3.19**). The second reporter line generated contained the promoter of *ARF7* plus the first exon and first intron (-2973 to + 374 genomic fragment) fused to 3xVenus-N7 (**Fig. 3.18**).

It has been revealed that including the first intron can elevate gene expression (Vasil *et al*., 1989 and Rose *et al*., 2008). In fact, introns near the start of transcription, like they are for *ARF7*, would therefore likely be enriched. This second transcriptional reporter line (*pARF7::ΔARF7-3xVenus*) exhibited expression in the primary root tip (**Fig. 3.20**) consistent with its role during LR development (and other auxin-related processes such as root gravitropism). By adding the first intron and exon, as with the second transcriptional reporter (**Fig. 3.20**), gene expression was significantly boosted. With an enhanced signal, *ARF7* expression was visualised in all nuclei throughout the root. Importantly, the *ARF7* reporter was expressed in pericycle cells from which LRP originate (**Fig. 3.20**).

To address whether the ARF7 protein was also expressed in early stage pericycle cells, a genomic *ARF7-YFP* reporter fusion line was created (*pARF7::gARF7-mVenus*

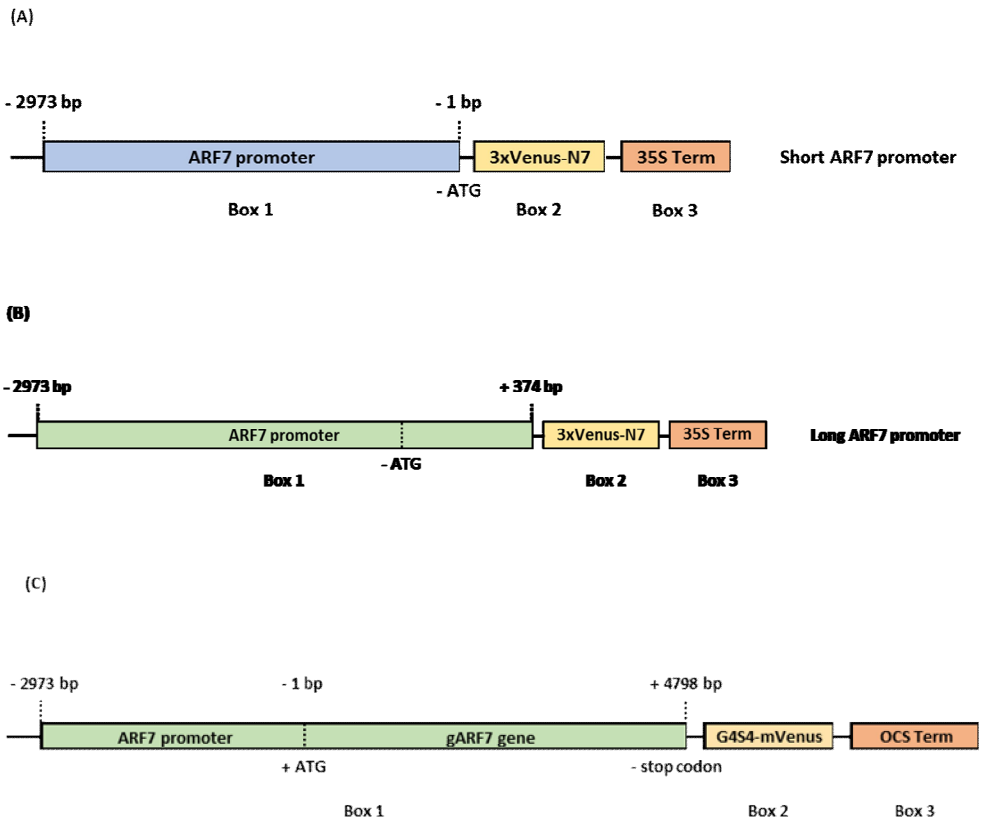


Fig. 3.18: ***ARF7* transcriptional + translational reporters specifying different promoter lengths.** Schematic representation of the promoter regions used to generate *ARF7* transcriptional and translational reporters. Both transcriptional reporters generated used an *ARF7* promoter (Box 1) fused to 3xVenus-N7 (Box 2) with a 35S terminator (Box 3) (*pARF7::3xVenus*). In the case of the 'shorter' promoter construct, a 2.9 kb region was created (-2973 to -1 bp) (A). Whereas the 'longer' promoter construct incorporated the same region as that of the 'shorter' promoter plus the first exon and intron (-2973 bp to +374 bp) (B). In fact, the first 374 bp (minus that start codon) of the *ARF7* genomic sequence (including the first intron) was used (transcriptional promoters images adapted from information sent by Jekaterina Truskina). The translational reporter generated used: an *ARF7* promoter with *gARF7* minus the stop codon (Box 1) fused to G4S4-mVenus (Box 2) with an OCS terminator (Box 3) (*pARF7::gARF7-mVenus)*. The 'shorter' promoter element of the *pARF7::gARF7-mVenus* was created as a continuous (Box 1) fragment (7771 bp). The *pARF7::gARF7-mVenus* was dipped into Col-0 and crossed into *arf7-1*.

Col-0) (Fig. 3.18) in Col-0. This transgenic line incorporated genomic *ARF7* rather than the coding region due to the importance of the first intron. In addition, the translational reporter was shown to be functional as it was also able to rescue the *arf7-1* loss of function LR phenotype. Compared to the promoter driven transcriptional reporter (Fig. 3.20), the translational reporter expressing *pARF7::gARF7-mVenus* Col-0 exhibited a weaker signal (Fig. 3.21). Nevertheless, *pARF7::gARF7-mVenus* Col-0 was clearly detectable in nuclei of cells of all tissues in the root meristem and elongation zones. Hence, *ARF7* appears to be expressed during the earliest stages of LR development.

The *pARF7::gARF7-mVenus* transgenic line was originally put into Col-0 background. To confirm that the *pARF7::gARF7-mVenus* was indeed functional and that its expression pattern reflected the spatial expression of *ARF7* required to regulate LR hydropatterning, we crossed it into the *arf7-1* background. The resulting *pARF7::gARF7-mVenus arf7-1* line rescued *arf7-1* LR hydropatterning and LR initiation defects. Therefore, the *pARF7::gARF7-mVenus* Col-0 reporters expression domain provides insight into those root tissues this transcription factor is required to function to control LR hydropatterning.

3.3 DISCUSSION

The developmental stages involved in the formation of a LR have been well defined (Casimiro *et al*., 2003; reviewed in Péret *et al*., 2009 and reviewed in Lavenus *et al*., 2013). LR priming in the basal meristem is the first key step to LR initiation. It was suggested that LR hydropatterning may act very early on in the development of a LR, via sensing of the local environment at the RT (Bao *et al*., 2014). A *pDR5::N7:Venus* reporter, that is initially expressed in pericycle cell nuclei, was used to visualise LRP

Transcriptional reporter – *pARF7::3xVenus*

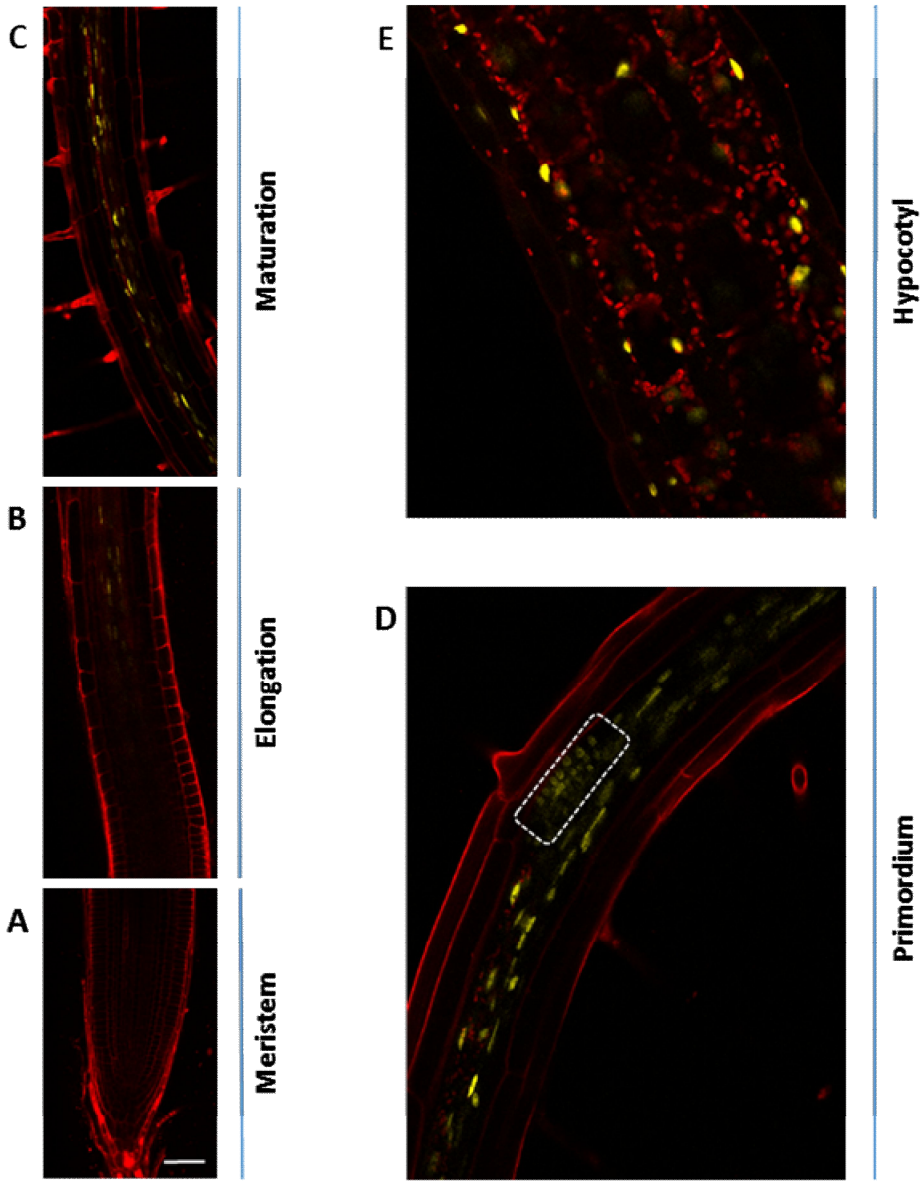


Fig. 3.19: Expression patterns of the *pARF7::3xVenus* reporter with the 'shorter' promoter. Confocal images of the *ARF7* transcriptional reporter generated with the 'shorter' promoter (Line 4) exhibited no Venus expression within the meristem and elongation zones of *Arabidopsis* roots (A and B). Expression became evident (in nuclei) towards the end of the elongation zone throughout the maturation zone (B and C) within the vasculature of the root. It was also revealed that expression was observed within primordia (circled in white) although weak (D). Only when viewing roots towards the SAM, did the Venus expression become stronger (E) (Scale bar, 50 µm) (Images reproduced from information sent by Jekaterina Truskina).

Transcriptional reporter – *pARF7::ΔARF7-3xVenus*

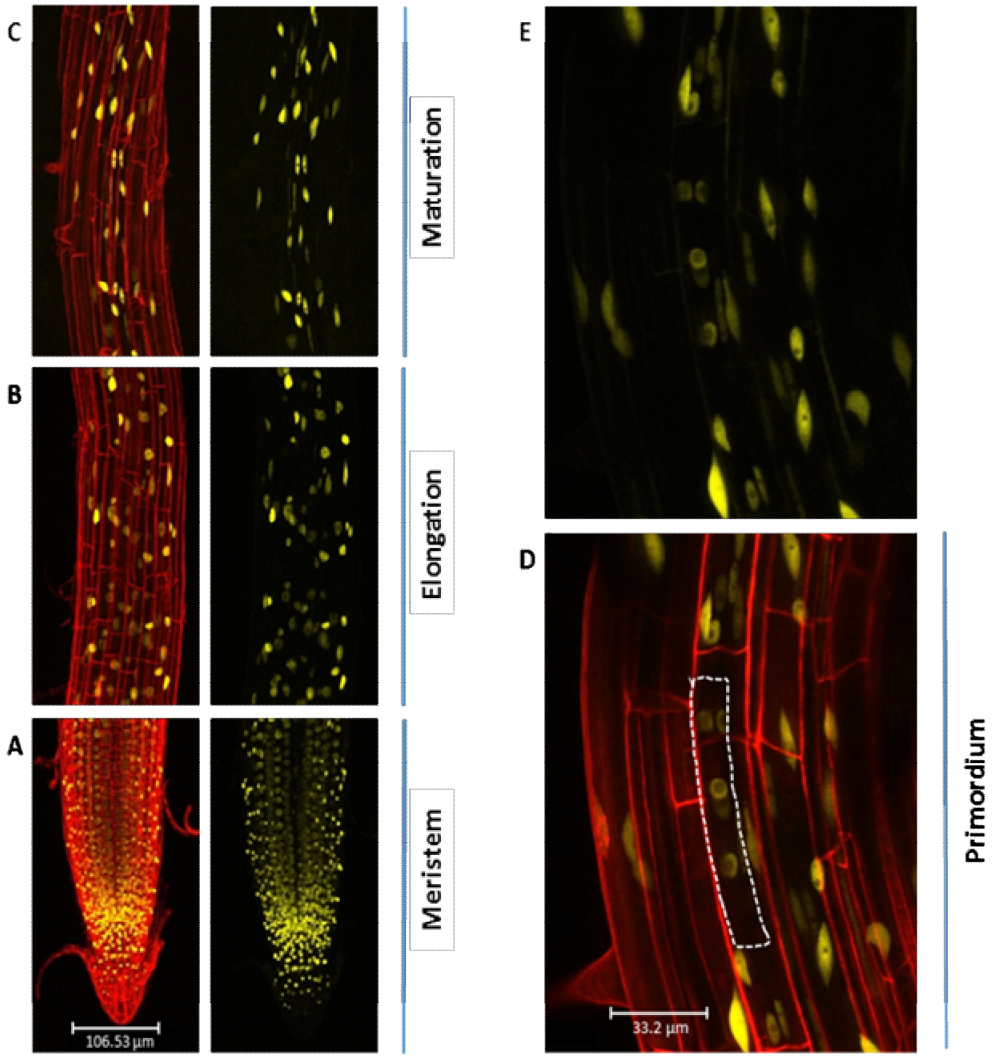


Fig. 3.20: Expression patterns of the *pARF7::ΔARF7-3xVenus* reporter with the 'longer' promoter. The *ARF7* transcriptional reporter generated with the 'longer' promoter (Line 3) exhibited bright Venus expression in nuclei throughout *Arabidopsis* roots. Clear expression patterns were evident everywhere from the RT (A), elongation zone (B) towards the maturation zone (C). The Venus expression was also present within pericycle cells where LRP originate. Therefore, it was evident that expression was visible in all cells radially across the root. It became apparent that higher up the root, the expression pattern was predominately within the stele (C to E). It was also revealed that expression was observed within primordia (circled in white) (D). Images are maximum projections of confocal image stacks. Scale bars – approx. 100 µm (A to C) and approx. 30 µm (D and E).

Translational reporter – *pARF7::gARF7-mVenus*

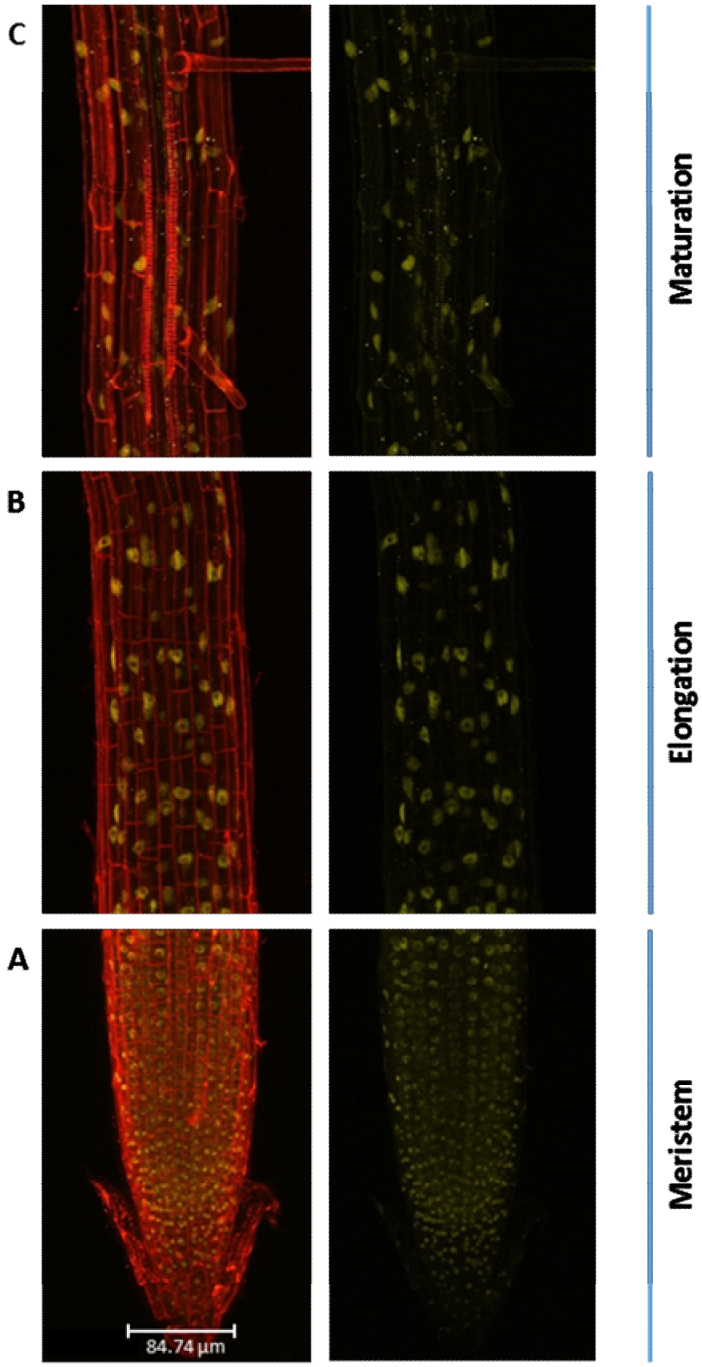


Fig. 3.21: Expression patterns of the *pARF7:gARF7-mVenus* reporter. *ARF7* translational reporter exhibited Venus expression in nuclei throughout *Arabidopsis* roots. Clear expression patterns were evident everywhere from the RT (A), elongation zone (B) and maturation zone (C). Unlike the transcriptional reporter with the 'longer' promoter, there was very weak Venus expression. Images are maximum projections of confocal image stacks. Scale bar, approx. 85 µm (A to C).

from the point of FC specification through to LR emergence. Interestingly, there was an increased number of LRP exhibited on the contact side rather than the air side in all stages of LRP development (Bao *et al*., 2014). No accumulation of pre-emerged LRP were observed on the air side that could account for differences between the two sides.

Hence, LR hydropatterning must be acting at FC specification prior to LR initiation (stage 1 LRP) (Bao *et al*., 2014). Essentially, a LR hydropatterning response must occur between the basal meristem and early elongation zones along the root. However, characterisation of the *twd1-3* mutant's root phenotype suggested that the LR patterning decision was made later on, i.e. after cells enter the elongation zone, since the *twd1-3* mutant displayed significant twisting in all root cell files within the elongation zone onwards. This conclusion is consistent with independent imaging data using a *pLBD16::gLBD16-GFP* reporter, which revealed asymmetric expression in xylem-pole pericycle cells prior to exiting the root elongation zone (**Fig. 3.2**).

LR hydropatterning response appears to influence LR development via an auxin-dependent mechanism (Bao *et al*., 2014). The complex interplay between auxin biosynthesis, transport and signalling results in the formation of a LR (Overvoorde *et al*., 2010). Bao *et al* (2014) reported that there were higher levels of auxin detectable on the contact (as opposed to the air) side of roots. *TAA1*-mediated auxin biosynthesis was found to be important for a LR hydropatterning response (Bao *et al*., 2014). The *TAA1* loss of function mutants, *wei8-1* and *sav3-1* both displayed a LR hydropatterning defect. Therefore, moisture was shown to activate the auxin biosynthesis response. PINs are important efflux carriers in the root for establishing auxin gradients that are ultimately responsible for the development of a LR (Friml *et al*., 2003). Mutations in *PIN3* (*pin3 pin7* double mutant) and *PIN7* (*pin7-2*), exhibited

small LR hydropatterning defects. However, other PINs did not have an effect on LR hydropatterning (Bao *et al*., 2014). This suggested that a functioning auxin transport pathway was partially required for maintaining auxin response gradients across the radial axis of the root.

ARF7 was the only activating ARF that displayed a LR hydropatterning defect. The *arf7-1* loss of function mutant exhibited a randomised patterning of LRs from all sides of the PR. This striking LR hydropatterning response was also observed in two other independent *arf7* loss of function mutant alleles. Hence, it appeared that *arf7* was unable to direct LR positioning towards the contact side of roots. This suggested that *ARF7* was essential for LR hydropatterning, most likely by functioning to create the observed auxin response gradient to trigger asymmetric expression of LRP regulatory genes like *LBD16* (and which is also a direct *ARF7* target; Lavenus *et al*, 2015).

The *ARF7* transcriptional and translational Venus reporters, clearly observed *ARF7* expression very early on in LR development. In fact, the ARF7 protein was expressed in early stage pericycle cells in a homogeneous manner. Hence, *ARF7* mRNA and protein did not appear to be differentially expressed. Essentially, *ARF7* is expressed in the expected root zones and tissues where LR hydropatterning is predicted to occur.

Why is *ARF7* more important for LR hydropatterning than other ARFs? It may simply reflect that, unlike other ARFs, *ARF7* is positioned at the top of the LR gene regulatory network (GRN) (Lavenus *et al*., 2015). However, the mechanism explaining how *ARF7* creates an auxin response gradient following a LR hydropatterning response is currently unclear. It is possible that *ARF7* regulates LR hydropatterning via either a post-translational or post-transcriptional mechanism. The next chapter will address this question.

Chapter 4: *ARF7* CONTROLS LR HYDROPATTERNING VIA A SUMOYLATION DEPENDENT POST TRANSCRIPTIONAL MECHANISM

Author list:

Nicola Leftley – Figures 4.1, 4.2, 4.3, 4.4, 4.5, 4.6, 4.10, 4.11, 4.12, 4.13 and 4.14

Ari Sadanandom *et al* (Contributed data) and Nicola Leftley – Figure 4.7

Ari Sadanandom *et al* (Contributed images) – Figure 4.8, 4.15, 4.16 and 4.17

Jekaterina Truskina (Contributed) and Nicola Leftley – Figure 4.9

Chapter 4: *ARF7* CONTROLS LR HYDROPATTERNING VIA A SUMOYLATION - DEPENDENT POST TRANSCRIPTIONAL MECHANISM

4.1 INTRODUCTION

Recently, it has been discovered that roots have the ability to distinguish between wet and dry environments and as a result adapt the positioning of lateral root branches (Bao *et al*., 2014). This newly discovered adaptive mechanism for controlling root branching, is referred to as LR hydropatterning (Bao *et al*., 2014). This root adaptive response comes about from local variations in water availability, resulting in LRs forming primarily on the side of the root that is in direct contact with water. Growing roots vertically on the surface of an agar plate triggers this adaptive response, whereby the formation of a meniscus results in opposite sides of the root to either be in direct contact with moisture or to the air.

Auxin is involved in almost all aspects of plant development. A complex interplay occurs between auxin biosynthesis, transport and signalling in the formation of a LR (Goh *et al*., 2012 and reviewed in Lavenus *et al*., 2013). Bao *et al* (2014) reported that there were higher levels of auxin detectable on the contact side as opposed to the air. Thereby suggesting that auxin biosynthesis or transport is moisture induced. Differences in the asymmetric moisture environment is known to trigger an auxin response gradient across the radius of the root, resulting in LRP forming predominately on the contact side (Bao *et al*., 2014).

It has been well documented that early auxin responsive gene expression is regulated by activating ARFs (reviewed in Péret *et al*., 2009). Out of the five activating ARFs in *Arabidopsis*, *ARF7* was the only member that (when mutated) displayed a LR hydropatterning defect (see **Chapter 3**), thereby confirming the importance of *ARF7* in

LR hydropatterning. *ARF7* is known to play a key role in every aspects of LR development, from LR priming through to LR emergence (Okushima *et al*., 2007). However, why *ARF7* is important for LR hydropatterning is unclear. The ARF7 protein is expressed in early stage pericycle cells (see **Chapter 3**) in a homogeneous manner. Hence, *ARF7* mRNA and protein are not differential expressed. This chapter examines how *ARF7* may regulate auxin response gradient formation and LR hydropatterning. The results reveal *ARF7* is a target for post-translational modification via SUMOylation which functions to inactivate its transcriptional activation ability.

4.2 RESULTS

4.2.1 LR hydropatterning is regulated by an ARF7-dependent post-transcriptional mechanism

LR hydropatterning is dependent on the transcription factor *ARF7* (**Chapter 3**). However, a functional *pARF7::gARF7-mVenus* reporter exhibited no differential expression in any root cell or tissue. This therefore suggested that *ARF7* may be a target for post translational regulation. To determine if *ARF7* regulated LR hydropatterning via either a transcriptional or post translational mechanism, the *ARF7* over expression transgene, *p35S::ARF7* was expressed in *arf7-1* to test if the mutant phenotype could be rescued.

Intriguingly, the *35S* driven *ARF7* expression was able to rescue the LR hydropatterning defect exhibited by the *arf7-1* mutant (**Fig. 4.1**). The *p35S::ARF7-Myc arf7-1* (L2-3) transgenic line exhibited a normal LR hydropatterning response comparable to WT (Col-0) roots. The distribution of LRs emerging towards the contact (75%) side was far greater than the air side (25%) and akin to wildtype.

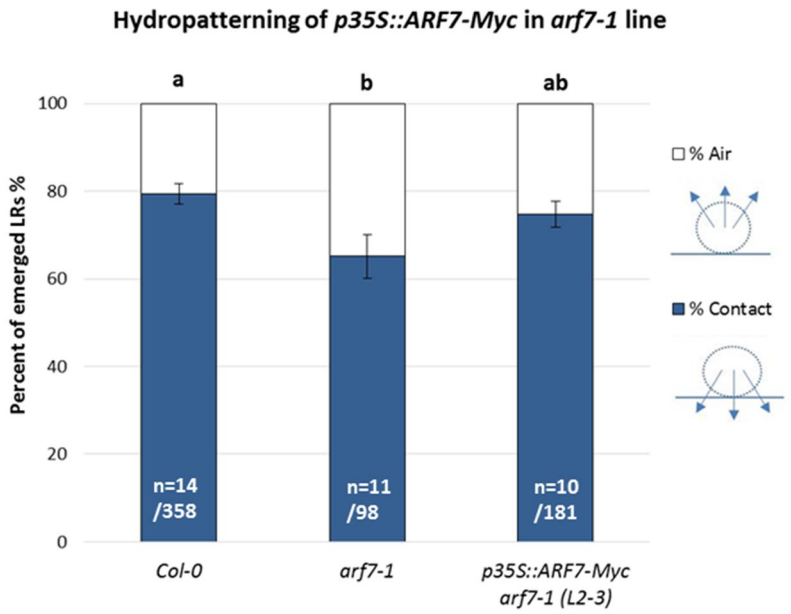


Fig. 4.1: Overexpression of *ARF7* rescued the LR hydropatterning defect. An ectopic expression of *ARF7* in the *p35S::ARF7-Myc arf7-1* (L2-3) transgenic line was able to rescue the *arf7-1* loss of function LR hydropatterning defect. The percent of LRs emerging towards the air and contact sides in the *p35S::ARF7-Myc arf7-1* (L2-3) transgenic line was similar to that seen by WT (Col-0) roots. Data shown is mean values ± S. E, (n = number of seedlings/number of LRs analysed). Statistical differences were analysed on the percent of emerged LRs emerging towards either contact (including horizontal) or air using a Tukey HSD test (P<0.05); statistically similar groups are indicated using the same letter. Biological replicates (1=4) were performed.

Visually, this *p35S::ARF7-Myc arf7-1* (L2-3) transgenic line appeared very similar to WT (Col-0) (Fig. 4.2) (A). Although, there was a significant increase in primary root length observed (Fig. 4.2) (B). It was also noted that the *p35S::ARF7-Myc arf7-1* (L2-3) transgenic line displayed double the amount of LRs compared to the *arf7-1* mutant (Fig. 4.2) (C). There was a clear increase in LR number when compared to *arf7-1* mutant which consequently impacted LR density (Fig. 4.2) (D). Although, when compared to WT (Col-0), the *p35S::ARF7-Myc arf7-1* (L2-3) transgenic line did not fully

complement LR number. This suggested that the ARF7 protein may be partially complemented or another transcription factor may be involved.

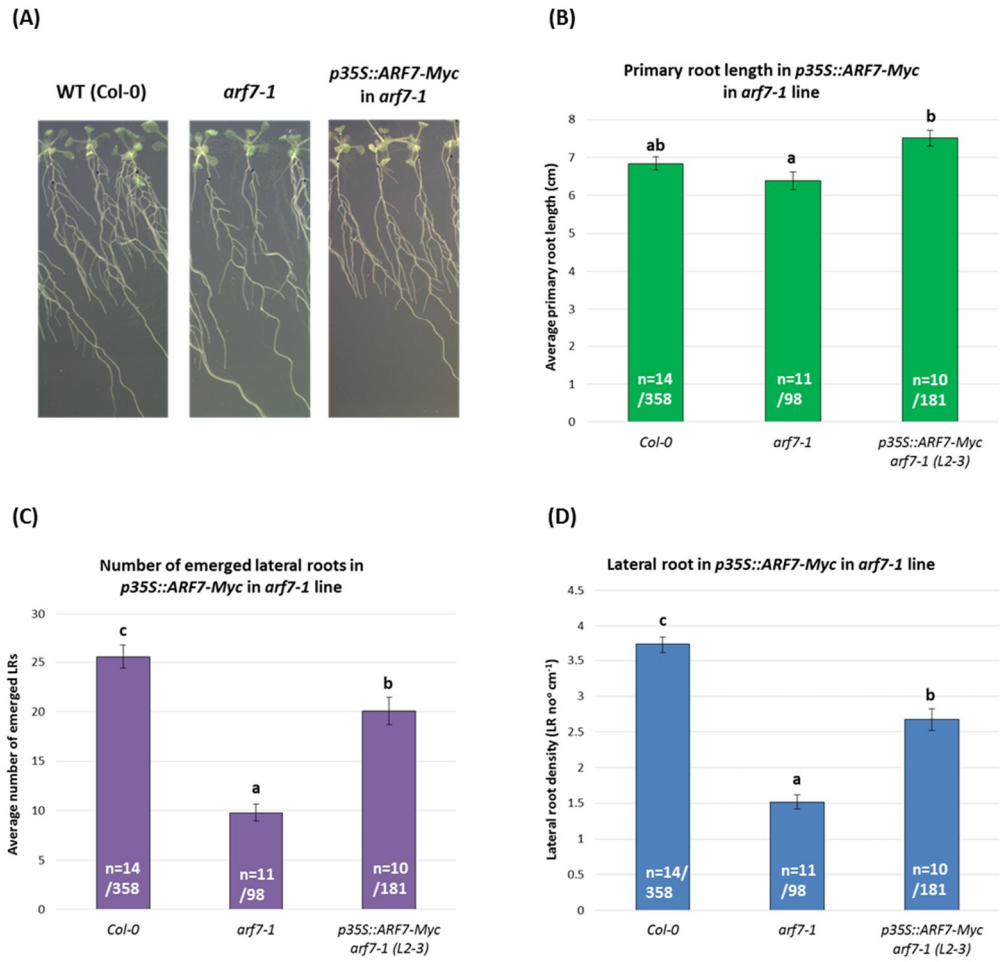


Fig. 4.2: ***ARF7* overexpression has a diverse root architecture.** Compared to WT (Col-0) *Arabidopsis* roots the *p35S::ARF7-Myc arf7-1* (L2-3) transgenic line appeared the same (A). Although, there was a significant difference in primary root length (B). In relation to *arf7-1*, the *p35S::ARF7-Myc arf7-1* (L2-3) transgenic line exhibited double the amount of LRs thereby rescuing the phenotype (C). When compared to WT (Col-0), instead of matching LR number there was a marked decrease. This therefore had an impact on LR density (D). Data shown is mean values ± S. E, (n = number of seedlings/number of LRs analysed). Significant differences were analysed using the Tukey HSD test ($P<0.05$); statistically similar groups are indicated using the same letter. Biological replicates (1=4) were performed.

Consistently, another *ARF7* overexpressor line *p35S::ARF7-HA* in *arf7-1* (L2-2) was created and observed to rescue the LR hydropatterning mutant defect (Fig. 4.3). In contrast to *arf7-1*, the majority of LRs emerged towards the contact (75%) side in the *p35S::ARF7-HA arf7-1* (L2-2) transgenic line. Knowing that both *p35S::ARF7* transgenic lines rescue *arf7-1* suggests that *ARF7* regulates LR hydropatterning via a post translational mechanism rather than be dependent on the endogenous *ARF7* promoter sequence.

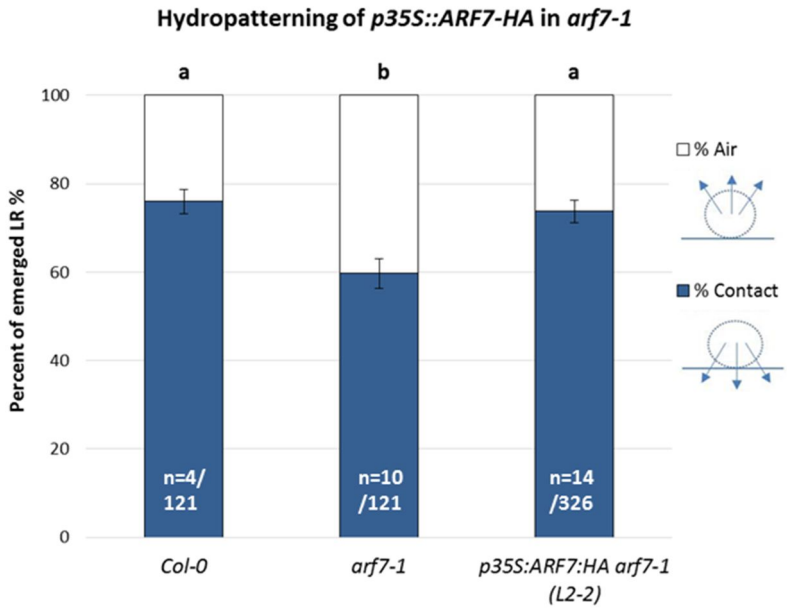


Fig. 4.3: **LR Hydropatterning is regulated post transcriptionally**. WT (Col-0) *Arabidopsis* roots and the *p35S::ARF7-HA arf7-1* (L2-2) transgenic line exhibited a normal LR hydropatterning response that was severely disrupted by the *arf7-1* loss of function mutant allele. There was a greater distribution of emerged LRs towards the contact side in the *p35S::ARF7-HA arf7-1* (L2-2) transgenic line compared to the *arf7-1* loss of function mutant. Data shown is mean values ± S. E, (n = number of seedlings/number of LRs analysed). Statistical differences were analysed on the percent of emerged LRs emerging towards either contact (including horizontal) or air using a Tukey HSD test ($P<0.05$); statistically similar groups are indicated using the same letter. Biological replicates (1=3) were performed.

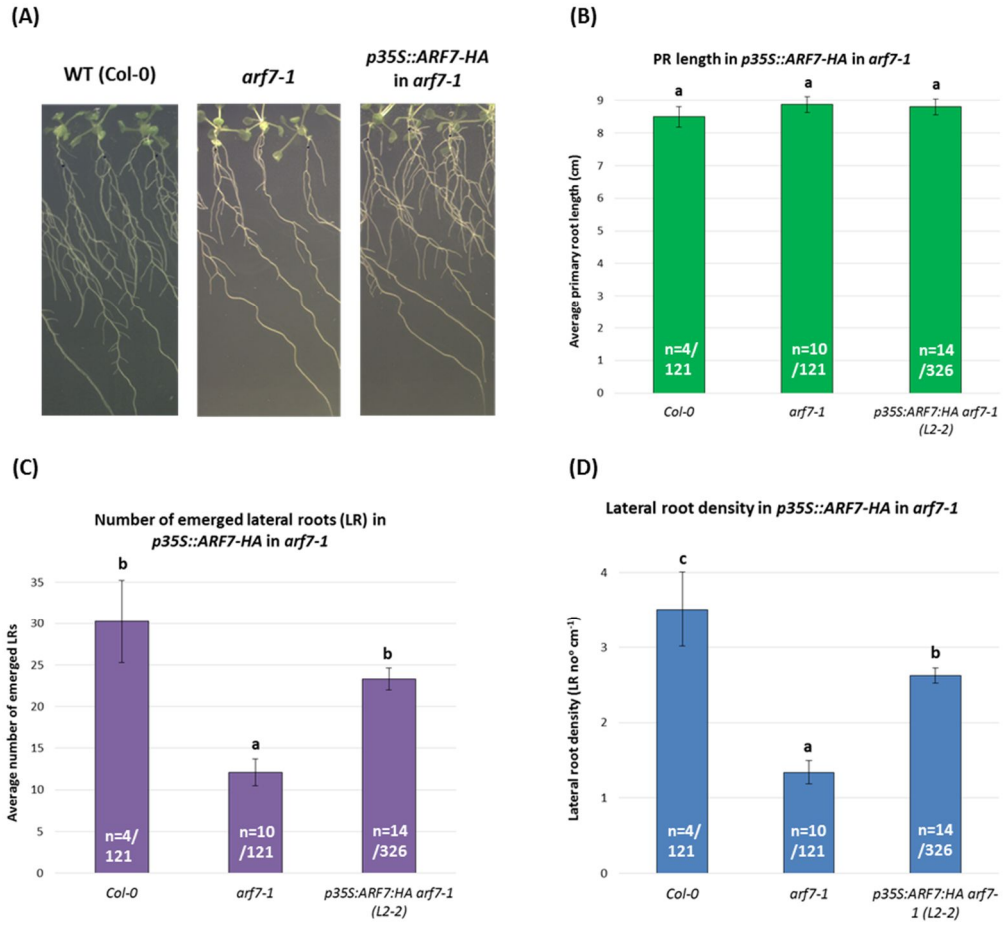


Fig. 4.4: *ARF7* overexpression impacts root architecture. Compared to WT (Col-0) *Arabidopsis* roots, the *p35S::ARF7-HA arf7-1* (L2-2) transgenic line appeared the same (A). There was no obvious difference in primary root length observed (B). In relation to *arf7-1* though, the *p35S::ARF7-HA arf7-1* (L2-2) transgenic line exhibited double the amount of LRs thereby rescuing the phenotype (C). When compared to WT (Col-0), instead of matching LR number there was a marked decrease. This therefore had an impact on LR density (D). Data shown is mean values ± S. E, (n = number of seedlings/number of LRs analysed). Significant differences were analysed using the Tukey HSD test ($P<0.05$); statistically similar groups are indicated using the same letter. Biological replicates (1=3) were performed.

Like the other *ARF7* overexpressor transgene, the *p35S::ARF7-HA arf7-1* (L2-2) transgenic line appeared quite distinct from the *arf7-1* loss of function mutant (Fig. 4.4) (A). Although, there was no difference in primary root length observed (Fig. 4.4)

(B). Consistent with the *p35S::ARF7-HA arf7-1* (L2-2) transgenic line being an overexpressor, there was a doubling of LR number compared to the *arf7-1* loss of function mutant allele (Fig. 4.4) (C). However, in relation to WT (Col-0), there was a marginal reduction in the number of LRs presented (Fig. 4.4) (C). Thereby, having an effect on LR density (Fig. 4.4) (D). Even though, both independent *p35S::ARF7* transgenic lines had a significant effect on *arf7-1* loss of function LR emergence. The fact that another 35S driven *ARF7* transgene was unable to fully rescue the WT (Col-0) LR phenotype suggested ARF7 may be functioning interdependently rather than alone.

4.2.2 SUMOylation influences LR hydropatterning

To determine how LR hydropatterning may control *ARF7*, mutants were examined that disrupt post-translational protein regulation. This included the SUMO protease mutant *ots1 ots2*. SUMO is a **s**mall **u**biquitin-like **mo**difier that can be added to and removed from proteins by E3 ligases and SUMO proteases, respectively.

It was revealed that the *ots1 ots2* mutant (SUMO protease deficient OVERLY TOLERANT TO SALT 1 and 2) phenocopied the *arf7-1* LR hydropatterning mutant defect (Fig. 4.5). Like the *arf7-1* loss of function mutant, the distribution of LRs emerging towards the air (40%) side was far greater than that seen by WT (Col-0) roots (20%). Hence, LR hydropatterning appeared to be dependent on *OTS1* and *OTS2* function.

Interestingly, there was a reduced number of LRs observed in the *ots1 ots2* mutant as opposed to WT (Col-0) roots (Fig. 4.6). This was also comparable with the *arf7-1* mutant. In fact, *arf7-1* had almost double the number of emerged LRs compared to the *ots1 ots2* mutant (Fig. 4.6) (C). This reduction in LR number exhibited by both the *ots1 ots2* and *arf7-1* mutants had a significant effect on LR density (Fig. 4.6) (D). Unlike

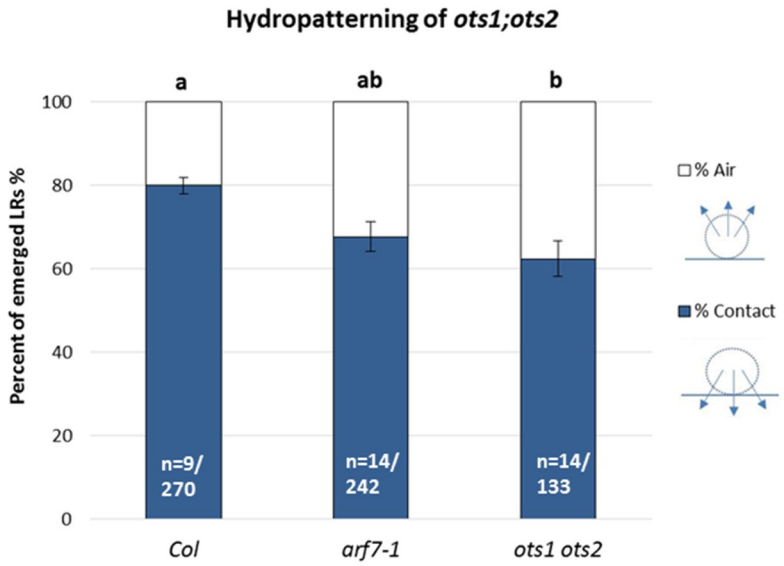


Fig. 4.5: LR hydropatterning dependent on *OTS1* and *OTS2*. WT (Col-0) *Arabidopsis* roots exhibited a LR hydropatterning response that was disrupted by *ots1 ots2* and *arf7-1* loss of function mutant alleles. The *ots1 ots2* loss of function and *arf7-1* loss of function mutants displayed almost identical responses. The percent of LRs emerging towards the air side in the *ots1 ots2* loss of function mutant was far greater than that seen by WT (Col-0) roots. Data shown is mean values ± S. E, (n = number of seedlings/number of LRs analysed). Statistical differences were analysed on the percent of emerged LRs emerging towards either contact (including horizontal) or air using a Tukey HSD test ($P<0.05$); statistically similar groups are indicated using the same letter. Biological replicates (1=6) were performed.

arf7-1 though, the *ots1 ots2* mutant has a much more severe root phenotype consistent with *OTS1 OTS2* being required for modifying many other proteins (**Fig. 4.6**) (**A and B**). *OTS1* and *OTS2* are nuclear localised and act by cleaving SUMO (Small Ubiquitin-like Modifier) from nuclear proteins like TFs (Conti *et al.*, 2008 and Conti *et al.*, 2014). *OTS1* and *OTS2* proteases are also destabilised by drought and salt stress, so SUMOylated proteins will accumulate in nuclei of cells exposed to these stresses (Conti *et al.*, 2008 and Conti *et al.*, 2014). Hence, SUMO represents a promising

mechanism to modify ARF7 activity in response to abiotic stress like a LR hydropatterning stimulus.

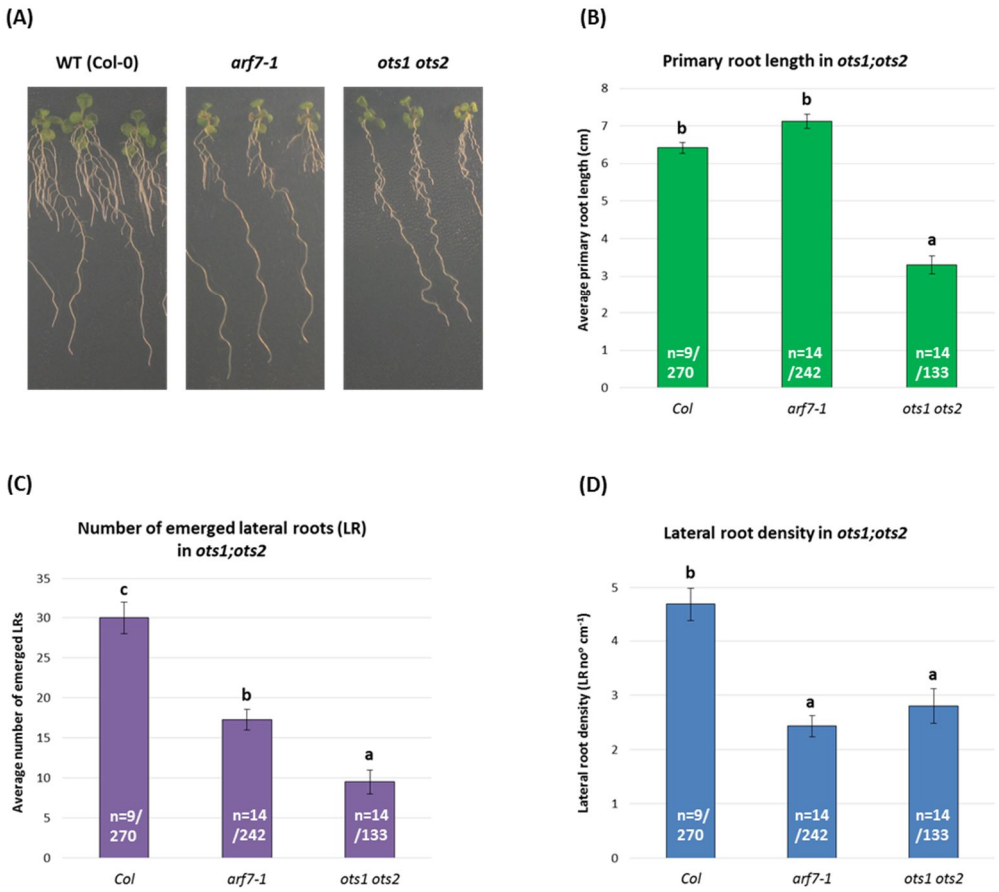
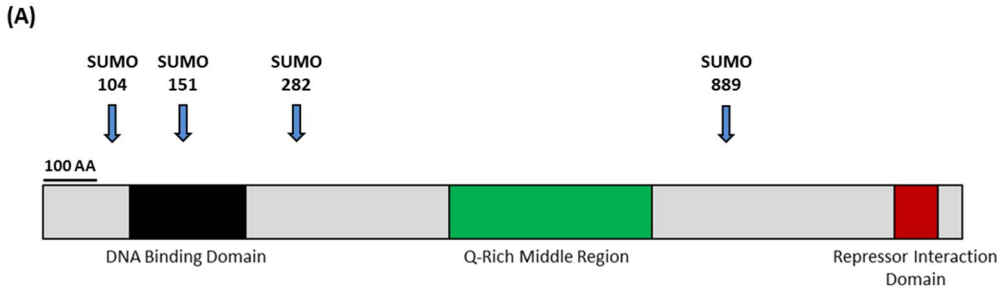


Fig. 4.6: *OTS1 OTS2* has a marked reduction in LRs. Compared to WT (Col-0) *Arabidopsis* roots the *ots1 ots2* loss of function mutant exhibit a striking LR phenotype (A). Primary root length in the *ots1 ots2* loss of function was significantly shorter than WT (Col-0) (B). There was also a marked reduction in LR number. In fact, the *arf7-1* loss of function mutant had double the amount of LRs than the *ots1 ots2* loss of function mutant (C). This reduction in LR number had a significant effect on LR density for both *ots1 ots2* and *arf7-1* loss of function mutant alleles (D). Data shown is mean values ± S. E, (n = number of seedlings/number of LRs analysed). Significant differences were analysed using the Tukey HSD test (P<0.05); statistically similar groups are indicated using the same letter. Biological replicates (1=6) were performed.



(B) **Predicted SUMO sites in ARFs**

```
AtARF7  (A)   CKTLTASDTSTHGGFSVPRRAAEKIFPALDFSMQPPCQELVAKDIHDNT
AtARF19 (A)   CKTLTASDTSTHGGFSVPRRAAEKIFPPLDFSMQPPAQEIVAKDLHDTT
AtARF5  (A)   CKTLTASDTSTHGGFSVPRRAAEKLFPPLDYSAQPPTQELVVRDLHENT
AtARF8  (A)   CKTLTASDTSTHGGFSVPRRAAEKVFPPLDYTLQPPAQELIARDLHDVE
AtARF6  (A)   CKTLTASDTSTHGGFSVPRRAAEKVFPPLDYSQQPPAQELMARDLHDNE
Pp-1    (A)   CKTLTASDTSTHGGFSIPRRAAEKVFPPLDYSQTPPAQELKARDLHDQE
AtARF9  (R)   SKVLTASDTSTHGGFSVLRKHATECLPPLDMTQQTPTQELVAEDVHGYQ
ARF1    (R)   CKTLTASDTSTHGGFSVLRRHADDCLPPLDMSQQPPWQELVATDLHNSE
AtARF2  (R)   CKTLTASDTSTHGGFSVLRRHADECLPPLDMSRQPPTQELVAKDLHANE
AtARF4  (R)   CKTLTASDTSTHGGFSVPRRAAEDCFAPLDYKQQRPSQELIAKDLHGVE
AtARF3  (R)   CKTLTASDTSTHGGFSVPRRAAEDCFPPLDYSQPRPSQELLARDLHGLE
Pp-2    (R)   CKTLTASDTSTHGGFSVPRRAAEECLPLLDHNMVPPCQELVAKDLHGKD
Pp-3    (R)   CKTLTASDTSTHGGFSVPRRAAEDCLPLLDHSMNPPCQELVAKDLHGKE
AtARF17 (R)   AKILTPSDANNGGGFSVPRFCADSVFPLLNFQIDPPVQKLYVTDIHGAV
Pp-4    (R)   AKTLTQSDANNGGGFSVPRYCAETIFPPLDYSSDPPVQTVLAKDVHGDV
Pp-5    (R)   AKTLTQSDANNGGGFSIPRYCAETIFPPLDYCIDPPVQTVLAKDVHGEV
AtARF10 (R)   AKTLTQSDANNGGGFSVPRYCAETIFPRLDYSAEPPVQTVIAKDIHGET
AtARF16 (R)   AKTLTQSDANNGGGFSVPRYCAETIFPRLDYNAEPPVQTILAKDVHGDV
                *.** **    ****                  * *     * *
```

Fig. 4.7: **Schematic representation of the *ARF7* protein coding sequence that contains post-translational regulatory motifs.** Within the ARF7 protein coding sequence there are several putative post-translational regulatory sites. These sites are for the addition of Small Ubiquitin Modifier (SUMO) proteins that are part of the SUMOylation pathway. *ARF7* has been found to have four SUMO sites located across its full length. One of which sits within the DNA binding domain (A). Using a SUMO predicted programme, the alignment of DNA binding motifs from (angiosperms) *Arabidopsis* (circled in green) and *Physcomitrella* ARF sequences revealed a highly conserved SUMOylation site (highlighted in red) in activators but not repressors (B) (Images reproduced from data supplied by Prof. Ari Sadanandom *et al*, The University of Durham).

4.2.3 *ARF7* is a target for SUMOylation

The results exhibited by the *ots1 ots2* mutant suggest that *ARF7* may be a target for SUMOylation, in fact, hyper-SUMOylated. Durham collaborators have recently discovered that *ARF7* has four SUMOylation sites (amino acids: 104, 151, 282 and 889) including one within the DNA binding domain (**Fig. 4.7**) (**A**). Interestingly, it is highly conserved among the activating ARFs (**Fig. 4.7**) (**B**). In contrast, there does not appear to be a SUMOylation site in the DNA binding domain of repressor ARF sequences. In fact, it is the N-Terminus DNA binding domain that binds to promoters of early auxin-response genes (Tiwari *et al.*, 2003). Hence, SUMOylation of *ARF7* (and other activating ARF proteins) is likely to affect DNA binding.

In order to examine the functional importance of *ARF7* SUMOylation, a non-SUMOylatable *ARF7* (4xKR) construct was generated alongside the complementary *ARF7* (WT) line (Dr Beatriz Orosa-Puente, The University of Durham) within which all four SUMOylation sites had been mutated by replacing lysine (K) with arginine (R) residues. Transient expression studies of both *pARF7::ARF7-GFP* (4xKR) and *pARF7::ARF7-GFP* (WT) transgenic lines revealed that mutating all four SUMOylation motifs blocked *ARF7* SUMOylation (**Fig. 4.8**).

An initial protein-complex co-immunoprecipitation (Co-IP) assay revealed no visible band on a western blot after probing the ARF7 (4xKR) protein with anti-SUMO-HA (**Fig. 4.8**) (**A**). This indicated that the ARF7 (4xKR) protein was no longer SUMOylated. In contrast, clear bands were exhibited in the ARF7 (WT) and ARF7 (single SUMO motif 104 mutated) proteins (**Fig. 4.8**) (**A**). The fact that a band was visible in the ARF7 (single SUMO motif 104 mutated) protein suggested that this particular SUMO site was not the sole SUMOylation site. Hence, it appeared that additional/all SUMO sites needed

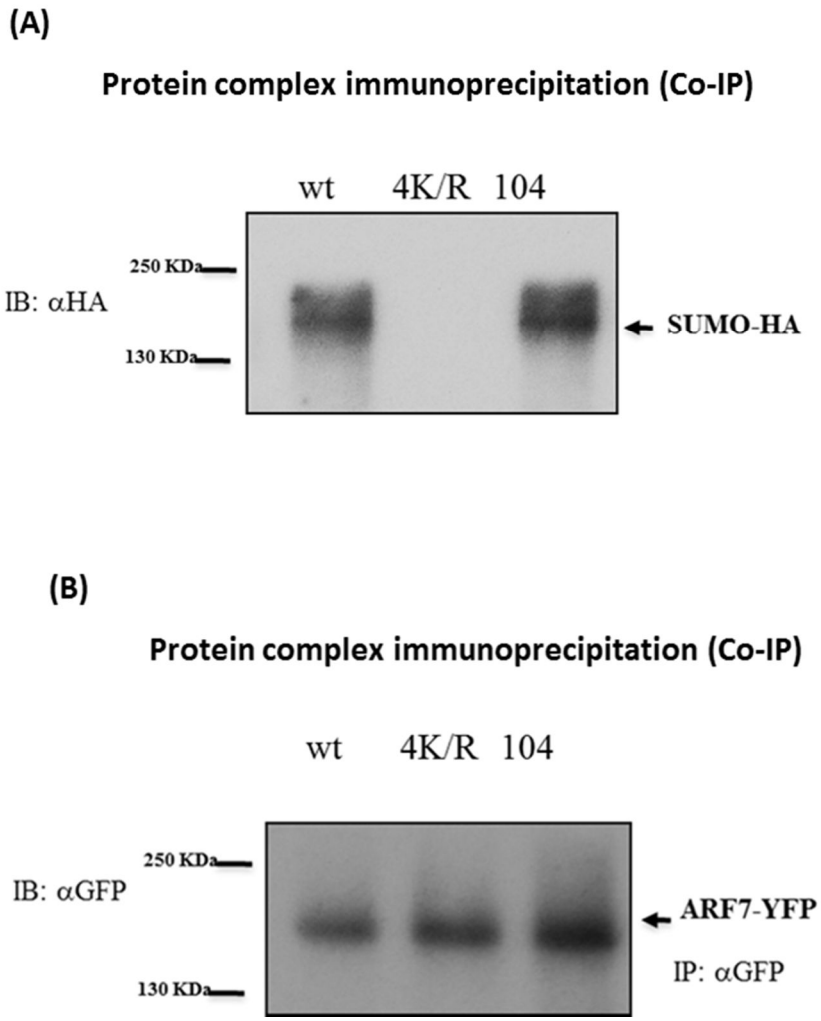


Fig. 4.8: ***ARF7* is a target for SUMOylation.** Western blots revealing protein-protein interactions from Co-IPs (protein complex immunoprecipitation). The initial Co-IP was first probed with anti-SUMO-HA and then re-probed with anti-HA antibodies (A). During SUMOylation, SUMO attaches to target proteins. Bands present in only WT (un-mutated ARF7) and 104 (single site mutated in ARF7) but not in 4xKR (all four SUMO sites mutated in ARF7) after probing with anti-SUMO-HA indicated that ARF7 is indeed a target for SUMOylation (A). The second Co-IP was to probe for the GFP tag that was present in both WT, 104 and 4xKR samples (B). Probing with anti-GFP and re-probing with anti-ARF7-YFP antibodies, confirmed the presence of GFP in the WT, 104 and 4xKR samples. Ultimately, mutating all four SUMO sites (4xKR) blocks ARF7 SUMOylation (Images from by Prof. Ari Sadanandom *et al*, The University of Durham).

(A)

***pARF7::ΔgARF7* (WT/4KR) construct**

Fragment 1

Plasmid as template: *pARF7::gARF7* (Box 1) (ATG plus 1st Intron)

Forward: GGGG ACA ACT TTG TAT AGA AAA GTT GGA AAGAGATGTCGCAAACCAGC
Reverse: TGGAGGCAACGAAATCAATGG

Tm = 67 Product size 3435bp

Fragment 2 (with stop codon)

Plasmid as template: (1) ARF7 (4K/R) cds (Box 2)
(2) ARF7 cds (Box 2)

Forward: CCATTGATTTCGTTGCCTCCA

Reverse: GGGG AC TGC TTT TTT GTA CAA ACT TGT TCACCGGTTAAACGAAGTGGC

Tm = 65 Product size 3429bp

Overlap PCR reaction (with stop codon)

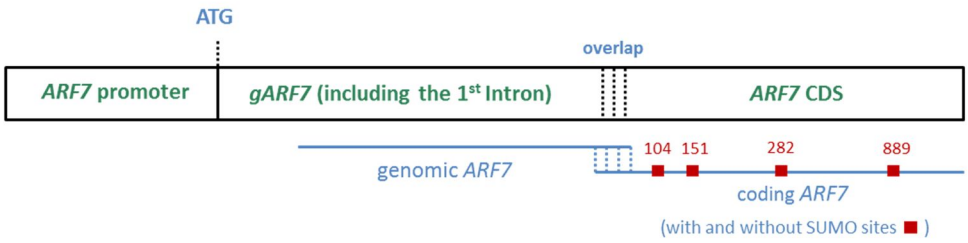
Forward: GGGG ACA ACT TTG TAT AGA AAA GTT GGA AAGAGATGTCGCAAACCAGC

Reverse: GGGG AC TGC TTT TTT GTA CAA ACT TGT TCACCGGTTAAACGAAGTGGC

Tm = 67 Product size 6809bp (approx)

(B)

Generating *pARF7::ΔgARF7* (WT/4KR) construct



(C)

Gateway - Box 1



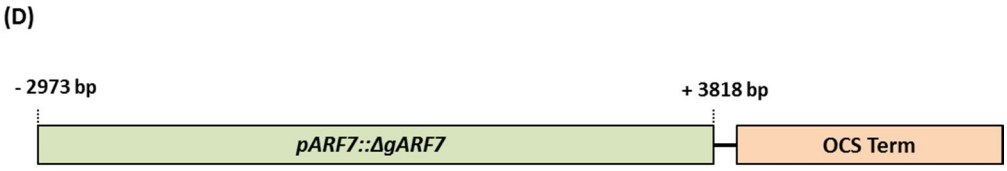


Fig. 4.9: Generating the mutated SUMO *ARF7* transgene. Schematic representation of the region used to create the *pARF7::gARF7* (WT/4xKR) constructs. The *ARF7* (4xKR) construct had been previously generated alongside the complementary ARF7 (WT) line (Dr Beatriz Orosa-Puente, The University of Durham). Both of these constructs used the CDS rather than the genomic sequence. These lines were used as the template DNA to create first intron constructs. In the first instance, PCR reactions generated fragment 1 and 2 (A). Purified fragments 1 and 2 were then used in an overlap PCR reaction (A). A pENTRY clone was generated using the overlapped DNA fragment (*gARF7* plus first intron then followed by *ARF7* CDS) incorporated with the 'longer' *ARF7* promoter (-2973 to +374bp) and pDONR P4-P1r (B and C). The *pARF7::gARF7* (WT and 4xKR) constructs generated used: *pARF7::gARF7* (Box 1), pENTRY gene mock (Box 2), an OCS terminator (Box 3) plus pBm43GW (D). Both the *pARF7::gARF7* (WT) and *pARF7::gARF7* (4xKR) constructs were dipped into the *arf7-1* background (Constructs made in connection with Jekaterina Truskina, The University of Nottingham/Lyon University).

to be mutated in order for the ARF7 protein not be SUMOylated. Hence, *ARF7* appears to be a target for SUMOylation.

4.2.4 *ARF7* controls LR hydropatterning via SUMOylation

To assess whether the non-SUMOylatable *ARF7* (4xKR) sequence can rescue *arf7-1* LR hydropatterning, a transgene was engineered. Given the importance of the first intron for *ARF7* expression (Chapter 3), a genomic based *ARF7* transgene was generated (Fig.

4.9) (Rose *et al*., 2008 and Park *et al*., 2014). Initially, two fragments were created that used: the 'longer' promoter (-2973bp to +374bp) incorporating the first exon and first intron (Chapter 3), plus *ARF7* (WT) and (4xKR) CDS (Fig. 4.9) (A). An overlapped PCR reaction joined the two fragments, 'longer' promoter (first exon and first intron) with either the *ARF7* (WT) or *ARF7* (4xKR) (Fig. 4.9) (B). This overlapped PCR product was

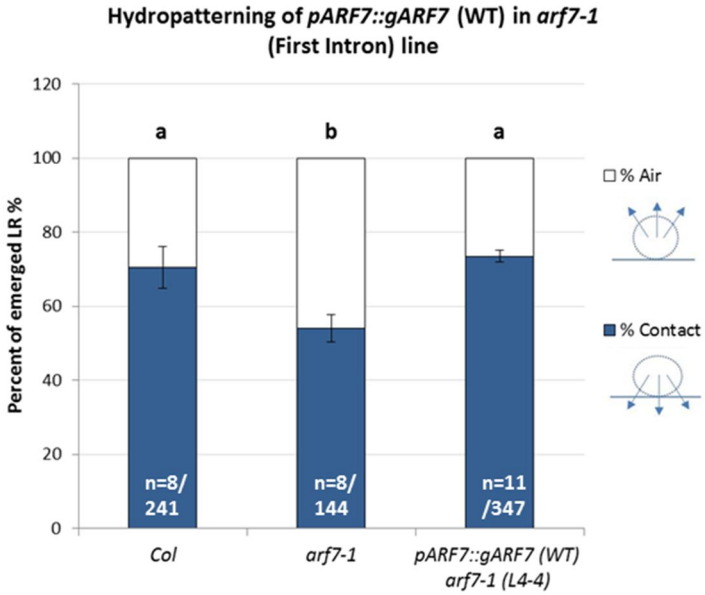


Fig. 4.10: **The WT *ARF7* transgene can rescue the *arf7* LR hydropatterning defect**. WT (Col-0) *Arabidopsis* roots and the *pARF7::gARF7 arf7-1* (WT) (L4-4) transgenic line exhibited a normal LR hydropatterning response that was severely disrupted by the *arf7-1* loss of function mutant allele. There was a greater distribution of emerged LRs towards the contact side in the *pARF7::gARF7 arf7-1* (WT) (L4-4) transgenic line compared to the *arf7-1* loss of function mutant. Hence, the *arf7-1* LR hydropatterning defect was rescued by the *pARF7::gARF7 arf7-1* (WT) (L4-4) transgenic line. Data shown is mean values ± S. E, (n = number of seedlings/number of LRs analysed). Statistical differences were analysed on the percent of emerged LRs emerging towards either contact (including horizontal) or air using a Tukey HSD test (P<0.05); statistically similar groups are indicated using the same letter. Biological replicates (1=5) were performed.

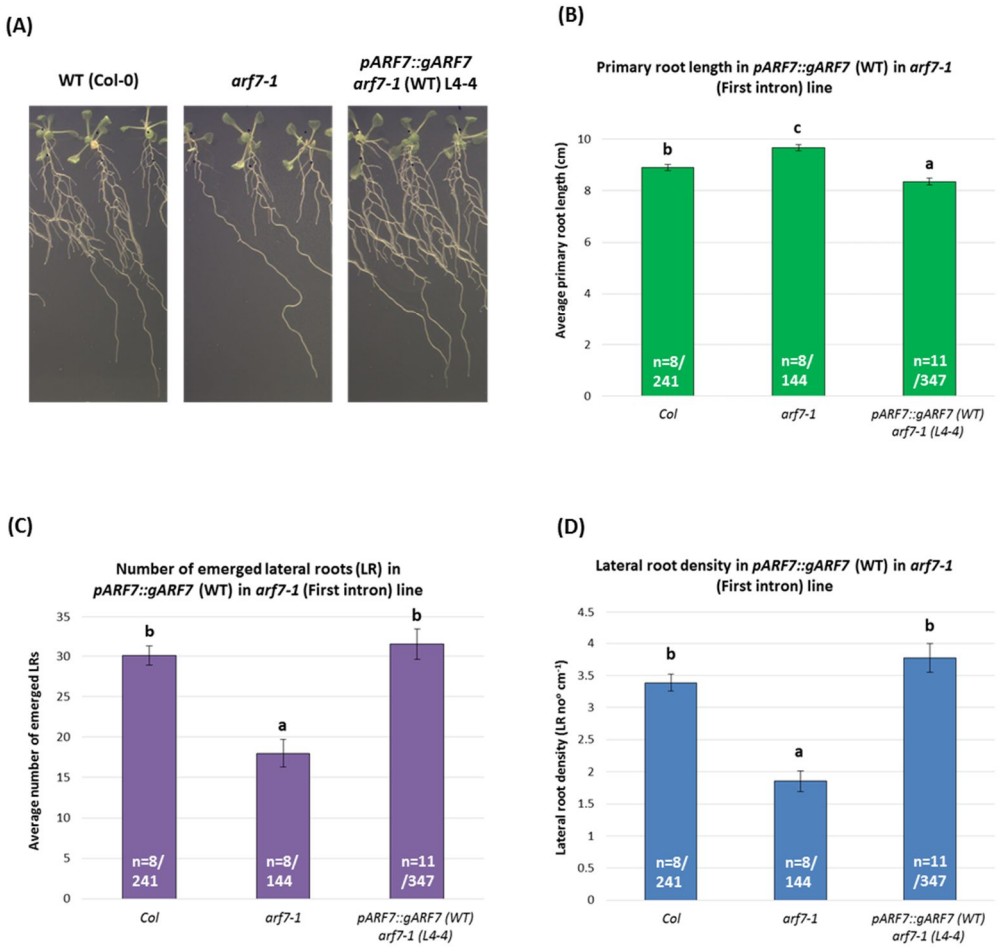


Fig. 4.11: SUMOylated *ARF7* (WT) is functional. Compared to WT (Col-0) *Arabidopsis* roots the *pARF7::gARF7 arf7-1* (WT) (L4-4) transgenic line appeared the same (A). Although, there was a slight reduction (0.5 cm) in primary root length observed (B). In relation to *arf7-1*, the *pARF7::gARF7 arf7-1* (WT) (L4-4) transgenic line displayed twice the amount of LRs thereby rescuing the phenotype (C). When compared to WT (Col-0) though, there was no obvious difference in LR number. The *pARF7::gARF7 arf7-1* (WT) (L4-4) transgenic line had a marginal increase in LR density in relation to WT (Col-0) roots (D). Data shown is mean values ± S. E, (n = number of seedlings/number of LRs analysed). Significant differences were analysed using the Tukey HSD test (P<0.05); statistically similar groups are indicated using the same letter. Biological replicates (1=5) were performed.

used to generate *pARF7::gARF7* (WT and 4xKR) pENTRY Gateway (Box 1) constructs (Fig. 4.9) (C). The resulting *pARF7::gARF7* (WT and 4xKR) transgenic lines (Fig. 4.9) (D) were engineered in the *arf7-1* background.

Interestingly, the *pARF7::gARF7 arf7-1* (WT) transgenic line was able to fully rescue LR hydropatterning (Fig. 4.10).

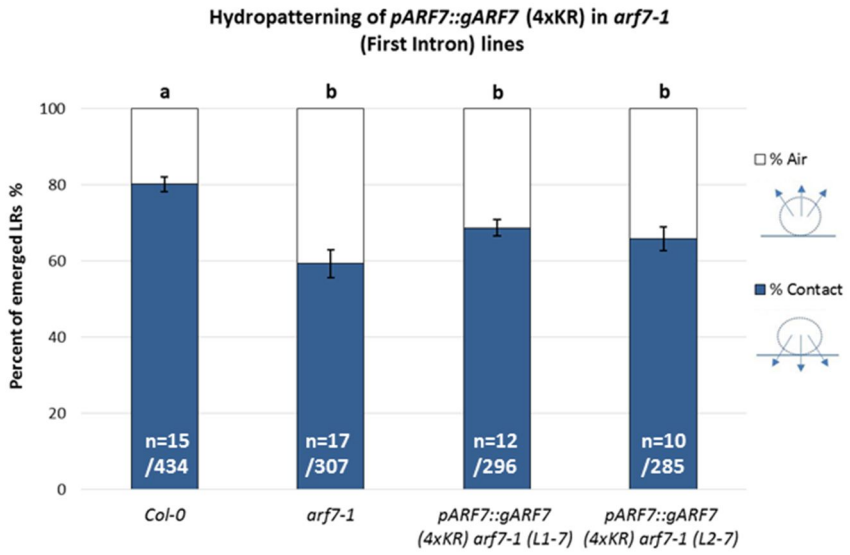
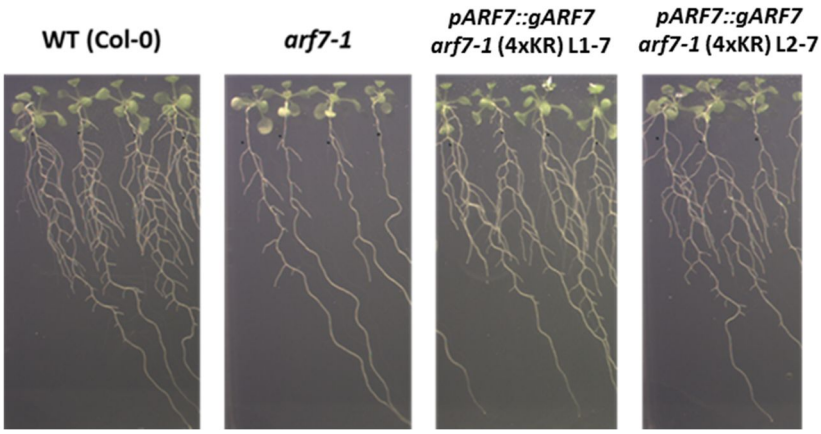
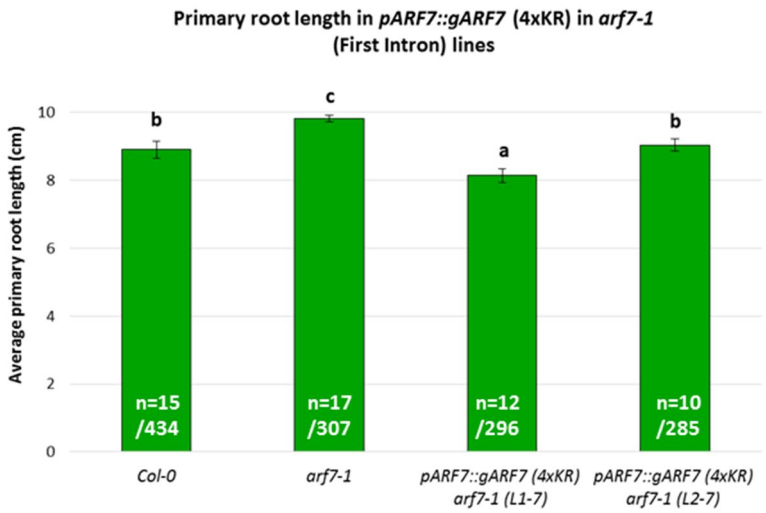


Fig. 4.12: *ARF7* SUMOylation is required for LR hydropatterning. WT (Col-0) *Arabidopsis* roots exhibit a LR hydropatterning response that is disrupted by *pARF7::gARF7 arf7-1* (4xKR) L1-7, L2-7 transgenic lines and *arf7-1* loss of function mutant. In fact, all these lines displayed almost identical responses. The percent of LRs emerging towards the air side in both *pARF7::gARF7 arf7-1* (4xKR) L1-7 and L2-7 transgenic lines was far greater than that seen by WT (Col-0) roots. Hence, the *pARF7::gARF7 arf7-1* (4xKR) results suggested that *ARF7* SUMOylation was a necessity for LR hydropatterning. Data shown is mean values ± S. E, (n = number of seedlings/number of LRs analysed). Statistical differences were analysed on the percent of emerged LRs emerging towards either contact (including horizontal) or air using a Tukey HSD test ($P<0.05$); statistically similar groups are indicated using the same letter. Biological replicates (1=5) were performed.

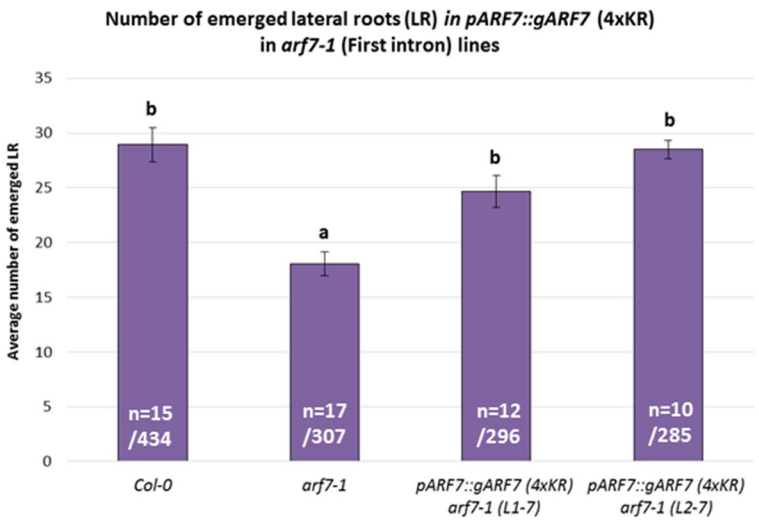
(A)


WT (Col-0)
arf7-1
pARF7::gARF7 arf7-1 (4xKR) L1-7
pARF7::gARF7 arf7-1 (4xKR) L2-7

(B)


Primary root length in pARF7::gARF7 (4xKR) in arf7-1 (First Intron) lines
Average primary root length (cm)
0
2
4
6
8
10
b
c
a
b
n=15 /434
n=17 /307
n=12 /296
n=10 /285
Col-0
arf7-1
pARF7::gARF7 (4xKR) arf7-1 (L1-7)
pARF7::gARF7 (4xKR) arf7-1 (L2-7)

(C)


Number of emerged lateral roots (LR) in pARF7::gARF7 (4xKR) in arf7-1 (First intron) lines
Average number of emerged LR
0
5
10
15
20
25
30
35
b
a
b
b
n=15 /434
n=17 /307
n=12 /296
n=10 /285
Col-0
arf7-1
pARF7::gARF7 (4xKR) arf7-1 (L1-7)
pARF7::gARF7 (4xKR) arf7-1 (L2-7)

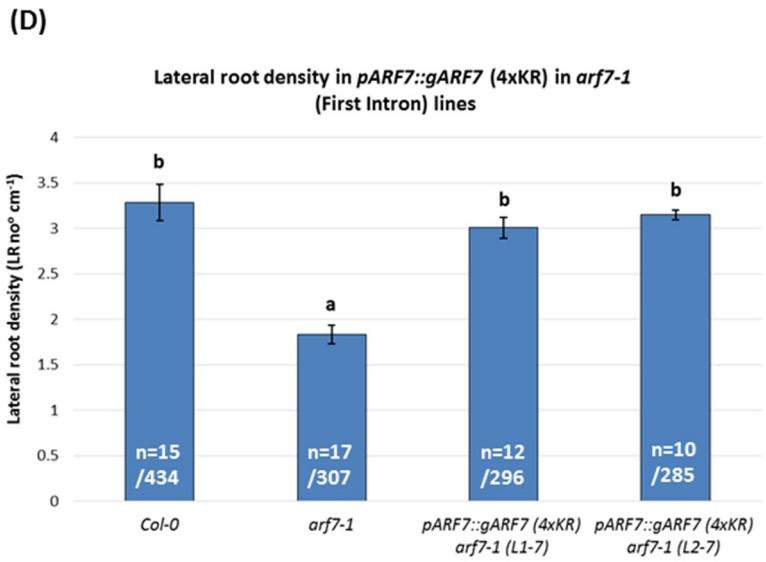


Fig. 4.13: Non-SUMOylatable *ARF7* is functional. Compared to WT (Col-0) *Arabidopsis* roots the *pARF7::gARF7 arf7-1* (4xKR) L1-7 and L2-7 transgenic lines appeared very similar (A). Although, the *pARF7::gARF7 arf7-1* (4xKR) L1-7 transgenic line exhibited marginal differences compared to L2-7. Hence, there was a significant reduction in primary root length observed (B). Whereas, the *pARF7::gARF7 arf7-1* (4xKR) L1-7 transgenic line was comparable with WT (Col-0) (B). In relation to *arf7-1*, the *pARF7::gARF7 arf7-1* (4xKR) (L2-7) transgenic line exhibited double the amount of LRs thereby rescuing the phenotype (C). On the other hand, the *pARF7::gARF7 arf7-1* (4xKR) (L1-7) transgenic line was able to rescue LR number but not to the same extent (C). Compared to WT (Col-0) though, there was a significant decrease in LR number. Although there was no impact on LR density for both *pARF7::gARF7 arf7-1* (4xKR) L1-7 and L2-7 transgenic lines (D). Data shown is mean values ± S. E, (n = number of seedlings/number of LRs analysed). Significant differences were analysed using the Tukey HSD test (P<0.05); statistically similar groups are indicated using the same letter. Biological replicates (1=5) were performed.

At least 70% of the emerged LRs were patterning towards the contact (rather than the air) side, unlike the *arf7-1* mutant. In addition, the *pARF7::gARF7 arf7-1* (WT)

transgene rescued the *arf7-1* LR related phenotypes (**Fig. 4.11**). In contrast, the *pARF7::gARF7 arf7-1* (4xKR) transgene failed to rescue LR

hydropatterning (**Fig. 4.12**). Two independent *pARF7::gARF7 arf7-1* (4xKR) transgenic lines (L1-7 and L2-7) both exhibited a similar LR hydropatterning response to the *arf7-1* mutant. The distribution of LRs emerging towards the air (35%) side was far greater than that seen by WT (Col-0) roots (20%), and more akin to *arf7-1*.

However unlike the *arf7-1* mutant, both LR number and LR density were restored in *pARF7::gARF7 arf7-1* (4xKR) (L1-7 and L2-7) transgenic lines (**Fig. 4.13**). Compared to WT (Col-0) though, the *pARF7::gARF7 arf7-1* (4xKR) transgenic line L1-7 displayed a slight reduction in LR number, although this did not affect LR density (**Fig. 4.13**) (**B to D**). Hence, whilst the ARF7 (4xKR) protein was functional and able to restore LR development, it was no longer able to rescue LR hydropatterning. This result was consistent with a regulatory role for SUMOylation during this root adaptive response.

4.3 DISCUSSION

Protein SUMOylation is known to play an important role during responses to environmental challenges, such as drought stress (Conti *et al*., 2008 and 2014). My results suggest that SUMOylation is also likely to play a key role during a LR hydropatterning response. The *ots1 ots2* mutant lacking these SUMO proteases exhibit a strong hydropatterning defect akin to the *arf7* mutant alleles. Consistent with *ARF7* being a target for *OTS1* mediated de-SUMOylation, pull down assays revealed that OTS1 can interact with ARF7 (Prof. Ari Sadanandom, personal communication). In addition, *ARF7* was shown to be a target for SUMOylation. Most compellingly, mutating all four SUMOylation sites in an *ARF7* transgene (termed 4xKR) abolished its

ability to rescue the *arf7* LR hydropatterning defect. Hence, ARF7 post-translational modifications by SUMO is therefore important for LR hydropatterning.

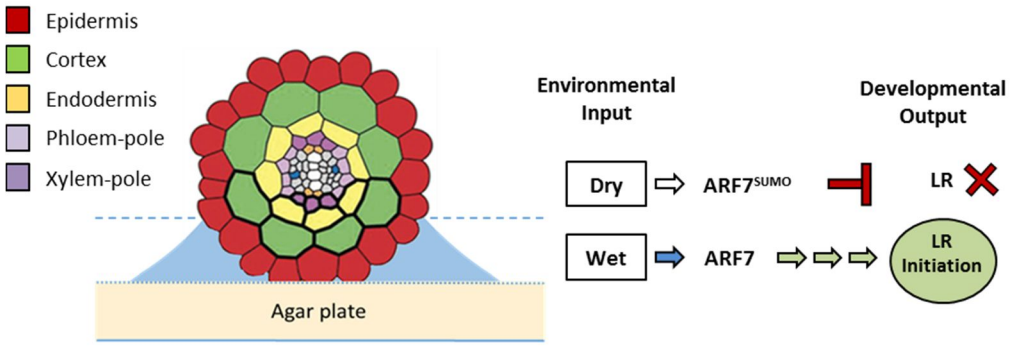


Fig. 4.14: Schematic representation of LR hydropatterning regulation via *ARF7* SUMOylation. Current model devised to depict what is happening to *ARF7* on either the dry or contact sides of the root. On the dry side, there is an accumulation of SUMOylated *ARF7* preventing growth. Whereas, non-SUMOylated *ARF7* on the contact side results in normal LR initiation.

SUMOylated *ARF7* is likely to cause protein inactivation during a LR hydropatterning stimulus, resulting in reduced LR development on the dry side of the root (Fig. 4.14). Consistent with this model, *ARF7* (4xKR) exhibits higher promoter affinity and auxin inducible gene expression (data not shown). So, why does SUMOylation of *ARF7* cause protein inactivation? During LR development the activity of *ARF7* is negatively regulated by Aux/IAA repressor proteins (Goh *et al*., 2012 and reviewed in Lavenus *et al*., 2015).

To determine if SUMOylation influences the interaction between *ARF7* and Aux/IAAs, repressor proteins IAA14/SLR and IAA3/SHY2 were examined. Pull down assays with Aux/IAA repressors IAA14 and IAA3 revealed that the ARF7-IAA3 interaction was

dependent on *ARF7*-SUMOylation (Fig. 4.15 and 4.16). The ARF7 (WT) protein was able to interact with both IAA14/SLR and IAA3/SHY2 repressor proteins. However,

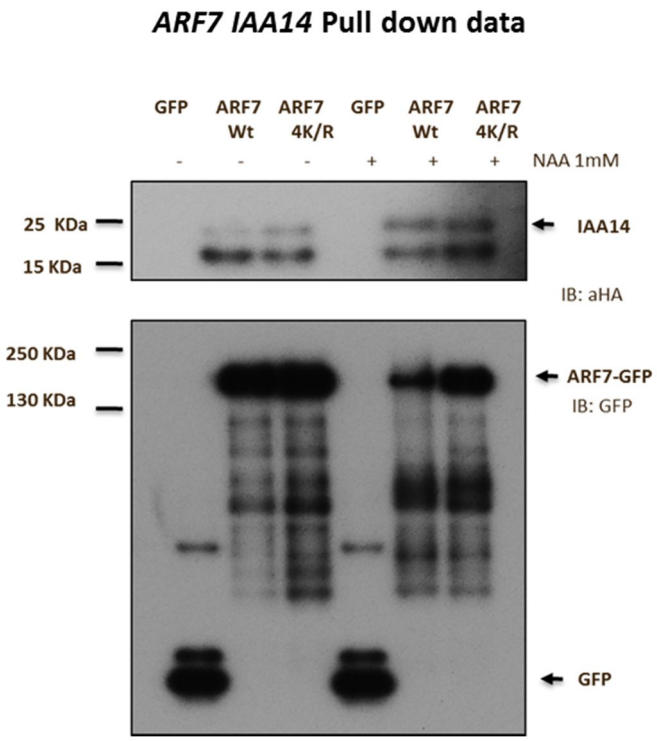


Fig. 4.15: ARF7-SLR/IAA14 interaction is SUMO independent. The initial Co-IP assay revealed that by mutating all SUMO sites (4xKR) *ARF7* can still interact with SLR/IAA14. Hence, independently of SUMOylation. Bands were present in both the WT (*pARF7::ARF7-GFP*) and 4xKR (*pARF7::ARF7-GFP*) with and without auxin (1mM NAA) after probing with anti-IAA14. The second Co-IP revealed that both proteins were present in the WT and 4xKR samples (Images from Prof. Ari Sadanandom *et al*, The University of Durham).

there was a significantly reduced ability in the *pARF7::ARF7-GFP* (4xKR) to pull down the IAA3/SHY2 protein. Whereas in contrast, the IAA14/SLR repressor protein was pulled down by pARF7::ARF7-GFP (4xKR) , akin to the ARF7 (WT) protein. Hence, the interaction between ARF7 and IAA14/SLR was independent of ARF7-SUMOylation.

IAA3/SHY2 (but not *IAA14/SLR*) was found to contain a SUMO interaction motif (SIM) (Prof. Ari Sadanandom, personal communication). Hence, the interaction between SUMOylated ARF7 and SHY2 proteins may be dependent on this SIM motif. Interestingly, mutating the IAA3/SHY2 SIM site disrupted its ability to interact with *ARF7*. Using the endodermal specific *CASP1* promoter, *SHY2* transgenic lines were engineered with and without the mutated SIM motif.

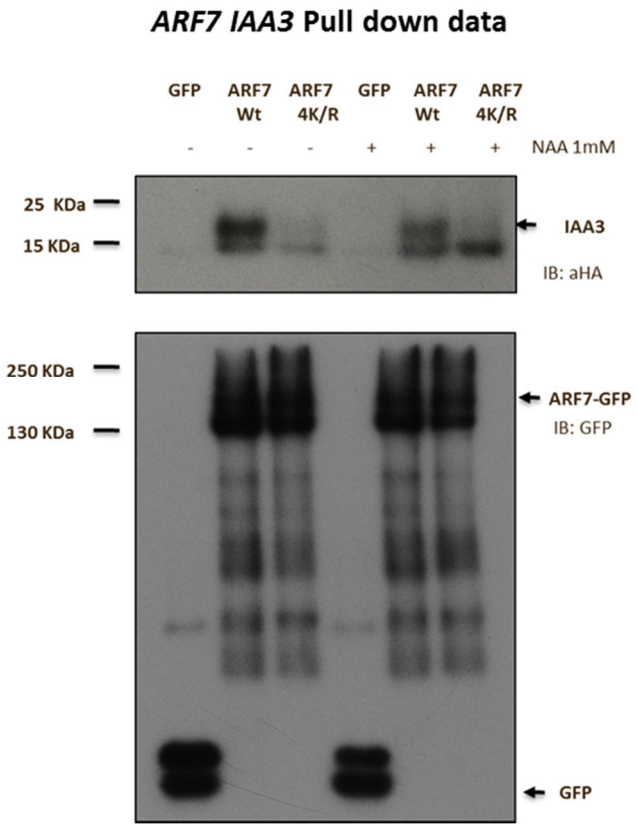


Fig. 4.16: ARF7-IAA3/SHY2 interaction is SUMO dependent. The initial Co-IP assay revealed that by mutating all SUMO sites (4xKR) *ARF7* cannot still interact with IAA3/SHY2. Hence, it is dependently on SUMOylation. Bands were present in WT (*pARF7::ARF7-GFP*) but not for 4xKR (*pARF7::ARF7-GFP*) with and without auxin (1mM NAA) after probing with anti-IAA3. The second Co-IP revealed that both proteins were present in the WT and 4xKR samples (Images from Prof. Ari Sadanandom *et al*, The University of Durham).

Intriguingly, mutating the IAA3/SHY2 SIM site in *pCASP1::shy2-2* (-SIM) (V/A) transgenes rescued LR initiation, akin to WT (Col-0) roots (Fig. 4.17). Whereas, the *pCASP1::shy2-2* (+SIM) (WT) transgenic lines exhibited a LR initiation defect.

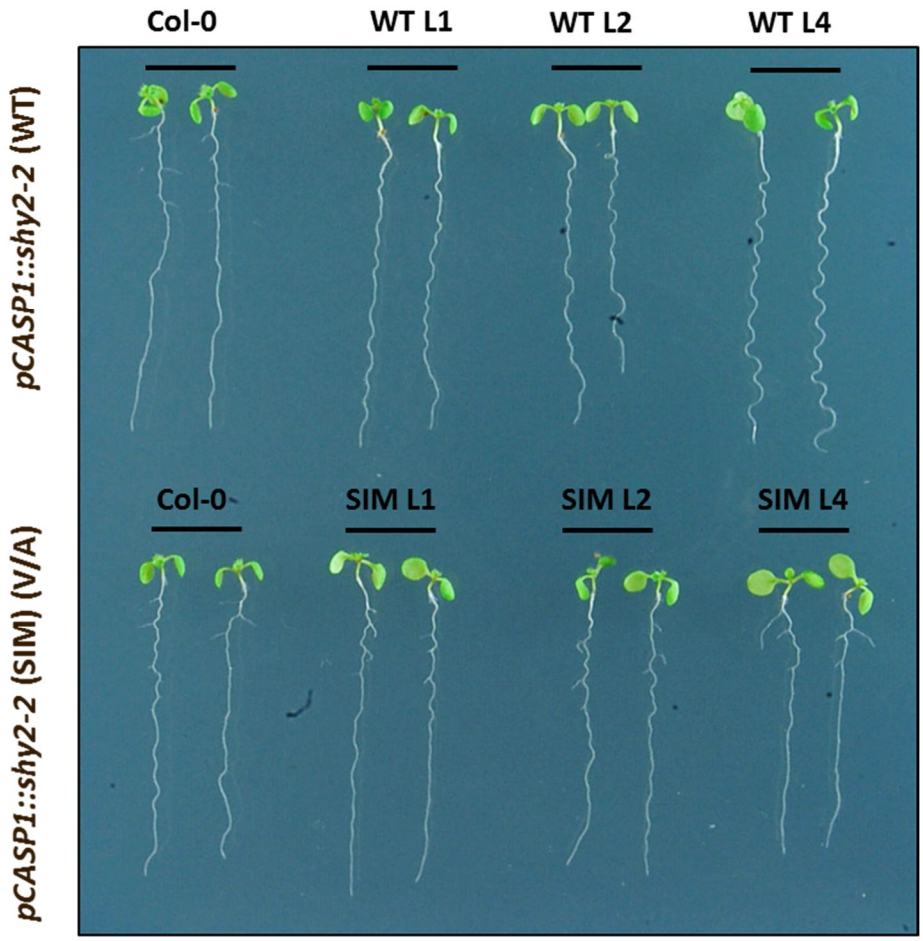


Fig. 4.17: Shy2-2 repression of LR initiation is dependent on the IAA3 SIM motif. Compared to WT (Col-0), *pCASP1::shy2-2* (no SIM) (V/A) transgenic lines no longer exhibited a LR initiation defect. In contrast, the *pCASP1::shy2-2* (SIM) (WT) displayed a LR initiation defect resulting in no emerged LRs. This suggested that the ability of IAA3/SHY2 to regulated LR development was dependent on the SIM domain (Image from Prof. Ari Sadanandom *et al*, The University of Durham).

This suggested that the ability of *IAA3/SHY2* to regulate LR development was dependent on the SIM domain. Hence, *IAA3* recruitment appears dependent on *ARF7*-SUMOylation and likely to control LR hydropatterning.

Chapter 5: DOWNSTREAM TARGETS OF *ARF7* EXHIBIT HYDROPATTERNING DEFECTS

Author list:

Nicola Leftley – Figures 5.1, 5.2, 5.4, 5.5, 5.7, 5.8, 5.9,

Daniel Von Wangenheim (Contributed data) and Nicola Leftley – Figure 5.3, 5.6

Chapter 5: DOWNSTREAM TARGETS OF *ARF7* EXHIBIT HYDROPATTERNING DEFECTS

5.1 INTRODUCTION

It has been revealed that roots have the ability to distinguish between wet and dry environments and as a result adapt the positioning of lateral root branches (Bao *et al*., 2014). LR hydropatterning is a newly discovered adaptive mechanism for adjusting root branching in relation to the local variations in water availability (Bao *et al*., 2014). Whereby LRs form primarily on the side of the root that is in direct contact with water. Growing roots vertically on the surface of an agar plate can mimic a similar adaptive response that is exhibited in soil (reviewed in Morris *et al*., 2017). This results in an asymmetric distribution of water that causes the formation of a meniscus on opposite sides of the root. Thereby, the root is either exposed to direct contact with moisture or the air.

The plant hormone auxin co-ordinates all aspects of plant development from the tip of the root to the shoot. The complex interplay between auxin biosynthesis, transport and signalling initiates LR formation (Overvoorde *et al*., 2010). It was determined that there were higher levels of auxin detectable on the contact side as opposed to the air (Bao *et al*., 2014). Thereby suggesting that auxin biosynthesis is moisture induced. Differences in the asymmetric moisture environment is known to trigger an auxin response gradient across the radius of the root resulting in LRP forming predominately on the contact side (Bao *et al*., 2014). Hence, an auxin response gradient appears to be regulated by a LR hydropatterning stimulus.

The auxin response factor *ARF7* was found to be important for LR hydropatterning. Overexpressing the *ARF7* gene rescued the LR hydropatterning defect exhibited by *arf7-1* loss of function mutant alleles. Hence, *ARF7* regulated the LR hydropatterning

stimulus post translationally. One possible post translational mechanism was SUMOylation. This mechanism has emerged as a major regulator of protein function during environmental stresses such as drought (Conti *et al*., 2009). *ARF7* was found to be a target for SUMOylation and exhibited four highly conserved SUMO domains. Mutating all four SUMO motifs in *pARF7::gARF7* (4xKR) *arf7-1*, was not able to restore the *arf7* LR hydropatterning defect. Whereas, the *pARF7::gARF7* (WT) *arf7-1* fully complimented *arf7* LR hydropatterning response and LR development. Hence, the post-translational modifications of ARF7 by SUMOylation are important for LR hydropatterning. During a LR hydropatterning stimulus, an accumulation of SUMOylatable *ARF7* occurs on the dry side of the root preventing LR initiation. Whereby, *ARF7* SUMOylation functions to inactivate transcriptional activation. However, it is unclear which genes are targets for *ARF7* regulation during a LR hydropatterning response. This chapter will examine *ARF7* targets and determine if they play a part in LR hydropatterning.

5.2 RESULTS

5.2.1 *LBD16* is a target for *ARF7* and required for LR hydropatterning

ARF7 plays a major role in the regulation of a wide selection of early auxin responsive genes (Okushima *et al*., 2005). A number of downstream targets of *ARF7* have been identified in the lateral root regulatory network (Lavenus *et al*., 2015). Several of the *LBD* transcription factor family represent direct targets for *ARF7*. To examine their importance during LR hydropatterning, *LBD* knockout lines were analysed. Interestingly, it was revealed that the *lbd16-2* loss of function mutant exhibited a striking LR hydropatterning response compared to WT (Col-0) roots (**Fig. 5.1**) (**A**). Instead of biasing LRs towards the contact side, the *lbd16-2* loss of function mutant

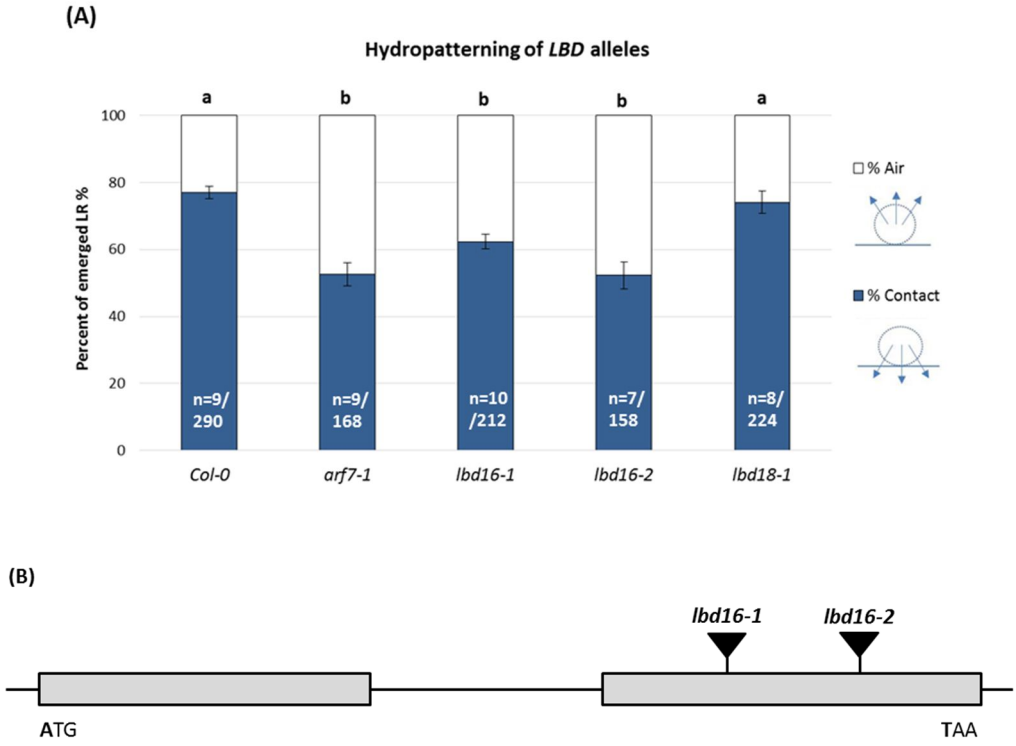


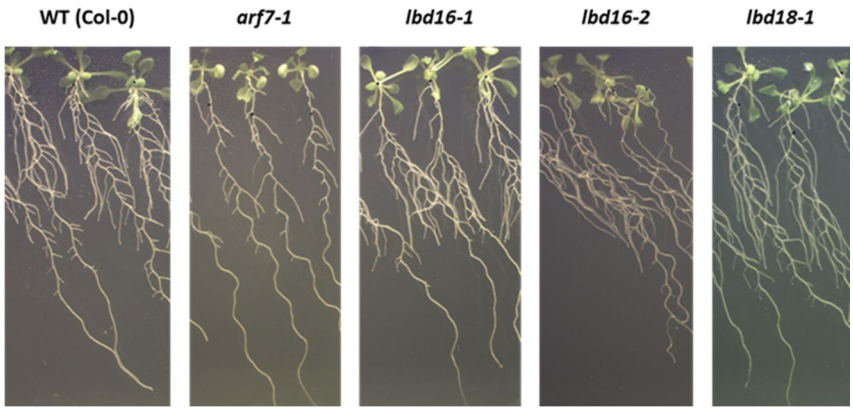
Fig. 5.1: *LBD16* is involved in LR hydropatterning. WT (Col-0) *Arabidopsis* roots exhibit a LR hydropatterning response that was disrupted by *lbd16* loss of function mutant alleles. Both *lbd16-1* and *lbd16-2* loss of function mutant alleles displayed very similar responses to the *arf7-1* loss of function mutant. There was a sporadic patterning of LRs rather than a bias towards the contact side. On the other hand, the *lbd18-1* loss of function mutant resembled WT (Col-0). Data shown is mean values ± S. E, (n = number of seedlings/number of LRs analysed). Statistical differences were analysed on the percent of emerged LRs emerging towards either contact (including horizontal) or air using a Tukey HSD test ($P<0.05$); statistically similar groups are indicated using the same letter. Biological replicates (1=5) were performed (A). Schematic representation of the *LBD16* domain structure specifying *lbd16* alleles. *LBD16* gene (At2g42430) (1985bp) and the positioning of *lbd16* mutations: *lbd16-1* (Salk_095791) (2nd Exon) and *lbd16-2* (Salk_040739) (2nd Exon). The location of the start (**A**TG) and stop (**T**AA) codons have been indicated. Exons (boxes) and introns (lines) were determined by comparing the full length DNA sequence with that of nucleotide sequences of *lbd16* mutant alleles (https://www.arabidopsis.org) (B).

displayed a randomised patterning of LRs from all sides of the PR. In fact, the *lbd16-2* mutant displayed almost identical results to that of the *arf7-1* loss of function mutant. The percent of LRs emerging towards the air sides (50%) was far greater than that seen by WT (Col-0) roots (22%). Another independent *lbd16* allele, *lbd16-1* loss of function mutant also exhibited a very similar response to the *arf7-1* mutant (**Fig. 5.1**) (**A**). Even though there was a slight reduction in the percent of LRs emerging towards the air (40%), it was still greater than that seen for WT (Col-0). Hence, it appeared that *LBD16* was important for LR hydropatterning.

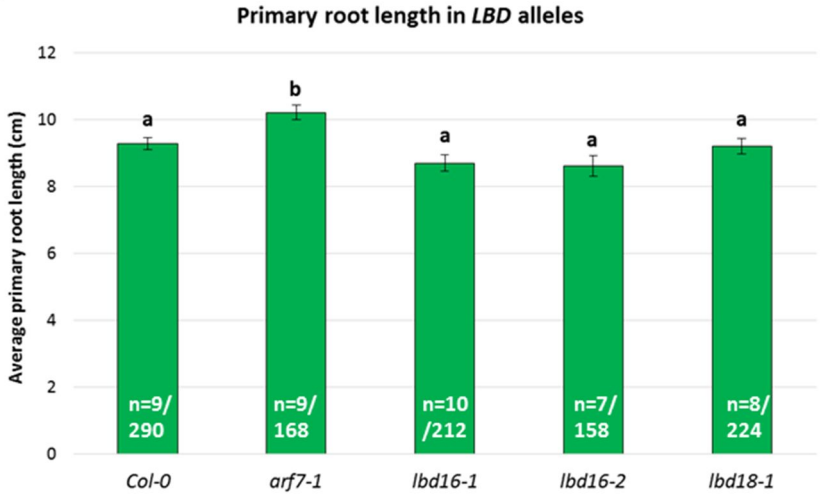
On the other hand, *lbd18-1* presented a similar LR hydropatterning phenotype to WT (Col-0) (**Fig. 5.1**) (**A**), where the distribution of LRs emerging from either the air (25%) or contact (75%) side was almost identical (**Fig. 5.1**) (**A**). Therefore, this suggested that *LBD18* was not important for LR hydropatterning. It has been well documented that both *LBD16* and *LBD18* are downstream targets of *ARF7* (Goh *et al*., 2012 and Lee *et al*., 2009). Both *lbd16* and *lbd18* loss of function mutant alleles display a reduced LR density similar to the *arf7-1* mutant (**Fig. 5.2**). In fact, both *LBD16* and *LBD18* are involved in LR formation, at the point of initiation and emergence (Lee *et al*., 2015). Hence, it was not surprising that compared to WT (Col-0), both *lbd16* loss of function mutants displayed a significantly reduced number of LRs (**Fig. 5.2**) (**C**). This was also evident with the *lbd18-1* loss of function mutant, but to a lesser extent. Therefore, our results suggest that *LBD16* and *LBD18* were both important for LR initiation, but only *LBD16* was important for LR hydropatterning.

Given the importance of *ARF7* to directly control the expression of many LR regulatory genes including *LBD16*, *Arabidopsis* roots expressing a *LBD16* reporter exposed to a hydropatterning stimulus were imaged. In order to determine exactly where *LBD16* expression was detected along the root, a functional *pLBD16::gLBD16-GFP* reporter

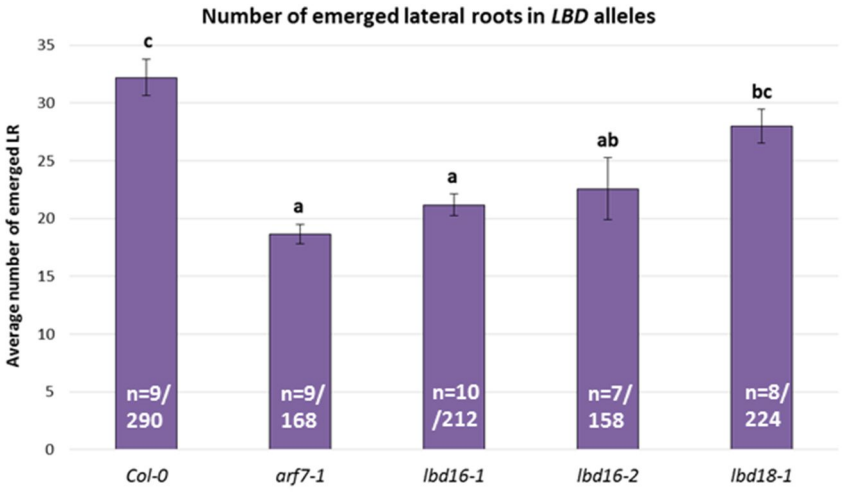
(A)


WT (Col-0)
arf7-1
lbd16-1
lbd16-2
lbd18-1

(B)


Primary root length in LBD alleles
Average primary root length (cm)
12
10
8
6
4
2
0
a
b
a
a
a
n=9/ 290
n=9/ 168
n=10 /212
n=7/ 158
n=8/ 224
Col-0
arf7-1
lbd16-1
lbd16-2
lbd18-1

(C)


Number of emerged lateral roots in LBD alleles
Average number of emerged LR
35
30
25
20
15
10
5
0
c
a
a
ab
bc
n=9/ 290
n=9/ 168
n=10 /212
n=7/ 158
n=8/ 224
Col-0
arf7-1
lbd16-1
lbd16-2
lbd18-1

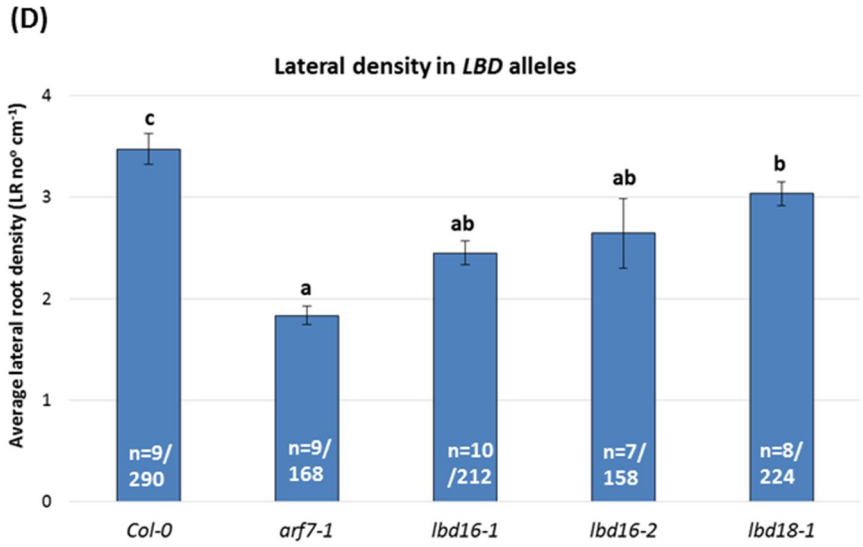


Fig. 5.2: ***LBD16* and *LBD18* have marked reductions in LRs.** Compared to WT (Col-0) *Arabidopsis* roots, the *lbd18-1* loss of function mutant phenotype appeared the same (A). On the other hand, there were fewer LRs observed in the *lbd16* loss of function mutant alleles (A). Primary root length was slightly enhanced in *lbd18-1* to that of WT (Col-0) compared to the *lbd16* loss of function mutant alleles (B). In contrast to the WT (Col-0), *lbd16-1*, *lbd16-2* and *lbd18-1* loss of function mutant alleles displayed a reduced number of LRs (C). This was more evident for the *lbd16* loss of function mutant alleles that had a similar LR number to *arf7-1*. The decrease in LR number had a marked effect on LR density for the *LBD* loss of function mutant alleles (D). Data shown is mean values ± S. E, (n = number of seedlings/number of LRs analysed. Significant differences were analysed using the Tukey HSD test (P<0.05); statistically similar groups are indicated using the same letter. Biological replicates (1=5) were performed.

was imaged using confocal microscopy. An asymmetric pattern of *gLBD16-GFP* expression was first observed in the late elongation zone within the root (**Fig. 5.3**) (**A**). Prior to this, there was no signal observed in the RAM. As described in **Chapter 3**, to image reporter expression following a LR hydropatterning stimulus (**Results: 3.2.1**) *LBD16* reporter roots were screened from multiple angles using a Light sheet

fluorescent microscope (LSFM). Intriguingly, reconstructed root images revealed that the *pLBD16::gLBD16-GFP* reporter was differentially expressed in xylem pole pericycle cells files orientated towards the contact side (**Fig. 5.3**) (**B and C**). It is known that *LBD16* is expressed in FCs, prior to LR initiation (Goh *et al*., 2012). Hence, confocal and LSFM imaging of the *LBD16* reporter revealed that its expression was differentially expressed in the root elongation zone, suggesting that *LBD16* regulated hydropatterning from a very early stage of LR development (i.e. prior to pericycle cell division).

5.2.2 *SHY2* is important for LR hydropatterning

Another gene that may be involved in LR hydropatterning is *SHY2/IAA3*. It was previously revealed (**Chapter 4**) that Aux/IAA repressor protein IAA3/SHY2 interacted with ARF7 in a SUMO-dependent manner. SHY2/IAA3 contains a SIM motif. Hence, it was suggested that ARF7 interacted with SHY2/IAA3 via this SIM motif. Mutating the SHY2/IAA3 SIM site disrupted ARF7 interactions (**Chapter 4**). *In Planta*, it was established that *SHY2/IAA3* was able to regulate LR development with the aid of its SIM domain (**Chapter 4**). Hence, *SHY2*/*IAA3* recruitment appears dependent on *ARF7*-SUMOylation and may control LR hydropatterning. To determine if *SHY2/IAA3* does control *ARF7* LR hydropatterning, a loss of function mutant allele was characterised.

Consistent with our model, the LR hydropatterning response was disrupted in the *shy2-31* loss of function mutant allele. The *shy2-31* mutant exhibited the same LR hydropatterning defect response as *lbd16-2* and *arf7-1* loss of function mutant alleles (**Fig. 5.4**) (**A**). The *shy2-31* mutant (Knox *et al*., 2003) exhibited a higher percent of LRs emerging from the air (50%) and contact (50%) sides compared to WT (L*er*). Hence, *SHY2* appeared important for LR hydropatterning. It is known that *SHY2/IAA3* is

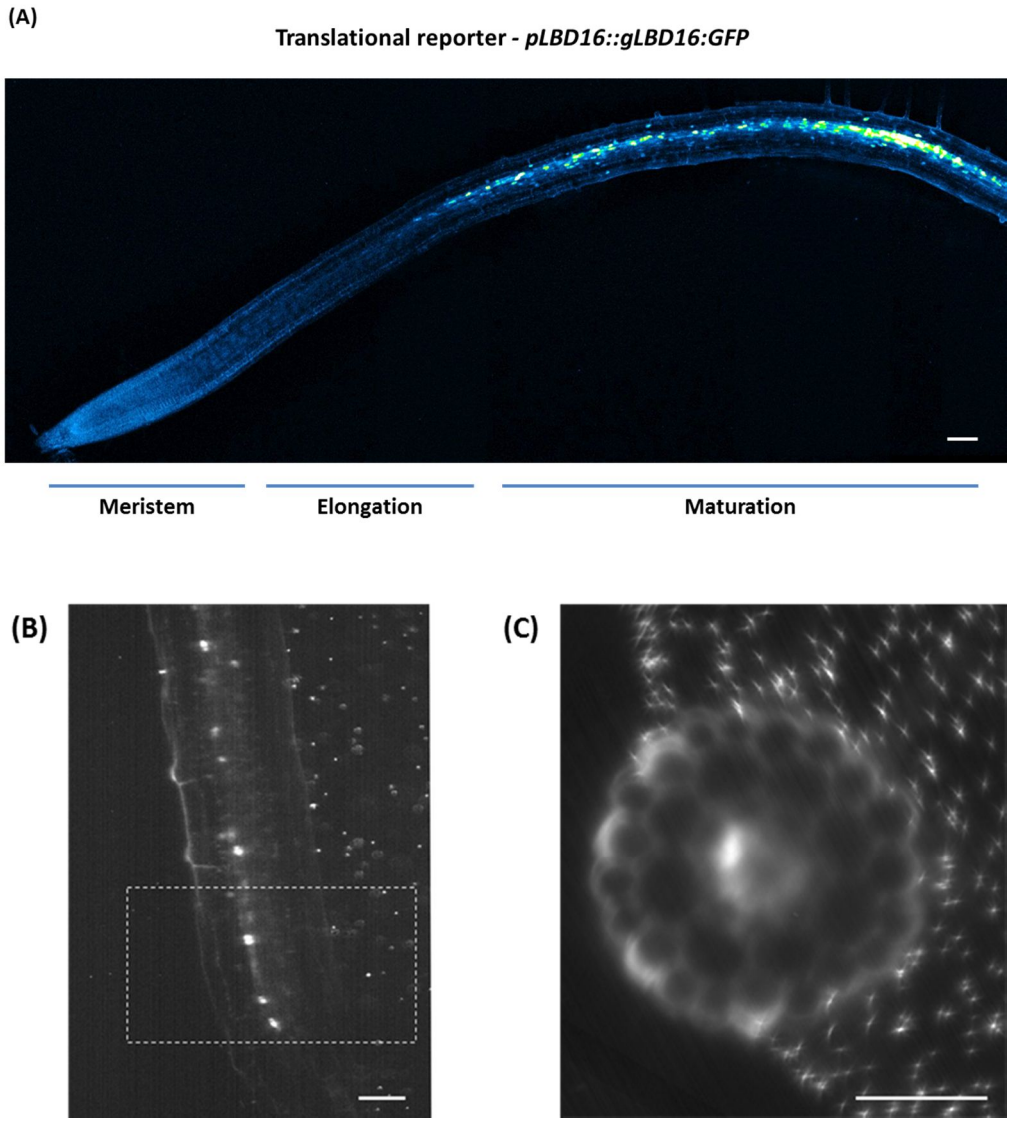
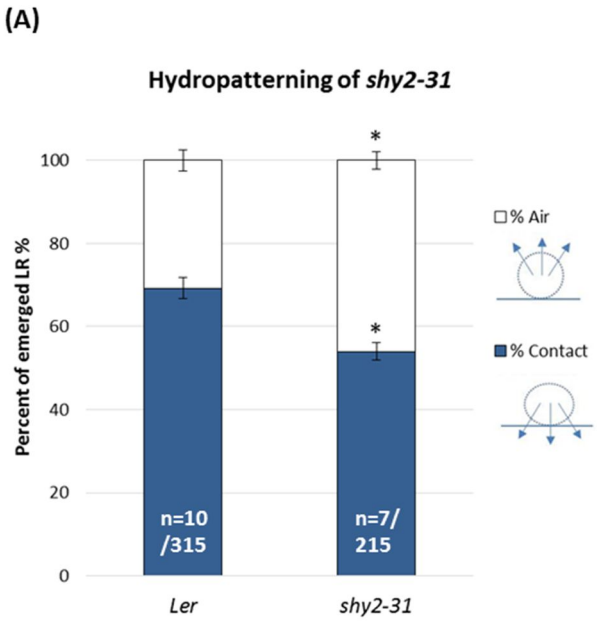
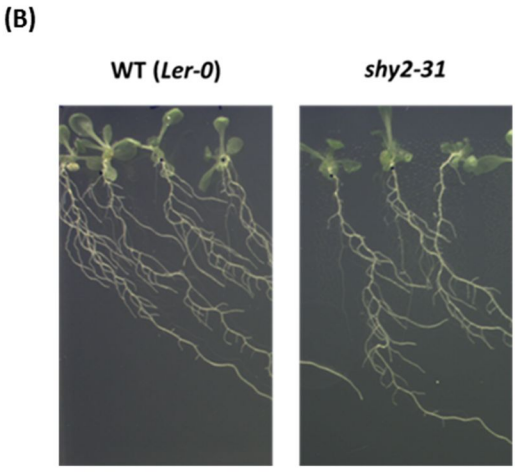
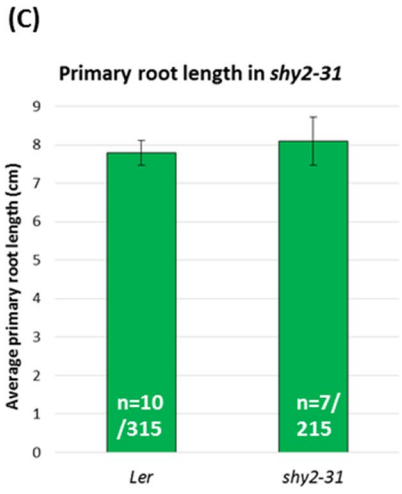


Fig. 5.3: ***LBD16* expression later in the elongation zone.** The *LBD16* (*pLBD16::gLBD16-GFP*) translational reporter exhibited bright GFP expression late in the elongation zone towards the maturation zone within *Arabidopsis* roots. It was evident that no GFP signal was present throughout the meristem and early elongation zones. Nuclei predominantly within the pericycle and stele displayed very clear expression patterns. Image was a maximum projection of confocal image stacks (A). Using the LSFM the *LBD16-GFP* reporter was differentially expressed in xylem-pole pericycle cells files oriented towards the contact side of the root. Fluorescence beads (white specks) depict the air side of the root from the contact side (white box) (B and C). Radial cross section (C). Scale bar – 100 µm (A) and 50 µm (B and C) (Images produced from data generated with Dr Daniel Von Wangenheim, The University of Nottingham).

involved with early stage LR development (Goh *et al*., 2012). The *shy2-2* gain of function mutant allele displayed significant decreased LR emergence although, the number of non-emerged LRP was vastly enhanced (Swarup *et al*., 2008 and Goh *et al*., 2012). In fact, *SHY2/IAA3* was shown to be important not only for LR formation but also LR emergence (Swarup *et al*., 2008 and Vermeer *et al*., 2014).







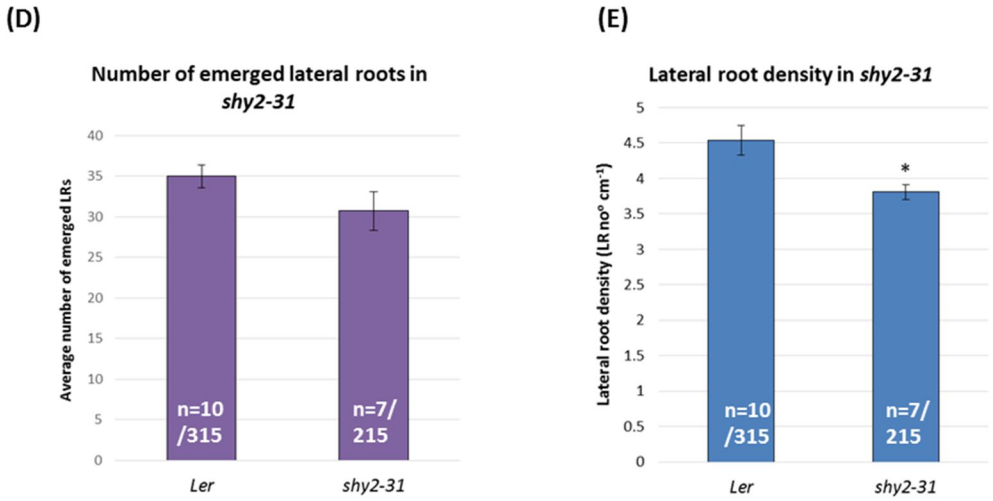


Fig. 5.4: IAA3/*SHY2* is required for LR hydropatterning. WT (L*er*) *Arabidopsis* roots exhibit a LR hydropatterning response that is disrupted by *shy2-31* loss of function mutant. The percent of LRs emerging towards the air side in the *shy2-31* loss of function mutant was greater than that seen by WT (L*er*) roots (A). The *shy2-31* loss of function mutant displayed a similar phenotype to WT (L*er*) roots (B). Primary root length in the *shy2-31* loss of function was also comparable with WT (L*er*) (C). There was a slight difference in LR number observed (D). This reduction in LR number had a significant effect on the LR density for the *shy2-31* loss of function mutant (E). Data shown is mean values ± S. E, (n = number of seedlings/number of LRs analysed). Asterisks indicate a significant difference from that of WT (L*er*) roots based on using a Student *t* test ($p<0.05$). Biological replicates (1=5) were performed.

Visually, it was observed that the *shy2-31* loss of function mutant resembled WT (L*er*) roots (Fig. 5.4) (B). Although, there was a significant difference in LR density revealed (Fig. 5.4). Compared to WT (Ler), the *shy2-31* loss of function mutant exhibited a slight reduction in LR number (Fig. 5.4) (D). Hence, supporting the notion that *SHY2/IAA3* is involved in LR emergence. The LR hydropatterning response presented by *LBD16* and *SHY2/IAA3*, suggest that both *ARF7* targets are important.

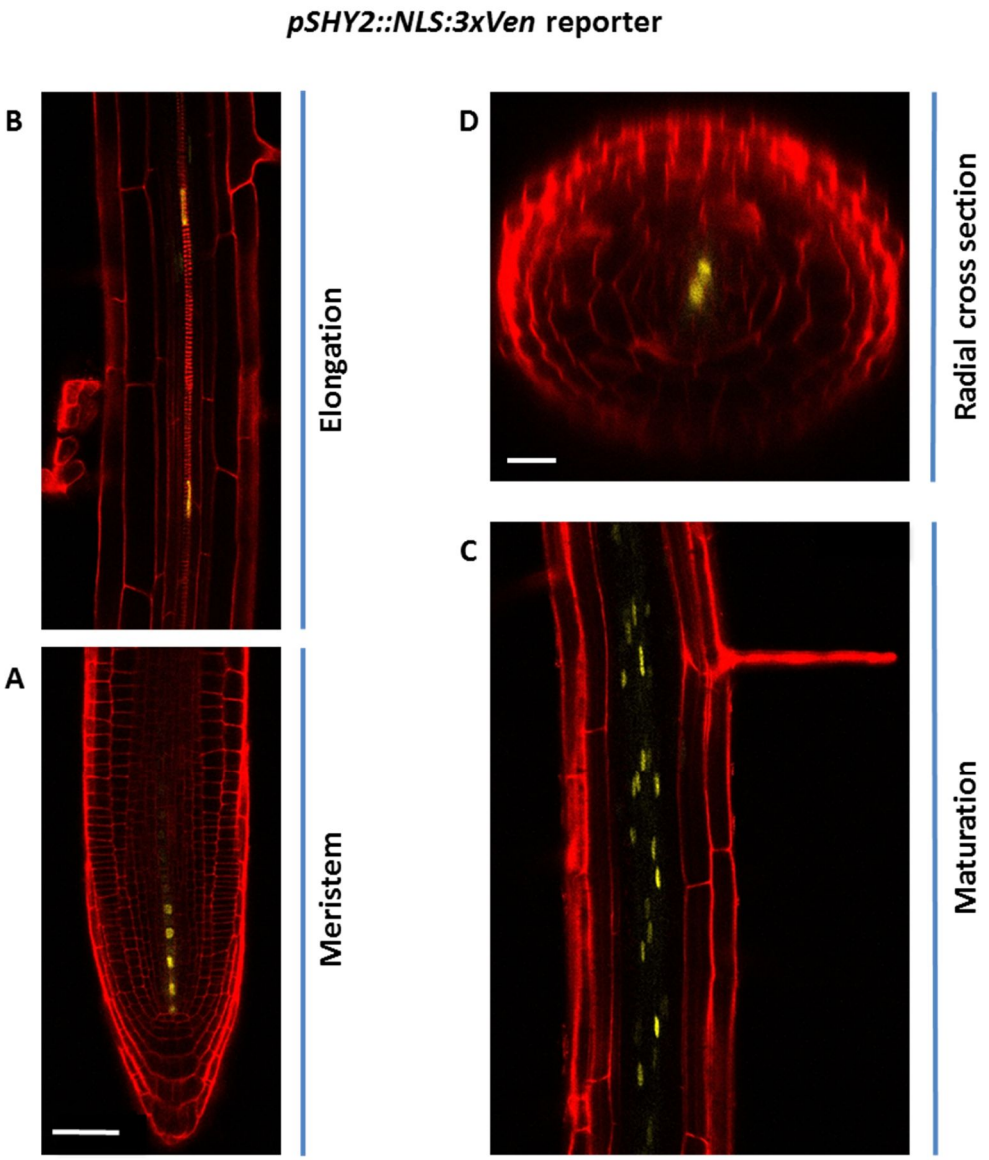


Fig. 5.5: Expression patterns of *pSHY2::NLS:3xVenus* reporter. Confocal images of *pSHY2::NLS:3xVenus* nuclear localised Venus reporter that exhibited Venus expression in nuclei throughout *Arabidopsis* roots. Clear expression patterns were evident everywhere from the RT (A), elongation zone (B) towards the maturation zone (C). Within the meristem and elongation zones, expression was only evident within the vasculature (D). It was also clear that expression was not continuous in the meristem but rather in the RAM (A). It became apparent that higher up the root, in the maturation zone, expression patterns were also visible in the endodermis and pericycle (C). Scale bars – 50 µm (A to C) and 20 µm (D).

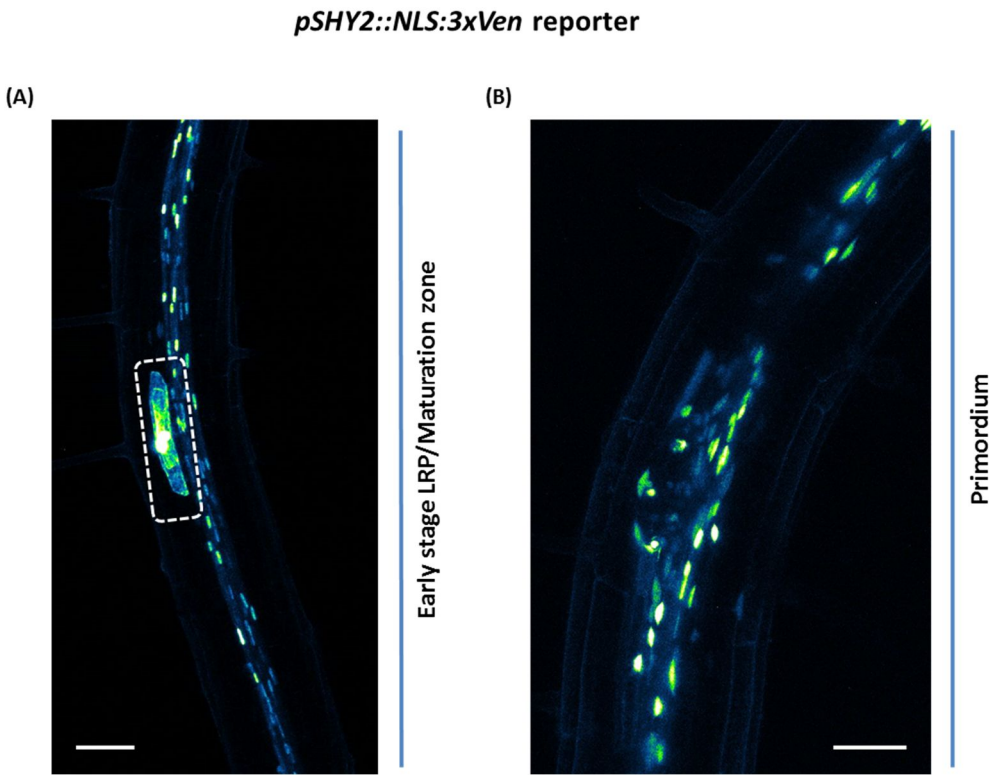


Fig. 5.6: ***pSHY2::NLS:3xVenus*** **expression in primordia.** Confocal images revealed that *pSHY2::NLS:3xVenus* expression was observed within endodermal and pericycle cells in the maturation zone (A). Strong expression was evident in pairs of pericycle cells that make up the LRP (circled in white) (A and B). Expression remains throughout the development of a LRP (B). Scale bars – 50 µm (A) and 100 µm (B) (Images produced from data generated with Dr Daniel Von Wangenheim, The University of Nottingham).

In fact, there is a direct link between *LBD16* and *SHY2IAA3* (Lavenus *et al*., 2015). LR gene regulatory network, has documented *SHY2/IAA3* to be downstream of *LBD16* (Lavenus *et al*., 2015). More interestingly, expression studies using the *SHY2::NLS-3xVenus* reporter have revealed that *SHY2/IAA3* is expressed in nuclei within several different tissues depending on the stage of development (**Fig. 5.5**). In the root meristem, *SHY2/IAA3* was expressed in the stele, then later in the endodermal cells

overlying newly initiated LRP (Fig. 5.5 and Fig. 5.6). Strong *SHY2/IAA3* expression around the pericycle cell layer indicated that it was also in the correct root zone region (Fig. 5.6). However, it is currently unclear exactly which tissue *SHY2/IAA3* may function in to control LR hydropatterning via *ARF7*.

5.2.3 *IAA28* is not important for LR hydropatterning

Like *IAA3/SHY2*, another Aux/IAA gene, *IAA28* also contained a SIM domain. Moreover, mutating the IAA28 SIM motif disrupted ARF7-IAA28 interactions. Hence, it appeared that the IAA28 SIM domain was important for its interaction with SUMOylated *ARF7*. It has been well documented that *IAA28* regulates early stages of LR development (De Rybel *et al*., 2010 and Rogg et al, 2001). In addition, *IAA28* is expressed in the basal meristem where LR hydropatterning is controlled, whilst the *IAA28* gain of function allele, *iaa28-1* disrupts LR development. To test whether *IAA28*, like *IAA3/SHY2*, controls LR initiation and LR hydropatterning *iaa28* gain and loss of function mutant alleles were characterised.

Interestingly, the *iaa28-ko* loss of function mutant exhibited a similar LR hydropatterning response to WT (Col-o) (Fig. 5.7). There was a strong bias of LRs towards the contact side (65%) as opposed to air (35%). Hence, the results from the *iaa28-ko* loss of function mutant revealed that *IAA28* was not important for LR hydropatterning. Although, it was clear that LR emergence was not totally disrupted in the *iaa28-ko* loss of function mutant allele (Fig. 5.8). Compared to WT (Col-0), the *iaa28-ko* loss of function mutant exhibited a slight reduction in the number of LRs (Fig. 5.8) (C). However, in agreement with Wang and Guo (2015) though, the *iaa28-ko* loss of function mutant lateral root phenotype mimicked WT (Col-0) roots.

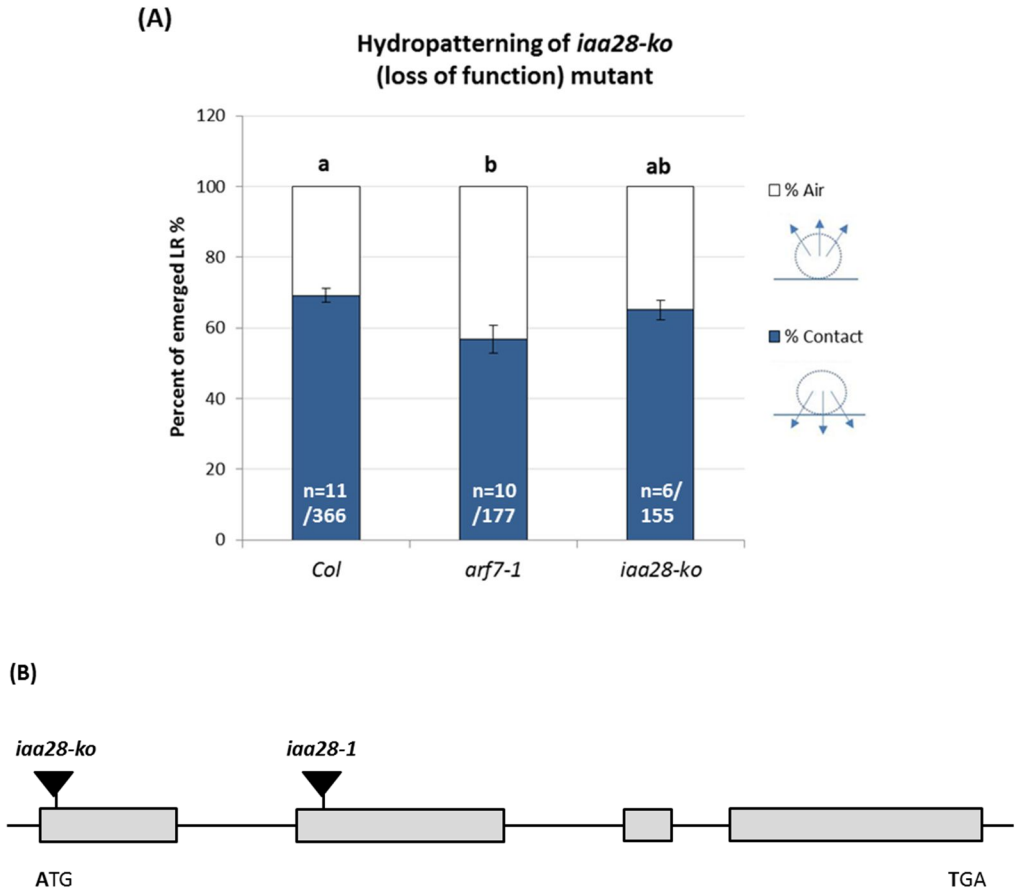


Fig. 5.7: ***IAA28* may be involved in LR hydropatterning.** Compared to WT (Col-0) *Arabidopsis* roots and the *iaa28-ko* loss of function mutant exhibit a similar LR hydropatterning response. Although, the *iaa28-ko* loss of function mutant had more LRs emerging towards the air than WT (Col-0) but less than *arf7-1* loss of function mutant. Data shown is mean values ± S. E, (n = number of seedlings/number of LRs analysed). Statistical differences were analysed on the percent of emerged LRs emerging towards either contact (including horizontal) or air using a Tukey HSD test ($P<0.05$); statistically similar groups are indicated using the same letter. Biological replicates (1=2) were performed (A). Schematic representation of the *IAA28* (At5g25890) gene structure (1937bp) and the positioning of *iaa28* mutations: *iaa28-1* (isolated from an IAA mutant screen, Rogg *et al.*, 2001) (2nd Exon) and *iaa28-ko* (Salk_129988C) (1st Exon). The location of the start (ATG) and stop (TGA) codons have been indicated. Exons (boxes) and introns (lines) were determined by comparing the full length DNA sequence with that of nucleotide sequences of *iaa28* mutant alleles (https://www.arabidopsis.org) (B).

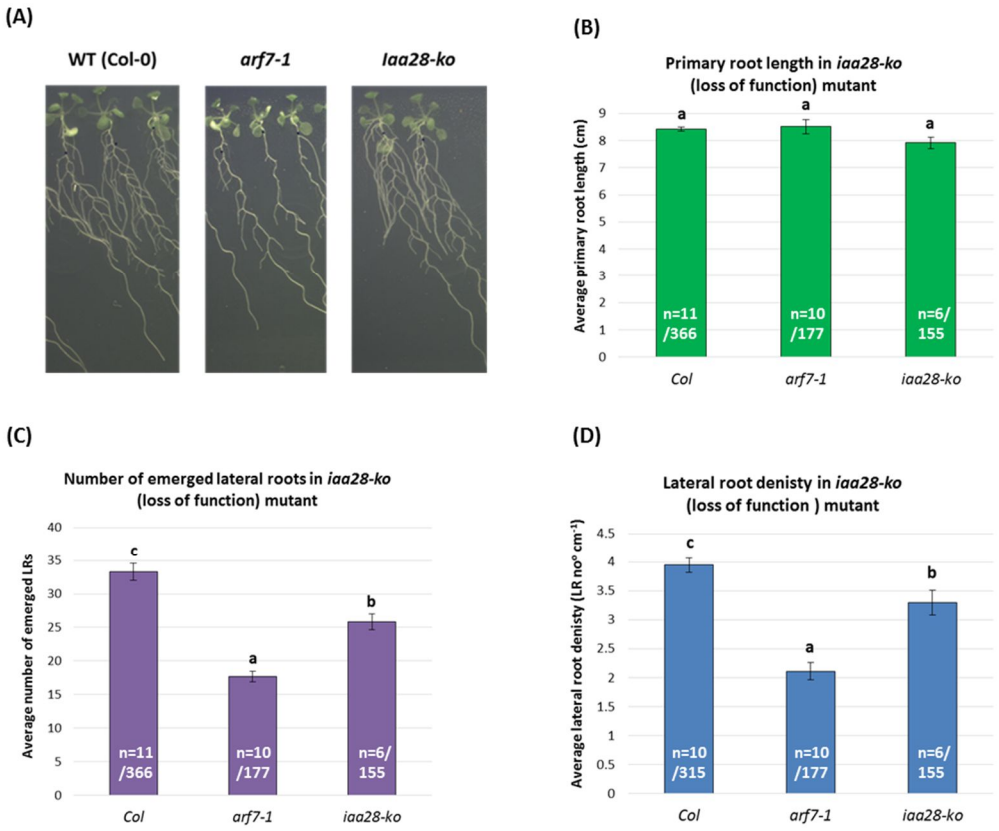
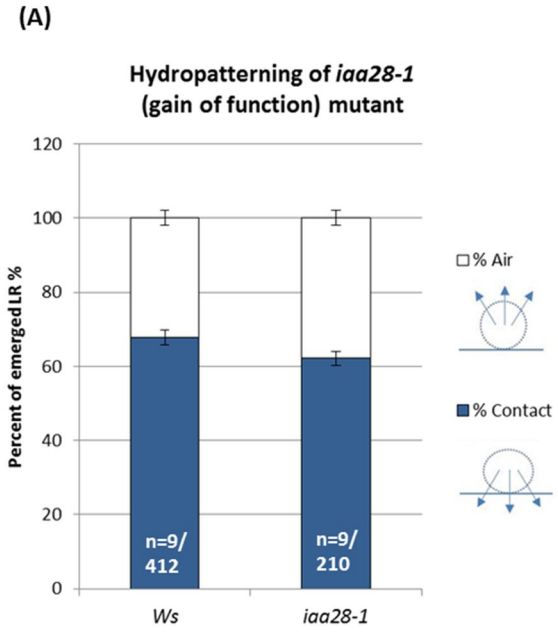
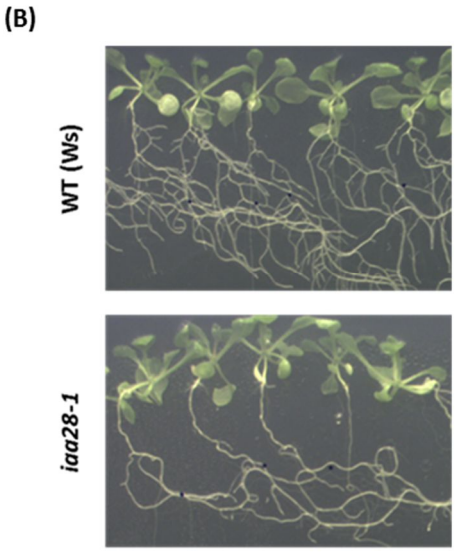


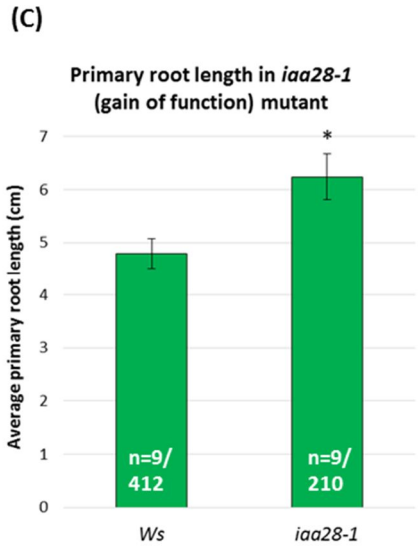
Fig. 5.8: ***iaa28-ko* displays diverse root architecture.** Compared to WT (Col-0) *Arabidopsis* roots, there was no obvious difference in phenotype observed in the *iaa28-ko* loss of function mutant (A). Although, there was a very slight reduction in primary root length (B). In relation to *arf7-1*, the *iaa28-ko* loss of function mutant displayed almost twice the amount of LRs (C). When compared to WT (Col-0) though, there was a marked decrease in LR number. Hence, there was a significant reduction in LR density seen in the *iaa28-ko* loss of function mutant when compared to WT (Col-0) roots (D). Data shown is mean values ± S. E, (n = number of seedlings/number of LRs analysed). Significant differences were analysed using the Tukey HSD test (P<0.05); statistically similar groups are indicated using the same letter. Biological replicates (1=2) were performed.

Like the *iaa28-ko* allele, the *iaa28-1* gain of function allele also displayed a WT LR hydropatterning response (Fig. 5.9) (A). The majority of the LRs emerged from the contact (62%) rather than the air side (38%), akin to WT (Ws). Therefore, *IAA28* did

not appear to control LR hydropatterning. Interestingly, the *iaa28-1* gain of function mutant displayed a striking LR phenotype (**Fig. 5.9**) (**B to E**). Compared to WT (Ws), the *iaa28-1* gain of function mutant exhibited a significant reduction in LR number thereby, affecting LR density (**Fig. 5.9**) (**D and E**). Consistent with previous research that the *iaa28-1* gain of function mutant strongly supresses LR development (Wang and Guo, 2015 and Rogg *et al*., 2001). Hence, LR initiation (but not LR hydropatterning) is controlled by *IAA28*.







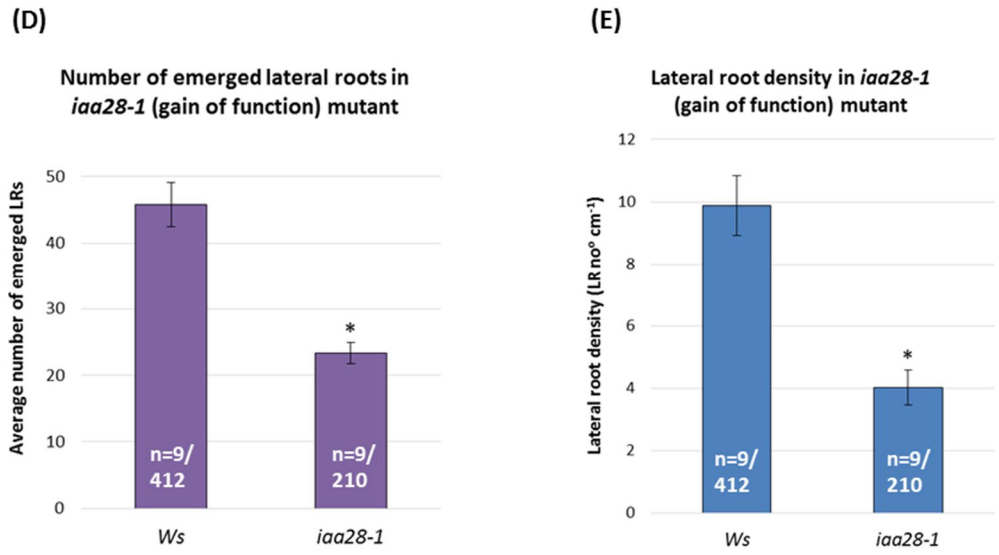


Fig. 5.9: *IAA28* gain of function exhibits normal LR hydropatterning. WT (Ws) *Arabidopsis* roots and the *iaa28-1* gain of function mutant exhibited a normal LR hydropatterning response. The percent of LRs emerging towards the air and contact sides in the *iaa28-1* gain of function mutant was similar to that seen by WT (Ws) roots (A). Compared to WT (Ws) *Arabidopsis* roots the *iaa28-1* gain of function mutant displayed striking LR phenotype resulting in fewer twisted LRs (B). Primary root length was significantly increased in *iaa28-1* gain of function mutant roots (C). The number of emerged LRs was reduced in *iaa28-1* gain of function mutant (D) Hence, this had an effect on LR density compared to WT (Ws) roots (E). Data shown is mean values ± S. E, (n = number of seedlings/number of LRs analysed). No significant difference was seen from that of WT (Ws) roots based on using a Student *t* test ($p<0.05$). Biological replicates (1=2) were performed.

5.3 DISCUSSION

Phenotypic studies have revealed that, in addition to *ARF7*, *LBD16* and *IAA3/SHY2* genes also regulate LR hydropatterning. *ARF7* has been shown to regulate several members of the *LBD* gene family during lateral root development. (Lavenus *et al*., 2015). *LBD* genes encodes a LATERAL ORGAN BOUNDARIES (*LOB*) domain that is

required for DNA binding (Majer and Hochholdinger, 2011). Among these family members, *LBD16* (plus *LBD17*, *LBD18* and *LBD29*) have been shown to be auxin inducible (Okushima *et al*., 2005). ChIP-PCR studies have revealed that *LBD16* is a direct target of *ARF7* (Lavenus *et al*., 2015). In fact, *LBD16* is involved in LR initiation very early on (Lee *et al*., 2009; Goh et al, 2012). Moreover, the *lbd16* loss of function mutant alleles exhibit striking LR hydropatterning and LR initiation defects that phenocopy *arf7* mutants. Collectively, this body of evidence suggests that *ARF7* regulates LR hydropatterning via *LBD16*.

Expression studies have shown that *LBD16* is expressed in FCs prior to LR initiation and after xylem pole pericycle cells have been primed (Goh *et al*., 2012) (**Fig. 5.3**). LSFM studies have revealed that a functional *pLBD16::gLBD16-GFP* reporter was asymmetrically expressed in xylem-pole pericycle cells prior to exiting the root elongation zone (**Chapter 3: Fig. 3.2**), which is the major site of water uptake in roots. Hence, *LBD16* is expressed in the expected root zones and tissues where LR hydropatterning is predicted to occur to influence which subset of xylem pole pericycle cells is selected to initiate a new LRP.

During LR development the activity of *ARF7* is negatively regulated by Aux/IAA repressor proteins such as *SHY2/IAA3* (Goh *et al*., 2012). *SHY2/IAA3* like *ARF7* is involved in the early stages of LR development (Swarup *et al*, 2008 and Goh *et al*., 2012). In fact, *SHY2/IAA3* plays a key role in LR emergence within the endodermis (Swarup *et al*., 2008). Pull down data recently revealed that ARF7 interacted with SHY2/IAA3 in a SUMO dependent manner (A. Sadanandom, pers. comm). Mutating this domain prevented the interaction between *SHY2/IAA3* and *ARF7*. Hence, the relationship between ARF7 and SHY2/IAA3 was dependent on the SUMO-SIM interaction. Consistent with a role during hydropatterning, a *SHY2/IAA3* loss of

function mutant *shy2-31* exhibited a LR hydropatterning defect. The *shy2-31* mutant exhibited a randomised distribution of LRs on all sides of the PR. Therefore, *SHY2/IAA3* recruitment by SUMOylated *ARF7* appears to control LR hydropatterning.

SHY2/IAA3 has been reported to act in the endodermis during LR emergence (Swarup *et al*., 2008). It is known that degradation of *SHY2/IAA3* in the endodermal layer is required for cell wall remodelling enzymes to be induced by auxin (Swarup *et al*., 2008). Hence, the cell separation reduces tissue tension enabling the LRP (stage I) to further develop (Swarup *et al*., 2008). It is possible that SUMOylatable *ARF7* is functioning in the endodermal layer thereby indirectly repressing LR initiation. However, imaging an *pSHY2::NLS:3xVenus* reporter line has revealed that the gene was also expressed in stele cells within the root basal meristem, hence SHY2/*IAA3* may function to influence early lateral root development via stele tissues (underlying FC) rather than via the endodermis.

Chapter 6: DISCUSSION

Chapter 6: DISCUSSION

6.1 DISCUSSION

The highly heterogeneous nature of soil has a marked impact on root systems architecture. Roots must adapt their architecture in order to access heterogeneously distributed water and nutrient resources (Morris *et al*., 2017). By being developmentally plastic, roots are able to optimise their foraging (Osmont *et al*., 2007). Plants have evolved a number of adaptive responses that link root growth and development with environmental signals such as root hydrotropism (Dietrich *et al*, 2017). A newly discovered adaptive mechanism termed lateral root hydropatterning, position new lateral branches where roots are in direct contact with water. With the aid of X-ray microCT imaging, this LR hydropatterning response towards water was visualised *in-situ* (Bao et *al*., 2014 and reviewed in Morris et *al*., 2017). LR hydropatterning is a highly conserved adaptive response in higher plants as it occurs in monocot and eudicot roots (Bao *et al*., 2014). Growing roots vertically on the surface of an agar plate mimics this adaptive response, where the formation of a meniscus results in opposite sides of a root either to be in direct contact with moisture or exposed to air.

LR hydropatterning was predicted to act early on in LR development at the point of LR initiation (Bao *et al*., 2014). Essentially, a LR hydropatterning response must occur between the basal meristem and early elongation zones along the root. Characterisation of a *TWD1* mutant in **Chapter 3** suggests that this patterning decision was taken much later in the elongation zone. Supporting this, a *pLBD16::gLBD16-GFP* reporter revealed asymmetric expression in xylem-pole pericycle cells prior to exiting the root elongation zone. Given that water is taken up by the root in the elongation zone, makes this a plausible zone where the LR hydropatterning decision is made.

Exposure to an asymmetric moisture environment triggers an auxin response gradient across the radius of the root, resulting in LRP forming predominately on the contact side (Bao *et al*., 2014). However, the mechanistic basis behind this radial auxin response gradient remains unclear. **Chapter 3** also investigated the auxin–based molecular mechanism(s) regulating LR hydropatterning and describes a new role for the transcription factor *ARF7*. Out of the five activating ARF genes in Arabidopsis, *ARF7* was found to be the only one important for LR hydropatterning.

The relative importance of *ARF7* most likely reflects its pole position in the LR gene regulatory network compared to other ARFs (Lavenus *et al*, 2015). New *ARF7* reporter lines revealed for the first time that this TF was expressed during early stages of lateral root development. However, it remains unclear which *ARF7* root tissue(s) domain are functionally required for LR hydropatterning. This could be revealed by expressing *ARF7* in individual root tissues of *arf7-1* to assess which can rescue the LR hydropatterning defect.

In **Chapter 4**, overexpressing *ARF7* was able to rescue the *arf7* loss of function LR hydropatterning defect. This suggested that *ARF7* regulates LR hydropatterning via a post-translational mechanism. Mutant studies suggested that LR hydropatterning may be controlled by *ARF7* via a process termed SUMOylation. SUMO has emerged as an influential protein modifier within plants (Conti *et al*., 2014 and Yates *et al*., 2016). Unlike ubiquitination, SUMOylation modifies the function (rather than levels) of target proteins (Johnson *et al*., 2004).

E3 SUMO ligases add SUMO to target proteins (Park *et al*., 2011), whilst *OTS1* and *OTS2* proteases cleave SUMO from target proteins, such as *ARF7* (Conti *et al*., 2008). The *ARF7* sequence contained four SUMOylation sites. Expressing wild type *ARF7* (WT) and a non-SUMOylated version (ARF7 4xKR) in *arf7* revealed that *ARF7* controls LR

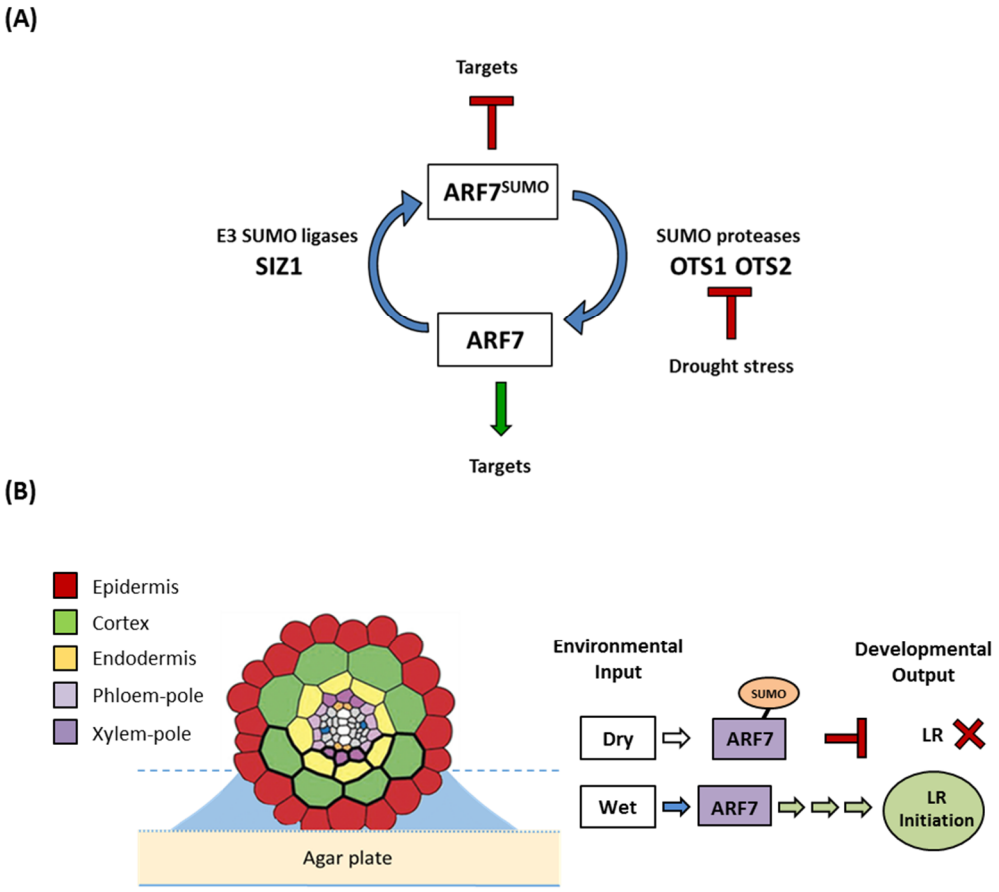


Fig. 6.1: Schematic representation of enhanced *ARF7* SUMOylation. SUMOylation of *ARF7* is enhanced following drought induced inactivation of *OTS1* and *OTS2*. A cyclic *ARF7* event occurs in the presence of E3 SUMO ligases (*SIZ1*) that covalently attaches SUMO. Thereby, resulting in an accumulation of SUMOylated ARF7 (A). Model devised to depict what is happening to *ARF7* on either the dry or contact side of the root. On the dry side, there is an accumulation of SUMOylated ARF7 preventing growth. Whereas, non-SUMOylated ARF7 on the contact side results in normal LR initiation (B).

hydropatterning via SUMOylation. Intriguingly, mutating all four sites in the *ARF7* sequence created a more active protein. This is consistent with our model where during a LR hydropatterning stimulus, *ARF7* is SUMOylated resulting in its inactivation whereas non-SUMOylated *ARF7* (ARF7 4xKR) remains active (Fig. 6.1).

Protein SUMOylation is known to play an important role during responses to environmental challenges, such as drought stress (Conti *et al*., 2008). So far, all four SUMO sites have been mutated revealing *ARF7* to be SUMOylated. In order to see if the other SUMO motifs have distinct regulatory functions, each ones needs to be mutated independently. For example, one of the SUMO motifs (151) in *ARF7* sits within the DNA binding domain. Hence, SUMOylation may block DNA binding, thereby depleting the pool of nuclear *ARF7* able to bind to DNA targets (such as *LBD16*) and activate auxin dependent gene expression.

Alternatively, an active repression mechanism may operate to recruit co-repressors. *ARF7* is negatively regulated by Aux/IAA repressor proteins during LR development (Lavenus *et al*., 2015). Pull down assays revealed that ARF7 interacted with SLR/IAA14 in a SUMO independent manner. In contrast, the interaction between ARF7 and SHY2/IAA3 was found to be SUMO dependent. IAA3/SHY2 as opposed to IAA14/SLR contained a SUMO interaction motif (SIM). Intriguingly, mutating the IAA3/SHY2 SIM site in *pCASP1::shy2-2* (-SIM) (V/A) transgenic lines was able to rescue LR initiation. Hence, *IAA3/SHY2* recruitment appears dependent on *ARF7*-SUMOylation and likely to control LR hydropatterning.

In **Chapter 5**, *SHY2/IAA3* was found to be important for LR hydropatterning. The *shy2-31* loss of function mutants displayed a striking LR hydropatterning response akin to *arf7* mutants. Like *ARF7*, *SHY2/IAA3* is known to be involved with LR development (Swarup *et al*., 2008). *ARF7* plays a key role in all areas of LR development from priming through to emergence (reviewed in Péret *et al*., 2009). Whereas *SHY2/IAA3*, expressed in the endodermis, is involved with LR emergence (Swarup *et al*., 2008). Another target of *ARF7*, *LBD16* has also been revealed to be important for LR hydropatterning. The *lbd16* loss of function mutants, especially *lbd16-2*, phenocopies *arf7* mutants LR

hydropatterning defect. The position of the *lbd16-2* mutation, further along the *LBD16* gene, may account for the increased LR hydropatterning defect observed compared to the other *lbd16* allele. *LBD16* is a direct target of *ARF7* and also involved in LR initiation (Goh *et al*., 2012). However, it is currently unclear exactly which root tissue(s) *SHY2/IAA3* and *LBD16* may function to control LR hydropatterning.

How is a gradient of *ARF7* SUMOylation generated across the radius of a root? *OTS1* and *OTS2* are known to be destabilised by an abiotic stress, resulting in an accumulation of their SUMOylated target proteins. The formation of a gradient of these *OTS* proteases across the root radius by a LR hydropatterning stimulus could provide the basis for this adaptive mechanism, where a gradient of *OTS1 OTS2* across a root exposed to a LR hydropatterning stimulus would result in an inverse gradient of SUMOylated *ARF7*. This would cause the ARF transcription factor on the air side of roots to recruit Aux/IAA repressor proteins IAA28 and IAA3/SHY2, thereby blocking auxin responsive gene expression associated with lateral root initiation. Essentially, mimicking being in a low auxin environment resulting in the inactivation of transcription.

In summary, LR hydropatterning provides a novel example where core components of the auxin response machinery are controlled via an environmentally post-translational mechanism. The knowledge gained so far promises to help reveal how plants explore the soil and position LRs to maximise water (and nutrient) foraging.

6.2 FUTURE DIRECTIONS

So far, *ARF7*, *SHY2* and *LBD16* have all been revealed to be important for LR hydropatterning. Although, it is currently unclear exactly where *ARF7* regulates LR

hydropatterning. In order to ascertain which *ARF7* root tissue(s) domain is functionally required for LR hydropatterning, *ARF7* will be expressed in individual root tissues of *arf7*-1. LR hydropatterning bio-assays will then reveal which tissue rescues the LR hydropatterning defect. Promoter specific *ARF7* transgenic lines will be generated that not only consider radial root tissues but also zones of growth (e.g. *pXPP*, *pSHR*, *pCASP1*, *pSCR*, *pEN7*, *pGL2*, *pCOBL9* and *pWER*).

It has been demonstrated that *ARF7* controls LR hydropatterning via the post-translational modification, SUMOylation. Four SUMO motifs (K104R, K151R, K282R and K889R) were found within the *ARF7* sequence. So far, all of these SUMO sites have been mutated (ARF7 4xKR). Although, it is not known if each SUMOylation site in *ARF7* has a distinct regulatory function. It is known that one of the SUMO sites (K151R) sits within a DNA binding domain. Hence, transcription may be blocked or there is the possibility of co-repressor recruitment. It is also noted, that the SUMO (K104R) motif is positioned just before the DNA binding domain which may ultimately affect transcription.

To establish if each SUMOylation motif has a separate regulatory function, each one will be mutated independently. Thereby, generating a non-SUMOylated version (ARF7 1xKR) for each individual SUMO site. Out of the four SUMO sites, one will be mutated. It is also possible that a combination of SUMO sites interact together as with the non-SUMOylated ARF7 (4xKR) version. Hence, it will be necessary to make non-SUMOylated ARF7 (3xKR) versions. Where three of the four SUMO sites are mutated.

Chapter 7: REFERENCES

Chapter 7: REFERENCES

7.1 REFERENCES

Babe A, Lavigne T, Severin J, Nagel K, Walter A, Chaumont F, Batoko H, Beeckman T and Draye X (2012) Repression of early lateral root initiation events by transient water deficit in barley and maize. *Philos Trans R Soc Lond B Biol Sci*. 367: 1534-1541.

Bailly A, Wang B, Zwiewka M, Pollman S, Schenck D, Lüthen H, Schulz A, Friml J and Geisler M (2013) Expression of TWISTED DWARF1 lacking its in-plane membrane anchor leads to increased cell elongation and hypermorphic growth. *Plant J*. 77: 108-118.

Bao Y, Aggarwal P, Robbins NE, Sturrock CJ, Thompson MC, Emami S, Tan HQ, Tham C, Duan L, Rodriguez P, Vernoux T, Mooney SJ, Bennett MJ and Dinneny JR (2014) Plant roots use a patterning mechanism to position lateral root branches towards available water. *PNAS*. 111: 9319-9324.

Berleth T and Jurgens G (1993) The role of the monopteros gene in organising the basal body region of the *Arabidopsis* embryo. *Development*. 118: 575-587.

Bouchard R, Bailly A, Blakeslee J, Oehring S, Vincenzetti V, Lee O, Paponov I, Palme K, Mancuso S, Murphy A, Schulz B and Geisler M (2006) Immunophilin-like TWISTED DWARF1 modulates auxin efflux activities of *Arabidopsis* P-glycoproteins. *J. Biol. Chem*. 281: 30603–30612

Bradnam K and Korf I (2008) Longer First Introns Are a General Property of Eukaryotic Gene Structure. *PLOS ONE*. 3.

Casimiro I, Beeckman T, Graham N, Bhalerao R, Zhang H, Casero P, Sandberg G and Bennett M (2003) Dissecting *Arabidopsis* lateral root development. *Trends in Plant Sci*. 8: 165-171.

Chen Q, Liu Y, Maere S, Lee E, Van Isterdael G, Xie Z, Xuan W, Lucas J, Vassileva V, Kitakura S, Marhavy P, Wabnik K, Geldner N, Benkova E, Le J, Fukaki H, Grotewold E, Li C, Friml J, Sack F, Beeckman T and Vanneste S (2015) A coherent transcriptional feed-forward motif model for mediating auxin-sensitive PIN3 expression during lateral root development. *Nature Communications*. 6:8821.

Clark N, Luis Balaguer M and Sozzani R (2014) Experimental data and computational modelling link auxin gradient and development in the *Arabidopsis* root. *Front. Plant Sci*. 5: 328.

Clough S and Bent A (1998) Floral dip: a simplified method for *Agrobacterium*-mediated transformation of *Arabidopsis thaliana. Plant J.* 16: 735-743.

Conti L, Price G, O'Donnell E, Schwessinger B, Dominy P and Sadanandom A (2008) Small ubiquitin-like modifier proteases OVERLY TOLERANT TO SALT1 and -2 regulate salt stress responses in *Arabidopsis*. *Plant Cell*. 20: 2894-2908.

Conti L, Nelis S, Zhang C, Woodcock A, Swarup R, Galbiati M, Tonelli C, Napier R, Hedden P, Bennett M and Sadanandom A (2014) Small ubiquitin-like modifier protein SUMO enables plants to control growth independently of the phytohormone Gibberellin. *Developmental Cell*. 28: 102-110.

Dietrich D, Pang L, Kobayashi A, Fozard A, Boudolf V, Bhosale R, Antoni R, Nguyen T, Hiratsuka S, Fujii N, Miyazawa Y, Bae T, Wells D, Owen M, Band L, Dyson R, Jensen O, King J, Tracy S, Sturrock C, Mooney S, Roberts J, Bhalerao R, Dinneny J, Rodriguez P, Nagatani A, Hosokawa Y, Baskin T, Pridmore T, De Veylder L, Takahashi H and Bennett M (2017) Root hydrotropism is controlled via a cortex specific growth mechanism. *Nature Plants*. 3. Article number: 17057, doi: 10.1038/nplants.2017.57.

De Smet I, Signora L, Beeckman T, Inzé D, Foyer C and Zhang H (2003) An abscisic acid-sensitive checkpoint in lateral root development of *Arabidopsis*. *Plant J*. 33: 543-555.

De Smet I, Tetsumura T, De Rybel B, Frei dit Frey N, Laplaze L, Casimiro I, Swarup R, Naudts M, Vanneste S, Audenaert D, Inzé D, Bennett M and Beeckman T (2007) Auxin-dependent regulation of lateral root positioning in the basal meristem of *Arabidopsis*. *Development*. 134: 681-690.

De Smet (2012) Lateral root initiation: one step at a time. *New Phytologist*. 193: 867-873.

De Rybel B, Vassileva V, Parizot B, Demeulenaere M, Grunewald W, Audenaert D, Campenhout J, Overvoorde P, Jansen L, Vanneste s, Möller B, Wilson M, Holman T, Van Isterdael G, Brunoud G, Vuylsteke M, Vernoux T, De Veylder L, Inzé D, Weijers D, Bennett M and Beeckman T (2010) A Novel Aux/IAA28 Signaling Cascade Activates GATA23-Dependent Specification of Lateral Root Founder Cell Identity. *Current Biology*. 20: 1697-1706.

Eapen D, Barroso M, Campos M, Ponce G, Corkidi G, Dubrovsky J and Cassab G (2003) A *no hydrotropic response* root mutant that responds positively to gravitropism in *Arabidopsis*. *Plant Physiol*. 131: 536-546.

Friml J, Vieten A, Sauer M, Weijers D, Schwarz H, Hamann T, Offringa R and Jürgens G (2003) Efflux-dependent auxin gradients establish the apical–basal axis of *Arabidopsis*. *Nature*. 426: 147-153.

Geisler M, Kolukisaoglu H, Bouchard R, Billion K, Berger J, Saal B, Frangne N, Koncz-Kálmán Z, Koncz C, Dudler R, Blakeslee J, Murphy A, Martinoia E and Schulz B (2003) TWISTED DWARF1, a unique plasma membrane-anchored immunophilin-like protein, interacts with *Arabidopsis* multidrug resistance-like transporters AtPGP1 and AtPGP19. *Mol. Biol. Cell.* 14: 4238–4249.

Goh T, Kasahara H, Mimura T, Kamiya Y and Fukaki H (2012) Multiple AUX/IAA-ARF modules regulate lateral root formation: the role of *Arabidopsis SHY2/IAA3*-mediated auxin signalling. *Philos Trans R Soc Lond B Biol Sci.* 367: 1461-1468.

Guilfoyle T (2007) Plant Biology: Sticking with auxin. *Nature*. 446: 621-622.

Harper R, Stowe-Evans E, Luesse D, Muto H, Tatematsu K, Watahiki M, Yamamoto K and Liscum E (2000) The *NPH4* Locus Encodes the Auxin Response Factor *ARF7*, a Conditional Regulator of Differential Growth in Aerial *Arabidopsis* Tissue. *Plant Cell*. 12: 757-770.

Ishida T, Yoshimura M, Miura K and Sugimoto K (2012) MMS21/HPY2 and SIZ1, Two *Arabidopsis* SUMO E3 Ligases, have distinct functions in development. *PLOS ONE*. 7.

Jeon J, Lee S, Jung K, Jun S, Kim C, An G (2000) Tissue-preferential expression of a rice alpha-tubulin gene, OsTubA1, mediated by the first intron. *Plant Physiol.* 123: 1005-1014.

Johnson ES (2004) Protein modification by SUMO. *Ann Rev Biochem*. 73: 355-382.

Knox K, Grierson C and Leyser O (2003) *AXR3* and *SHY2* interact to regulate root hair development. *Development*. 130: 5769-5777.

Lampropoulos A, Sutikovic Z, Wenzl C, Maegele I, Lohmann J and Forner J (2013) GreenGate - A Novel, Versatile, and Efficient Cloning System for Plant Transgenesis. *PLOS ONE*. 8.

Lavenus J, Goh T, Roberts I, Guyomarc'h S, Lucas M, Smet I, Fukaki H, Beeckman T, Bennett M and Laplaze L (2013) Lateral root development in *Arabidopsis*: fifty shades of auxin. *Trends in Plant Sci*. 18: 450-458.

Lavenus J, Goh T, Guyomarc'h S, Hill K, Lucas M, Voß U, Kenobi K, Wilson M, Farcot E, Hagen G, Guilfoyle T, Fukaki H, Laplaze L and Bennett M (2015) Inference of the *Arabidopsis* Lateral Root Gene Regulatory Network Suggests a Bifurcation Mechanism That Defines Primordia Flanking and Central Zones. *Plant Cell*. 27: 1368-1388.

Lee H, Kim N, Lee D and Kim J (2009) *LBD18/ASL20* regulates lateral root formation in combination with *LBD16/ASL18* downstream of *ARF7* and *ARF19* in *Arabidopsis*. *Plant Physiol*. 151: 1377-1389.

Lee H, Cho C and Kim J (2015) *Lateral organ boundaries domain 16 and 18* act downstream of the AUXIN1 and LIKE-AUXIN3 Auxin influx carriers to control lateral root development in *Arabidopsis*. *Plant Physiol*. 168: 1792-1806.

Liu N, Wu S, Van Houten J, Wang Y, Ding B, Fei Z, Clarke T, Reed J and Van Der Knapp E (2014) Down-regulation of AUXIN RESPONSE FACTORS 6 and 8 by microRNA 167 leads to floral development defects and female sterility in tomato. *Journal of exp. Botany.* 65: 2507-2520.

Majer C and Hochholdinger F (2011) Defining the boundaries: structure and function of LOB domain proteins. *Trends in Plant Sci*. 16: 47-52.

Malamy J (2005) Intrinsic and environmental response pathways that regulate root system architecture. *Plant, Cell and Environment*. 28: 67–77

Malamy J and Benfey P (1997) Organization and cell differentiation in lateral roots of *Arabidopsis thaliana*. *Development*. 124: 33-44.

Miyazawa Y and Takahashi H (2007) How do *Arabidopsis* roots differentiate hydrotropism from gravitropism? *Plant Signal Behav.* 2: 388-389.

Morello L, Bardini M, Sala F and Breviario D (2002) A long leader intron of the Ostub16 rice beta-tubulin gene is required for high-level gene expression and

can autonomously promote transcription both in vivo and in vitro. *Plant J*. 29: 33-44.

Moreno-Risueño M, Van Norman J, Moreno A, Zhang J, Ahnert S and Benfey P (2010) Oscillating Gene Expression Determines Competence for Periodic *Arabidopsis* Root Branching. *Science*. 329: 1306-1311.

Moriwaki T, Miyazawa Y, Kobayashi A and Takahashi H (2013) Molecular mechanisms of hydrotropism in seedling roots of *Arabidopsis thaliana* (*Brassicaceae*). *Am. J. Bot*. 100: 25-34.

Morris E, Griffiths M, Golebiowska A, Mairhofer S, Burr-Hersey J, Goh T, Von Wangenhiem D, Atkinson B, Sturrock C, Lynch J, Vissenberg K, Ritz K, Wells D, Mooney S and Bennett M (2017) Shaping 3D root system architecture. *Current Biology*. 27: 919-930 (review).

Nakagawa T, Kurose T, Hino T, Tanaka K, Kawamukai M, Niwa Y, Toyooka K, Matsuoka K, Jinbo T and Kimura T (2007) Development of series of gateway binary vectors, pGWBs, for realising efficient construction of fusion genes for plant transformation. *J. Biosci. Bioeng*. 104: 34-41.

Okushmia Y, Overvoorde P, Arima K, Alonso J, Chan A, Chang C, Ecker J, Hughes B, Lui A, Nguyen D, Onodera C, Quach H, Smith A, Yu G and Theologis A (2005) Functional Genomic Analysis of the *AUXIN RESPONSE FACTOR* gene family members in *Arabidopsis thaliana*: unique and overlapping functions of *ARF7* and *ARF19*. *Plant Cell*. 17: 444-463.

Okushmia Y, Fukaki H, Onoda M, Theologis A and Tasaka M (2007) ARF7 and ARF19 regulate lateral root formation via direct activation of *LBD/ASL* genes in *Arabidopsis*. *Plant Cell*. 19: 118-130.

Osmont KS, Sibout R and Hardtke CS (2007) Hidden branches: developments in root system architecture. *Annu. Rev. Plant Biol*. 58: 93-113.

Overvoorde P, Fukaki H and Beeckman T (2010) Auxin control of root development. *Cold Spring Harb. Perspect. Biol*. 2: 1-16.

Parizot B, Laplaze L, Ricaud L, Boucheron-Dubuisson E, Bayle V, Bonke M, De Smet I, Poethig S, Helariutta Y, Haseloff J, Chriqui D, Beeckman T and Nussaume L (2008) Diarch Symmetry of the Vascular Bundle in *Arabidopsis* Root Encompasses the Pericycle and Is Reflected in Distich Lateral Root Initiation. *Plant Physiol*. 146: 140-148.

Park HJ, Kim W, Park HC, Lee S, Bohnert H and Yun D (2011) SUMO and SUMOylation in plants. *Mol. Cells.* 32: 305-316.

Park S, Hannenhalli S and Choi S (2014) Conservation in first introns is positively associated with the number of exons within genes and the presence of regulatory epigenetic signals. *BMC Genomics*. 15: 526

Péret B, Larrieu A and Bennett M (2009) Lateral root emergence: a difficult birth. *Journal of exp. Botany.* 60: 3637-3643.

Péret B, De Rybel B, Casimiro I, Benková E, Swarup R, Laplaze L, Beeckman T and Bennett M (2009) *Arabidopsis* lateral root development: an emerging story. *Trends in Plant Sci*. 14: 399-408 (review).

Quint M and Gray W (2006) Auxin signalling. *Curr. Opin. Plant Biol*. 9: 448-453.

Robbins N and Dinneny J (2015) The divining root: moisture-driven responses of roots at the micro- and macro-scale. *Journal of exp. Botany.* 66: 2145-2154.

Rogg L, Lasswell J and Bartel B (2001) The gain of function mutation in *IAA28* supresses lateral root development. *Plant Cell*. 13: 465-480.

Rose A, Elfersi T, Parra G and Korf I (2008) Promoter-Proximal Introns in *Arabidopsis thaliana* are enriched in dispersed signals that elevate gene expression. *Plant Cell*. 20: 543-551.

Scheres B, Benfey P and Dolan L (2002) Root development. *Arabidopsis Book.* 1.

Smith S and De Smet I (2012) Root systems architecture: insights from *Arabidopsis* and cereal crops. *Phil. Trans. R. Soc. B*. 367: 1441–1452.

Swarup K, Benková E, Swarup R, Casimiro I, Péret B, Yang Y, Parry G, Nielsen E, De Smet I, Vanneste S, Levesque M, Carrier D, James N, Calvo V, Ljung K, Kramer E, Roberts R, Graham N, Marillonnet S, Patel K, Jones J, Taylor C, Schachtman D, May S, Sandberg G, Benfey P, Friml J, Kerr I, Beeckman T, Laplaze L and Bennett M (2008) The auxin influx carrier LAX3 promotes lateral root emergence. *Nature Cell Biol*. 10: 946-954.

Tian Q and Reed J (1999) Control of auxin-regulated root development by the *Arabidopsis thaliana SHY2/IAA3* gene. *Development*. 126: 711-721.

Tian C, Muto H, Matamura T, Tatematsu K, Koshiba T and Yamamoto K (2004) Disruption and overexpression of auxin response factor 8 gene of *Arabidopsis* affect hypocotyl elongation and root growth habit, indicating its possible involvement in auxin homeostasis in light condition. *Plant J*. 40: 333-343.

Tiwari S, Hagen G and Guilfoyle T (2003) The roles of auxin response factor domains in auxin-responsive transcription. *Plant Cell*. 15: 533-543.

Yadav S, Bishopp A and Helariutta Y (2010) Plant development: early events in lateral root initiation. *Current Biology*. 20: 843-845.

Van Norman J, Xuan W, Beeckman T and Benfey P (2013) To branch or not to branch: the role of pre-patterning in lateral root formation. *Development*. 140: 4301-4310.

Vasil V, Clancy M, Ferl R, Vasil I and Hannah L (1989) Increased Gene Expression by the First Intron of Maize Shrunken-1 Locus in Grass Species. *Plant Physiol*. 91: 1575-1579.

Verbelen JP, Cnodder T, Le J, Vissenberg K and Baluška F (2006) The root apex of *Arabidopsis thaliana* consists of four distinct zones of growth activities. *Plant Signal Behav*. 1: 296-304.

Vermeer J, Von Wangenheim D, Barberon M, Lee Y, Stelzer E, Maizel A and Geldner N (2014) A spatial accommodation by neighboring cells is required for organ initiation in *Arabidopsis*. *Science*. 343: 178-183.

Vermeer J and Geldner N (2015) Lateral root initiation in *Arabidopsis thaliana*: a force awakens. *F1000 Prime Reports*. 7: 32

Verstraeten I, Schotte S and Geelen D (2014) Hypocotyl adventitious root organogenesis differs from lateral root development. *Front. Plant Sci*. 5: 495 (review).

Wang B, Bailly A, Zwiewka M, Henrichs S, Azzarello E, Mancuso S, Maeshima M, Friml J, Schulz A and Geisler M (2013) *Arabidopsis* TWISTED DWARF1 Functionally Interacts with Auxin Exporter ABCB1 on the Root Plasma Membrane. *Plant Cell*. 25: 202-214.

Wang J and Guo H (2015) Cleavage of *INDOLE-3-ACETIC ACID INDUCIBLE28* mRNA by MicroRNA847 Upregulates Auxin Signalling to Modulate Cell Proliferation and Lateral Organ Growth in Arabidopsis. *Plant Cell*. 27: 574-590.

Wilmoth J, Wang S, Tiwari S, Joshi A, Hagen G, Guilfoyle T, Alonso J, Ecker J and Reed J (2005) *NPH4/ARF7* and *ARF19* promote leaf expansion and auxin-induced lateral root formation. *Plant J*. 43: 118-130.

Xuan W, Audenaert D, Parizot B, Möller B, Njo M, De Rybel B, De Rop G, Van Isterdael G, Mähönen A, Vanneste S and Beeckman T (2010) Root cap derived auxin pre-patterns the longitudinal axis of the *Arabidopsis* root. *Current Biology*. 25: 1381-1388.

Yates G, Srivastava A and Sadanandom A (2016) SUMO proteases: uncovering the roles of deSUMOylation in plants. *Journal of exp. Botany.* 67: 2541-2548.

Chapter A: APPENDICES

Chapter A: APPENDICES

A.1 PRIMERS

A.1.1 Sequencing/Genotyping primers (page 140)

A.1.2 GREENGATE sequencing primers (page 141)

A.1.1 Sequencing/Genotyping Primers

NL41	gtccaaactgaaactg	54	ARF7		At5g20730	Reverse	5' end gene	R			ARF7_RV1	
NL42	gtttcaattactactactggc	57	ARF7		At5g20730	Reverse	Middle of the gene	R			ARF7_RV2	
NL43	cttggacttttgctgacc	55	ARF7		At5g20730	Reverse	3' end gene	R			ARF7_RV3	
NL44	TGGTGAGCCGACCTCAGG	61	ARF7		At5g20730	Reverse	3' end gene	F			ARF7_FW1	
NL45	GCTGGAGGCAACGAAATCA	57	ARF7		At5g20730	Reverse	After the ATG	R			ARF7_RV4	
NL46	TTGTCAGCAGCGAAAAGGC	54	ARF7		At5g20730	Reverse	5' end gene	F			ARF7_FW2	
NL47	GACATCCTCCTCGTCGGCG	63	ARF7		At5g20730	Reverse	100bp from the stop codon	F			ARF7_FW3	
NL75	ACAGAGTCTCCAGCAAAG	50	ARF7		At5g20730	Reverse	After SUMO site 151	R			pARF7_ARF7_YFP_RV2	
NL76	GACTCAGCGAATGCGAAC	53	ARF7		At5g20730	Reverse	Towards the end of the gene	F	(NL76 + NL77) 1038bp		pARF7_ARF7_YFP_FW3	
NL77	cagctagtggttgtcgggc	56	YFP Tag				Middle of the tag	R			pARF7_ARF7_YFP_RV3 (Also for YFP)	
NL84	AAGAGGATGTCGCGAAACCAGCTCATGTCACC	64	pARF7		At5g20730	Reverse	Approx 3300bp from ATG	F	(NL84 + NL85) 3347bp		pARF7_FW1 (No overhangs)	
NL85	CCTTTCTCCTGCATTCACACAACATCAAAGCTGT	64	pARF7		At5g20730	Reverse	Towards the ATG of the ARF7 gene	R			pARF7_RV1 (No overhangs)	
NL91	TCGCCTTCCACCAACAACTG	57	ARF7		At5g20730	Reverse	Towards the end of the gene	F			ARF7_FW5	
NL92	CTTGACGGTGATTCCAGG	55	ARF7		At5g20730	Reverse	Towards the end of the gene	F			ARF7_FW6	
NL93	gcatagtcaggaacatcgta	51	HA Tag				Middle of the Tag	R			HA_Tag_RV1	
NL94	gttcacgttcaaatcttctt	51	Myc Tag				Middle of the Tag	R			Myc_Tag_RV1	
NL97			ARF4		At5g60450	Reverse		F			ARF4_FW1	
NL98			ARF4		At5g60450	Reverse		R			ARF4_RV1	
NL99	AGTGAGTATGAGAGAGAAG	52	pCASP1		At2g36100	Reverse	Promoter	F			pCASP1_FW1	
NL100	TGACTCTTTCTAAGTGGACC	55	pCASP1		At2g36100	Reverse	Promoter	R			pCASP1_RV1	
NL101	ATTAGTTTCCCACCACAA	49	pCASP1		At2g36100	Reverse	Promoter	F			pCASP1_FW2	
NL102	GCTGCTGAGAAAATCTTTCCTGCT	61	ARF7 SUMO		At5g20730	Reverse	SUMO site 151 (DNA binding domain)	F			ARF7_SUMO_Un_FW7	
NL110	CCTTTCTCCTGCATTCACACA	57	pARF7		At5g20730	Reverse	Promoter	R			pARF7_RV1	
NL111	AAGAGGATGTCGCGAAACCAGC	57	pARF7		At5g20730	Reverse	Promoter	F			pARF7_FW1	
NL112	ATGCGTGAAGACAGAAGT	51	pARF7		At5g20730	Reverse	Promoter	R			pARF7_RV2	
NL113	agaaacgaaatggatcggcaaacg	61	pSCR		At3g54220	Forward	Promoter	F			pSCR_FW1	
NL114	attggaaggatgtggttggagga	61	pSCR		At3g54220	Forward	Promoter	R			pSCR_RV1	
NL115	aatactcttttatcttcaat	43	pSCR		At3g54220	Forward	Promoter	R			pSCR_RV2	
NL116	gtgttgaatggatcaggga	48	pSCR		At3g54220	Forward	Promoter	F			pSCR_FW2	
NL117	atgaggagatgggatgaaga	48	pSCR		At3g54220	Forward	Promoter	R			pSCR_RV3	
NL118	AGTCTAAGCAACTTCAAC	49	ARF7		At5g20730	Reverse	Promoter	F			ARF7_FW9	
NL119	agaagcgttcactgttgt	51	pCo2				Promoter	R			pCo2_FW1	
NL120	ctaaagagtccgtgaaat	45	pCo2				Promoter	R			pCo2_RV1	
NL121	gtgacttgtatgggtgt	50	pCo2				Promoter	R			pCo2_RV2	
NL124	ACCATACAAAGTGTTCCTA	46	pCRE1		At2g01830	Reverse	Promoter (approx -1.5kb upstream ATG)	F			pCRE1_FW1	
NL125	ATGAGTTGTGAGAGGATTG	48	pCRE1		At2g01830	Reverse	Promoter (840bp upstream ATG)	R	(NL124 + NL125) 1627bp		pCRE1_RV1	
NL126	ATCTTTGGCGATAATGACA	48	pCRE1		At2g01830	Reverse	Middle of the promoter	R	(NL124 + NL126) 648bp		pCRE1_RV2	
NL140	ATAATAACGCTGCGGACATCTACATTTTT		GK LB				Gabi Kat LB				GK_LB_O8474 GABI_LB_08474	
NL141	gatggttagagaggcttacgc		35S				CE Promoter				35S_FW2	
NL142	GACACCATACGGACACAC	51	pARF7		At5g20730	Reverse	Promoter	F			pARF7_FW2	
NL143	ATGAAACTCAGAACCAACCA	51	pARF7		At5g20730	Reverse	Promoter	F			pARF7_FW3	
NL144	ATGTCGCTACTCACTGC	51	pARF7		At5g20730	Reverse	Promoter	F			pARF7_FW4	
NL145	AGTTGTCGGAAAGGGATG	51	pARF7		At5g20730	Reverse	Promoter	R			pARF7_RV3	
NL147	GATCACTCAACTTTACTTTCTCTGAA	53	pARF7		At5g20730	Reverse	Promoter	R			pARF7_RV4	
NL148	CAGCTAGATCGTTCGAAATGG	59	ARF7		At5g20730	Reverse	3' end gene (628bp from the end)	R	(NL148 + NL149) 1040bp		ARF7_A_LP SALK_040394C (ARF7 allele)	
NL149	AGCACATCACCATTTAGGTGC	60	ARF7		At5g20730	Reverse	3' end gene (1645bp from the end)	F			ARF7_A_RP SALK_040394C (ARF7 allele)	
NL150	AGTGGATGAATATGCAGCAGC	60	ARF7		At5g20730	Reverse	Middle of the gene	F	(NL150 +NL151) 1275bp		ARF7_B_LP SALK_040394.55.10 (ARF7 allele)	
NL151	AAGAGGAAGGTGCATCTCCTC	59	ARF7		At5g20730	Reverse	Middle of the gene	R			ARF7_B_RP SALK_040394.55.10 (ARF7 allele)	
NL152	TGCACTCCTCTTTGAACCATC	60	ARF7		At5g20730	Reverse	3' end gene (2132bp from the end)	F	(NL152 + NL153) 1172bp		ARF7_C_LP SALK_040394.31.25 (ARF7 allele)	
NL153	CACGAGTTCTTGTTTTAGCCG	59	ARF7		At5g20730	Reverse	3' end gene (981bp from the end)	R			ARF7_C_RP SALK_040394.31.25 (ARF7 allele)	
NL154	TTCTATTGGCACGGTAAGTGC	60	ARF7		At5g20730	Reverse	After the 3' UTR	R	(NL154 + NL155) 1253bp		ARF7_D_LP SALK_067623.50.65 (ARF7 allele)	
NL155	AGTTCTTGGTGGTGGATTGTG	59	ARF7		At5g20730	Reverse	3' end gene (592bp from the end)	F			ARF7_D_RP SALK_067623.50.65 (ARF7 allele)	
NL156	TGACCGAAAACCAATTCAATTC	59	ARF7		At5g20730	Reverse	Within the 2nd intron	R	(NL156 + NL157) 1192bp		ARF7_E_GK_LP GABI_402D05 (ARF7 allele)	
NL157	TTGCCAAAACATATATGTACGCAC	59	ARF7		At5g20730	Reverse	Within the 1st intron	F			ARF7_E_GK_RP GABI_402D05 (ARF7 allele)	
NL158	TGTAGATGCTCGTTGTGCGACTG	60	ARF7		At5g20730	Reverse	3' end gene (1785bp from the end)	R	(NL158 + NL159) 1089bp		ARF7_F_GK_LP GABI_798F08 (ARF7 allele)	
NL159	AAAACTCTCAGTGGCGGAATC	60	ARF7		At5g20730	Reverse	Just past the middle of the gene	F			ARF7_F_GK_RP GABI_798F08 (ARF7 allele)	
NL166	ccgagtttatacgaagttcagtc		LRK1		AT3G45420			R			pLRK1_RV1	
NL167	gagatggcttgtgacgac		LRK1		AT3G45420			F			pLRK1_FW1	

A.1.2 GREENGATE Sequencing Primers

NL78	aacaggtctcgacctTTAATCTGCATAAAAGTGAGTATGAGAGAGAAG	56	pCASP1	Promoter module (A)	pGGA proCASP1F
NL79	accaggtctcgtgttTTCTCTTGCAATTGGGGTTTAAAAGAAAG	57	pCASP1	Promoter module (A)	pGGA proCASP1R
NL80	aacaggtctcgggctATGAAAGCTCCTTCATCAAATGGAGTTTCTCC	60	ARF7	Gene module C (with stop)	pGGC ARF7_PCR1F (with stop codon)
NL81	aacaggtctcCCCGTTcAGACCAGGAGGCTGCTGCTGTTC	68	ARF7	Gene module C (with stop)	pGGC ARF7_PCR1R (with stop codon)
NL82	CCTCCTGGTCTCAACGGGCAGAATCAGCAAAC	67	ARF7	To remove the Bsa1 site	pGGC ARF7_PCR2F (with stop codon)
NL83	aacaggtctcgctgaTCACCGGTTAAACGAAGTGGCTGAGTTATC	62	ARF7	To remove the Bsa1 site	pGGC ARF7_PCR2R (with stop codon)
NL86	aacaggtctcgacctATCGCGTAGATACGACCACCACC	69	pSCR	Promoter module (A)	pGGA_pSCR_PCR1F
NL87	TTCTCCGGTCTCTCTCCGGTCAATCCTCT	64	pSCR	Promoter module (A)	pGGA_pSCR_PCR1R
NL88	aacaggtctcCGGAGAaAGACCGGAGAAAGATGGGA	68	pSCR	To remove the Bsa1 site	pGGA_pSCR_PCR2F
NL89	accaggtctcgtgttGGATCCggagattgaaggttgttgg	70	pSCR	To remove the Bsa1 site	pGGA_pSCR_PCR2R
NL90	aacaggtctcgctgaCCGGTTAAACGAAGTGGCTGAGTTATCAT	69	ARF7	Gene module C (without stop)	pGGC_ARF7_no stop_PCR_2R
NL95	GTTTTCCCAGTCACGACGTT	55	ENTRY Control	End of ENTRY vector facing insert	ENTRY_Vector_Cont_R (GG control primer)
NL96	gtggaattgtgagcggataac	53	ENTRY Control	End of ENTRY vector facing insert	ENTRY_Vector_Cont_F (GG control primer)
NL107	ATACAGCGACTTAGTTTACC	53	Destination Control	End of Destination vector facing insert	pGGZ001_RV1 (GG Destination primer)
NL108	tcaccaaggtagtcggca	56	Destination Control	Middle of the Destination vector	pGGZ001_RV2 (GG Destination primer)
NL109	tcgggcttctggatttc	52	Destination Control	End of Destination vector facing insert	pGGZ001_FW1 (GG Destination primer)
NL122	AACAGGTCTCGACCTaactccattatttacgactgtgccactct	67	pCo2	Promoter module (A)	pGGA_pCo2_PCR1F
NL123	ACCAGGTCTCGTGTTatcgttattaactaggttcttgaaatttttc	64	pCo2	Promoter module (A)	pGGA_pCo2_PCR1R
NL127	AACAGGTCTCGAACAggtggtggtggcggatg	63	YFP Tag	N Tag module (B)	YFP_N_PCR1F
NL128	AACAGGTCTCTAGCCcttgtacagctcgtccatgccg	60	YFP Tag	N Tag module (B)	YFP_N_PCR1R
NL129	AACAGGTCTCGTCAGggtggtggtggcggtgag	64	YFP Tag	C Tag module (D)	YFP_PCR_1F
NL130	AACAGGTCTCTGCAGttacttgtacagctcgtccatgccgagagt	64	YFP Tag	C Tag module (D)	YFP_PCR_1R
NL131	aacaggtctcgacctgtgtttggttcgtaattatatacc	50	pGRP (XPP)	Promoter module (A)	pGRP_PCR_1F (XPP)
NL132	accaggtctcgtgttttggaaatcttcgtgtgttaa	50	pGRP (XPP)	Promoter module (A)	pGRP_PCR_1R (XPP)
NL133	tcatagtggaaccatagattagt	50	pGRP (XPP)	Promoter (1580bp upstream ATG)	PGRP_FW1 (XPP)
NL134	tagataggtaagatagagagtgatg	50	pGRP (XPP)	Promoter (285bp upstream ATG)	pGRP_RV1 (XPP)
NL135	atagtagcaaggtgaaagca	50	pGRP (XPP)	Promoter (724bp upstream ATG)	pGRP_FW2 (XPP)
NL136	aacaggtctcgacctgtgtttggttcgtaattatatacccttccatattcga	60	pGRP (XPP)	Promoter module (A)	pGRP_PCR1F (XPP)
NL137	accaggtctcgtgttttttggaaatcttcgtgtgttaagacttgcc	60	pGRP (XPP)	Promoter module (A)	pGRP_PCR1R (XPP)
NL138	aacaggtctcgacctAAGAGATGTCGCAAACCAGCTCATGT	60	pARF7	Promoter module (A)	pGGA_pARF7_PCR_1F (primer has overhangs)
NL139	accaggtctcgtgttCCTTTCTCCTGCATTCACACAACATCAAA	60	pARF7	Promoter module (A)	pGGA_pARF7_PCR_1R (primer has overhangs)
NL146	accaggtctcgtgttGATCACTCAACTTTACTTTCTCTGAA	65	pARF7	Promoter module (A)	pGGA_pARF7_PCR1R (primer has overhangs)

A.2 CLONING (GATEWAY AND GREENGATE)

A.2.1 List of Greengate pENTRY vectors (page 143)

A.2.2 List of Greengate Destination vectors (page 144)

A.2.3 List of Gateway plasmids (page 145)

A.2.1 List of Greengate pENTRY vectors

Greengate Promoter modules	Greengate CDS modules
Promoter XPP	*CDS ARF7* (WT) stop
Promoter SCR	*CDS ARF7* (WT) no stop
Promoter CASP1	*CDS ARF7* (4xKR) stop
Promoter LRK1	*CDS ARF7* (4xKR) no stop
Promoter EN7	
Promoter Co2	
Promoter GL2	

A.2.2 List of Greengate Destination vectors

pXPP::ARF7 arf7-1	Pericycle specific
pSCR::ARF7 arf7-1	Endodermal specific
pCASP1::ARF7 arf7-1	Endodermal specific
pLRK1::ARF7 arf7-1	Expressed in the elongation zone
pEN7::ARF7 arf7-1	Endodermal specific
pCo2::ARF7 arf7-1	Cortex specific
pWER::ARF7 arf7-1	Epidermal specific (root hair cells)
pGL2::ARF7 arf7-1	Epidermal specific (non-root hair cells)
pCOBL9::ARF7 arf7-1	Epidermal/lateral root cap specific

A.2.3 List of Gateway plasmids

pARF7::ARF7 (4xKR) arf7-1	first exon and intron with stop codon	Basta/hygromycin
pARF7::ARF7 (4xKR) arf7-1	first exon and intron with no stop codon	
pARF7::ARF7 (WT) arf7-1	first exon and intron with stop codon	Basta/hygromycin
pARF7::ARF7 (WT) arf7-1	first exon and intron with no stop codon	
p35S::ARF7:HA arf7-1	no stop codon	
p35S::ARF7:HA Col	no stop codon	
p35S::ARF7:Myc arf7-1	no stop codon	
p35S::ARF7:Myc Col	no stop codon	
pARF7::ARF7:3xVenus Col		